Process Design and Simulation of Light Calcination of Magnesite with High Efficiency

by

Ping An

Supervisor: Professor Dr Guoqing Guan

A Dissertation Presented to

the Graduate School of Science and Technology

of Hirosaki University in partial fulfillment of the requirement for

the degree of Doctor of Philosophy in Safety Science and Technology

HIROSAKI UNIVERSITY

2021

ABSTRACT

Magnesia has been widely used in the fields of fire-resistant materials, construction materials, chemical industries, environmental protections, pharmaceutical industries, agriculture, magnesium metal and magnesium alloys. For decades, the combination of water gas generator and reverberatory furnace has been adopted in traditional caustic calcined magnesia (CCM) production process with undesirable characteristics of high energy consumption, difficult quality control, and serious environment pollution. Thus, the technology for the production of CCM needs to be greatly upgraded.

This study mainly focuses on the design and simulations of novel light magnesite calcination technique with high energy efficiency for CCM production using a two-stage fluidized bed gasification (TSFBG) system with a transport bed flash calcination (TBFC) process. Firstly, a TSFBG system for fuel gas production is systematically simulated by Aspen Plus to identify the pre-drying effect of coal with its initial water content varying from 10 to 65 wt.% on gasification performance, particularly relating to the energy efficiency. The results show that the energy efficiencies based on lower heating value (LHV) (η_{LHV}) and higher heating value (HHV) (η_{HHV}) of feed coal are about 1.5%-7% and 1.5%-5% higher when coal is fed to the system directly without the pre-drying. For the TSFBG system, the higher the water content is, the greater the energy efficiency reduction by the pre-drying is. The analysis of energy allocations

reveals that the heat loss due to the pre-drying of coal is mainly responsible for the decrease of energy efficiency in operations with the pre-drying. With an increase in the initial water content from 10 to 65 wt.%, the η_{LHV} of the TSFBG system without the pre-drying of coal using air/steam as gasification agent reaches its maximum of about 91% at an initial water content of 26 wt.%. The η_{LHV} and η_{HHV} of the TSFBG system using oxygen/steam as the gasification agent increases energy efficiency by about 1-2% compared to that using air/steam. For TSFBG using air/steam to gasify coal without the pre-drying, the preferred initial water content of coal is below 50 wt.%.

Then, a TBFC process applied to magnesite is systematically investigated through a process simulation to optimize the energy-saving strategy. The high-temperature calciner flue gas is used to preheat the fed magnesite, while the sensible heat with the CCM product is cooled by air sending to the calciner. Pre-decomposition of magnesite during preheating is considered on basis of the kinetics measured using a micro fluidized bed reaction analyzer (MFBRA) that allows the minimized effect of external diffusion on reaction. With staged fuel gas supply, the TBFC process allows the equivalence ratios around 1.2 for combustion. The preferred arrangement of stages for magnesite preheating and CCM cooling are 4 and 2 respectively, leading to the energy consumption of 4100 kJ/kg-CCM and the energy efficiency of 66.8%, which is almost doubly higher than the 33.9% of the conventional reverberatory furnace (RF). The pre-decomposition occurs mainly in the 1st-stage preheater, and the maximal conversion is about 13%. Varying the stages of preheating appears more influential on the energy

saving than varying the cooling stages, while residence time above 1 s in the preheaters has limited effect.

Finally, the detailed and comprehensive $CaCO_3$ (with a similar decomposition performance as the $MgCO_3$) decomposition under different flue gas atmospheres and different pressures through simulation are conducted to provide more fundamental and complete information for the reaction in the product gas strongly inhibited atmospheres and certain reference values for industrial applications. The results show that CO_2 seriously inhibits the decomposition of $CaCO_3$ and this inhibition seems to be more obvious on the initial decomposition temperature when compared with the complete decomposition temperature. The higher CO_2 concentration of flue gas may lead to a narrower but higher whole temperature range for the decomposition of $CaCO_3$. Both the initial and complete decomposition temperatures of $CaCO_3$ increase with the increase of reaction pressure for different CO_2 concentrations in the flue gas, indicating that the decrease of pressure is favorable for the decomposition of $CaCO_3$.

All in all, in this work, the high energy efficiency for light calcination of magnesite for CCM production is successfully achieved by the optimum process design and simulation. It is expected to give the guidance for the design and application for the upgrading of CCM production technique.

ACKNOWLEDGMENTS

I am grateful to all those who have offered me instruction, encouragement, support, care and help during my PhD study.

First of all, I wish to thank my supervisor, Professor Dr. Guoqing Guan, who is very respectable and knowledgeable. He has offered me valuable instruction, suggestions, and encouragement during my PhD study. At the same time, I'm sincerely grateful to his help in my daily life in Japan.

I would like to thank Professor Dr. Abuliti Abudula, Graduated School of Science and Technology, Hirosaki University, for his kind help and support during my PhD study especially in the doctoral course affairs.

I would like to thank Professor Dr. Akihiro Yoshida for his help and advice.

I would like to sincerely thank Professor Dr. Guangwen Xu, Shenyang University of Chemical Technology, China, for recommending me for PhD study in this laboratory. Moreover, I'm very grateful to his valuable instruction and great support on my research.

I would like to thank Professor Dr. Dingrong Bai, Shenyang University of Chemical Technology, China, for his insightful advice and kind help.

I also would like to sincerely thank Professor Dr. Zhennan Han, Shenyang University of Chemical Technology, China, for his careful instruction, great efforts, insightful suggestions with incomparable patience on my research.

I would like to thank all professors and staff at Institute of Regional Innovation

(IRI), and at Graduated School of Science and Technology, Hirosaki University, for all of their kind advices and supports of my study.

I would like to thank all members in our research group for their helps and supports to my research and daily life.

I would like to thanks all members in the Professor Guangwen Xu`s group at Shenyang University of Chemical Technology, China, for their helps and supports to my research.

Finally, I would like to thank my family for all their support, for their love, encouragement, and understanding all through these years.

Thank you all very much.

Ping An

TABLE OF CONTENTS

LIST OF TABLES

LIST OF FIGURES

CHAPTER 1

Introduction

1.1 General introduction

Magnesium materials have been widely used in refractory materials, metallurgy, building materials, construction materials, automobiles, electronics, chemical industry, aviation, agriculture, aerospace, pharmaceutical, animal husbandry and other fields [1]. Its demand is growing continuously and has become one of the important and indispensable materials in the development of economy. Due to the high-quality and rich magnesium resources in China (i.e., magnesite), which are mainly distributed in Liaoning province and Shandong province, it has become the largest producer and exporter of magnesium-based materials in the world [2]. As the characteristic industry in Liaoning province and key technology of magnesium industry, caustic-calcined magnesia (CCM, also known as active magnesium oxide) production from magnesite calcination is crucial for the developments of industry and economy in Liaoning province.

The CCM production process is usually equipped with the fuel gas generator which will supply the energy for system. For decades, the combination of water gas generator (a fixed bed gasification technology) and reverberatory furnace has been adopted in traditional production process with undesirable characteristics of high energy consumption, only application to large partials, difficult quality controlling and serious environment pollution [3]. Thus, the production technology of CCM needs to be

upgraded comprehensively. The detailed introductions for CCM production, including the gasification technology for fuel gas production, are introduced in the following sections.

1.2 Gasification technology

The unstable oil prices have promoted researchers to investigate other energy sources such as carbon-based solid fuels. Coal, as a representative of carbon-based solid fuels, is still an important energy source nowadays. In general, the coal quality is determined by carbon, volatiles and moisture amount, which determine the heating value. For the high-quality coals with high heating value, the combustion technology is generally used and still dominates the generation of heat and power. However, the concerns of global climate change [4] and environmental pollution have restricted its applications. On the other hand, the high-quality coals are not abundantly reserved. The gasification technology is developed for possibly using low-quality coals with high moisture, high volatiles, and low heating values [5].

Different from the direct combustion, gasification can use coals more efficiently and cleanly with significant carbon dioxide emission reducing, since the obtained gas (fuel gas or syngas) from it can be applied for the production of not only heat and power but also value-added chemicals [6]. Gasification refers to the thermochemical process that a solid fuel reacts with gasifying agents (air/steam/O_2/CO_2) to produce a combustible gas (mainly CO and H_2). During this process, fuel drying, fuel pyrolysis,

char gasification, cracking and reforming of hydrocarbons and tar, combustion of combustibles [7] could occur. The major reactions except for combustion, are shown in the following Eqs. (1.1) - (1.5) [5].

$$C+CO_2 \leftrightarrows 2CO \quad \Delta H_{R1}=172.5kJ/mol \tag{1.1}$$

$$C+H_2O \rightarrow H_2+CO \quad \Delta H_{R2}=131.3kJ/mol \tag{1.2}$$

$$CO+H_2O \leftrightarrows H_2+CO_2 \quad \Delta H_{R3}=-41.2kJ/mol \tag{1.3}$$

$$C+2H_2 \rightarrow CH_4 \quad \Delta H_{R4}=-74.5kJ/mol \tag{1.4}$$

$$CH_4+H_2O \leftrightarrows CO+3H_2 \quad \Delta H_{R5}=205.8\ kJ/mol \tag{1.5}$$

There are numerous gasification technologies which have been developed and are commercially available. Based on the reactor bed where fuels are gasified, these gasifiers can be generally categorized into three types including fixed bed, fluidized bed, and entrained flow gasifiers.

1.2.1 Fixed bed gasification

In fixed bed gasifiers or moving bed gasifiers, the solids are always in a fixed or moving state with respect to the gas [8]. Based on the relative positions of solid feedstocks and gasifying agents into the gasifier, as illustrated in **Figure 1.1**, it can be classified into updraft fixed bed (UD-FB) gasifier (co-current) and downdraft fixed bed (DD-FB) gasifier (counter-current) [9]. In the UD-FB gasifier, fuel is introduced into the gasifier from the top whereas the gasifying agent is provided from the bottom. The gas-solid convection is beneficial to enhance the contact between fuels and gasifying agents, reduce pressure drop of the bed and generate a small amount of slag. However, primary

tar flows from high temperature zone to low temperature zone and the upward moving gas shortens the reforming time of tar, resulting in high tar content (e.g., as high as 50 g/Nm^3_{db}). It is reported that the obtained fuel gas is usually composed of 1.6-50 vol.% H_2, 13-25 vol.% CO and 1.5-10 vol.% CH_4 with high heating values in the range of 2.4-12.1 MJ/Nm^3_{db} when the reaction temperature changes from a minimum range of 650-700 °C to a maximum range of 950-1150 °C under different gasification conditions [10,11]. In the DD-FB reactor, both fuel and gasifying agent are firstly delivered in the drying zone, and the volatiles from pyrolysis are carried to the combustion and reduction zones, which always yield low-tar fuel gas (<20 g/Nm^3_{db}) with low particulate content [12]. However, it is difficult to control the temperature and the products, easily leading to the problems of bridging and slagging in the gasifier. Usually, the downdraft gasifier can generate a lower-tar-content product gas [8] with a lower heating value [13] compared with the updraft gasifier. In addition, due to the lack of versatility for treating different feedstocks, downdraft gasifier is not as flexible as updraft gasifier [8].

The fixed bed gasifier was firstly proposed and fabricated in Finland, and successfully applied in one power generation company. From 1985-1986, eight UD-FB gasifiers were commercialized with the output range of 4-5MW_{th} [14]. The two most popular commercial gasifiers are Sasol-Lurgi dry bottom gasifiers and British Gas Lurgi (BGL) (slagging type), shown in **Figure 1.2** [15]. The fixed bed gasifiers can only adopt large-particle raw materials, usually more than 20 mm and 10 mm for the atmospheric reactors and the pressurized Lurgi reactors, respectively. Fixed bed

gasifiers always have lower heat/mass transfer rates and poor adaptability for the powder feedstock as well as difficulty in scaling up, which still restricts their applications in large scale. Fixed bed gasifiers have the most obvious merit of high conversion while they are limited to operational temperatures below1000 °C [9].

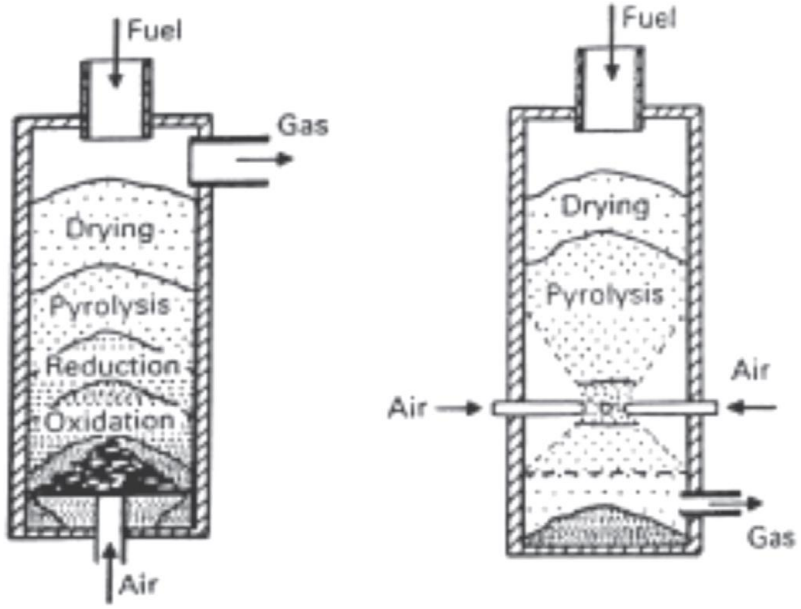

Figuer 1.1 Fixed bed reactor configurations. (Reprinted with permission from Ref. [9]).

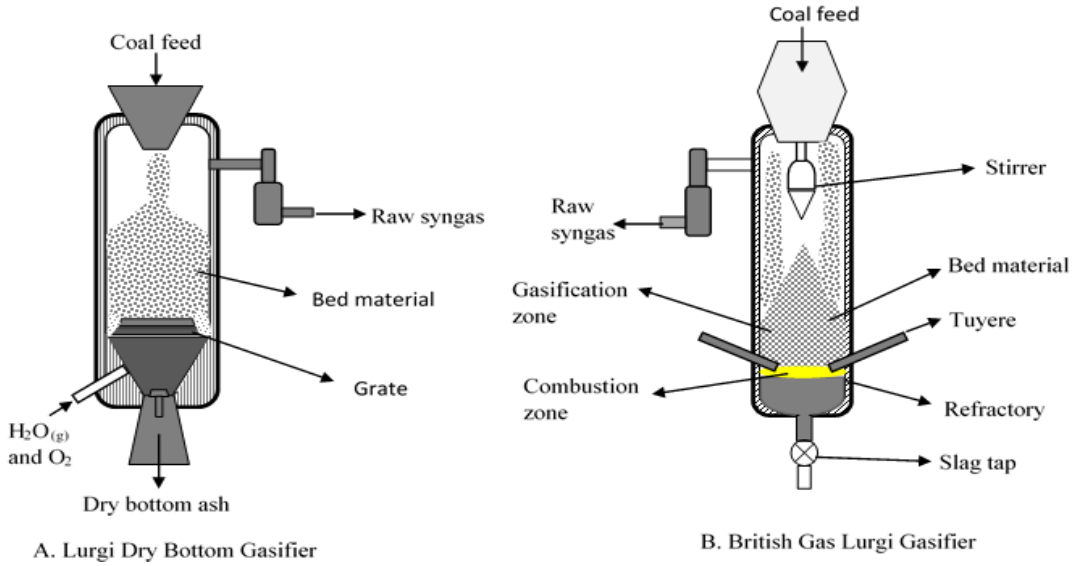

Figure 1.2 Schematic of fixed bed gasifiers (A) Sasol-Lurgi Dry Bottom Gasifier; and (B) British Gas/Lurgi (BGL) Slagging Gasifier [15].

1.2.2 Fluidized bed gasification

Fluidized bed gasifiers (FBGs) have been widely applied to coals in continuous operation. The gasifying agent flows from the bottom of gasifier and the coal enters near the bottom of gasifier [5]. As shown in **Figure 1.3**, there are three common types of FBGs: bubbling fluidized bed (BFB), circulating fluidized bed (CFB), and dual fluidized bed (DFB) gasifiers. Due to the main advantage of better distribution, FBGs can reduce limitations of heat and mass transfer. FBGs also have desirable characteristics of high capacity, good adaptability of solid fuels in a wide particle size distribution (below 10 mm) and low investment. However, FBGs still suffer from the problems of high tar content in produced fuel gas [16]. Tar will be condensed when the temperature is below 300 °C and thus causes many operational problems, such as catalyst deactivation, erosion and blocking of pipeline and equipment, and serious environmental pollution of phenol wastewater [17]. Han *et al.* [18] reported that the tar contents in produced gas form BFB and CFB gasifiers in low operating temperatures respectively ranged around 10–40 g/Nm^3_{db} and 5–12 g/Nm^3_{db}, while it could vary about 0.5 - 40 g/Nm^3_{db} which was influenced by the type of DFB gasifier, bed material as well as operating condition.

For the BFB gasifier (Fig. 1.3a), the solids bed and the fluidization agent undergo a vigorous bubbling state and the pyrolysis and gasification of fuels occur to produce char, tar and gases. The bubbling type is composed of one chamber for gasification and it may suffer from the problem of fluidization control. The O_2 exists in the bubbles in

this gasifier, thus the combustion could occur anywhere in the whole reactor, which significantly decreases gasification efficiency [8]. Tar is usually generated in high-temperature solids bed, then cracked to about 5-20 g/Nm^3_{db} and transported to low-temperature gas phase zone [19]. As the bed temperature is in the range of 700-900 °C, the produced fuel gas usually contains 30-60 vol.% of H_2, 10-25 vol.% of CO and 8-12 vol.% of CH_4 with 7.3-14 MJ/Nm^3_{db} [20]. The dust is always carried out either from the bottom or with the product gas. The BFB gasifiers have lower carbon conversion because of reaction gas dilution by product gas and shorter reaction time compared with CFB gasifiers [21]. Particles entrainment of fine char and reduction of oxidant diffusion from bubble phase to emulsion phase are also big problems for bubbling bed. While CFB and transport bed reactors can effectively solve these problems. The transport bed gasifier is significantly different from CFB and BFB in the particle size of feedstock, residence time of particle as well as gas velocity [21].

For the CFB gasifier (Fig. 1.3b), solids circulate between the reactor and the cyclone, in which the ash is separated while the bed material together with char are moved back to the reactor. Compared with the bubbling design, the CFB has a capability of handling large feedstock throughputs due to its very high gas velocity. Moreover, the efficiency for CFB does not reduce since bubbles do not exist in such a circulating reactor [8]. The FBG usually operates from 800 to 1000 °C, which can prevent ash accumulation. Thus, these reactors can adopt high-ash feedstock in this temperature range [8]. While the main difficulty in operation is the possible slagging at

low temperatures when the ash melt may occur below 1000 °C [9]. The main consideration is to remove ash, which has been almost neglected in the bubbling fluidized bed reactors but its impacts on agglomeration and defluidization in fluidized bed reactors have been widely studied [22]. It is reported that the obtained fuel gas contains 22-27 vol.% of H_2, 27-40 vol.% of CO and 7-9 vol.% of CH_4 with 8.3-12 MJ/Nm^3_{db} under the temperature ranged in 650-850 °C [20, 23]. Compared with the BFB gasifier, the CFB gasifier can improve carbon conversion efficiency, but the high tar content in produced gas and dust problems still limit its applications.

The DFB gasifiers (Fig. 1.3c) separate the fuel pyrolysis and partial gasification from the combustion of unreacted char. The middle caloric fuel gas is expected to be produced by DFB gasifiers even though using gasification agents of air/steam/air-steam mixture since product gas dilution by N_2 from air and CO_2 from combustion can be avoided. The feeding coal is pyrolyzed to generate char and gas which could complete within 10 s with the temperatures of more than 800 °C [24], and then the char is gasified whereas it takes several minutes [25]. Compared with char, the O_2 in atmosphere would prefer to react with the pyrolysis gas. Moreover, the gasification reaction of char would be suppressed by the coexistence of pyrolysis gas and char. This could lead to low efficiency of gasification and low-quality product gas. Hence, the concept of DFB gasifiers technology is proposed, in which the fuel pyrolysis is separated from the char gasification. The issue of different bed combinations for DFB gasifiers was first addressed by Xu *et al.* [26]. From the experimental results of 5 kg/h DFB gasifier with

electrical heating, the combination of ‘‘riser combustor and low-velocity fluidized bed gasifier’’ was proved to be superior because it enabled the DFB gasifier to perform with high conversions of C and H, high efficiency of gasification as well as good tar elimination capability [27].

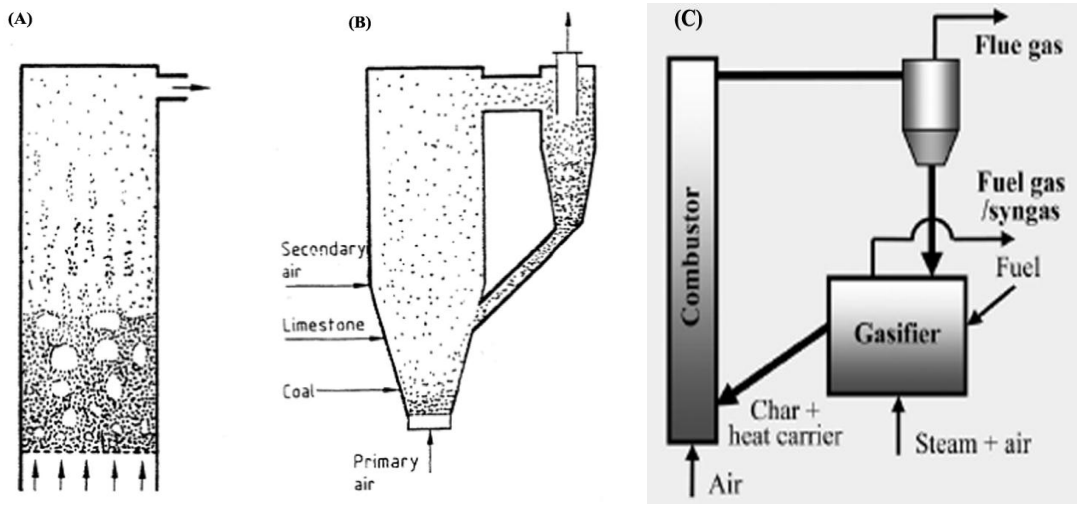

Figure 1.3 Fluidized bed reactors used for gasification:(A) bubbling bed, (B) circulating bed, (C) dual fluidized bed. (Reprinted with permission from Ref. [9], [27]).

In the 1920s, the German Winkler firstly discovered the phenomenon of fluidization and applied it to the development of coal gasification. Then the Winkler gasification technology (**Figure 1.4**) was successfully developed and its first plant for industrial application was built in Leuna, Germany in 1926 [28]. This created a precedent for the industrial application of fluidization technology, which was the major breakthrough in the development of coal gasification technology. After that, fluidized bed gasification technologies such as U-Gas technology and KRB technology have been successfully developed and their industrial demonstrations have been well carried out [29].

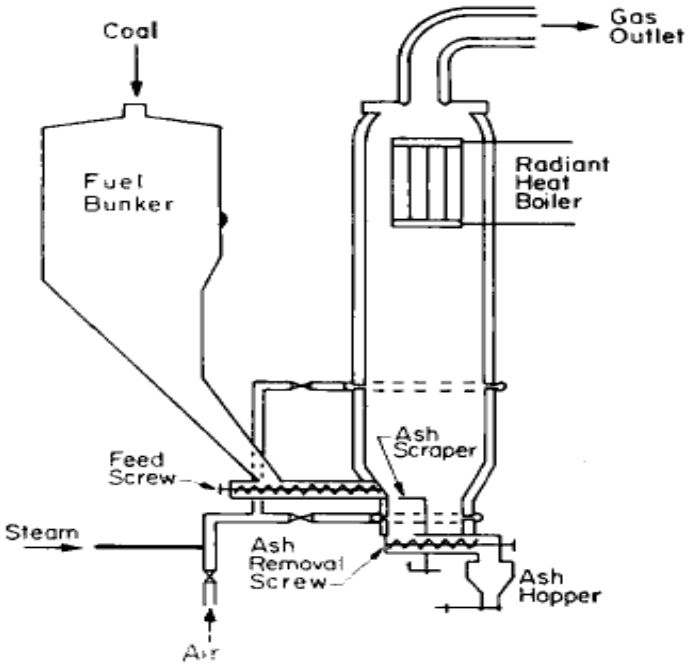

Figure 1.4 Winkler gasifier [30]. (Reprinted with permission from Ref. [30]).

1.2.3 Entrained bed gasification

In entrained flow gasifiers (EFGs), the feedstock particles (below 75 μm) together with agents for gasification usually enter the reactor from top. The gas velocity is high enough to entrain all the feedstock particles. Compared with fixed bed gasifiers and FBGs, the EFGs have the obvious characteristics of very high temperatures (more than 1473 K), large load capacity and short residence time [31]. Generally, the high-temperature (even reaching 1700 °C) and high-pressure (usually 3.0-4.0 MPa) EFGs are very suitable to produce the syngas for chemical synthesis. The high-capacity (e.g., 2000 t/d coal) EFGs usually have much heavy invest and they generally treat the high-heating-value coals with low-content (e.g., less than 10 wt.%) ash and low ash-melting point (e.g., above 1250 °C) considering economics and technology reasons [32]. In EFGs, slurry or dry coals can be fed into the reactor while bottom slag and fly ash can be

correspondingly produced from the removal of slag/ash [31]. EFGs are widely used type of gasifier for industrialization due to quite low content of tar in product gas, flexibility as well as very high conversion of char. While it is quite challenging to obtain the required feed size and the material of construction can be a restriction for EFGs. It is essential to perform an efficient cooling for syngas to removal sulfur and improve gas handling [5].

In the 1930s, Koppers of Germany and Texaco of the United States started to investigate entrained bed coal gasification technology [28]. In 1952, the industrialization of Koppers-Totzek entrained bed gasifier (K-T gasifier, shown in **Figure 1.5**) is successfully achieved, which is another major breakthrough in the history of coal gasification technology. In the early 1970s, due to the first crisis of petroleum, Shell, Texaco, Dow and other multinational companies have invested heavily in research and development of coal gasification. Coal-water slurry gasification technology and pulverized coal pressurized gasification technology gradually completed large-scale industrial demonstrations in fields of coal to bulk chemicals, direct and indirect coal liquefaction, coal to natural gas, IGCC power generation and hydrogen production [29]. In 1980, the entrained bed coal-water slurry gasification was first introduced into China for ammonia synthesis [33]. The coal-water slurry was fed at the top of the reactor to react with oxygen at the temperatures of 1300-1400 °C to ensure that the ash is in melting state in the chamber of gasification (**Figure 1.6**). The syngas produced from this gasification process usually has H_2/CO ratio of 0.7-0.85 and a low concentration of

CH_4, which is quite suitable for FT synthesis. Additionally, water slurry feeding could utilize some of polluted water, which is beneficial to environmental protection. Although many experiences have been already obtained in large-scale applications, such a gasification system still has the main disadvantages of large oxygen consumption and lower efficiency because of low density of energy in water diluted feeding. The original Texaco gasifier used only one jet at the top of reactor vessel. After continuous research and development, the latest design for coal–water slurry gasifiers are equipped with multiple jets in the upper zone of the reactor with a top jet. Consequently, a better flow field in the chamber of combustion and a higher carbon conversion is realized. This type of gasifier with multiple jets could be easily scaled up to a processing capacity of 3000-4000 t coal per day [34].

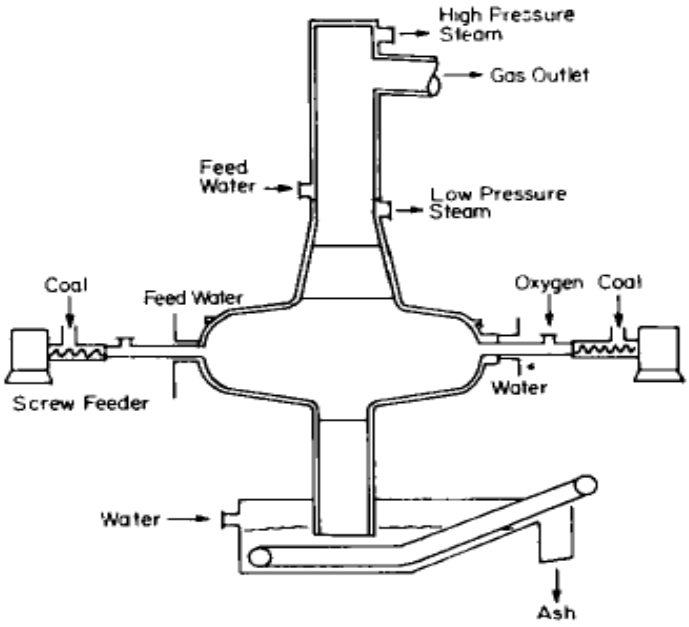

Figure 1.5 Koppers-Totzek entrained bed gasifier. (Reprinted with permission from Ref. [30]).

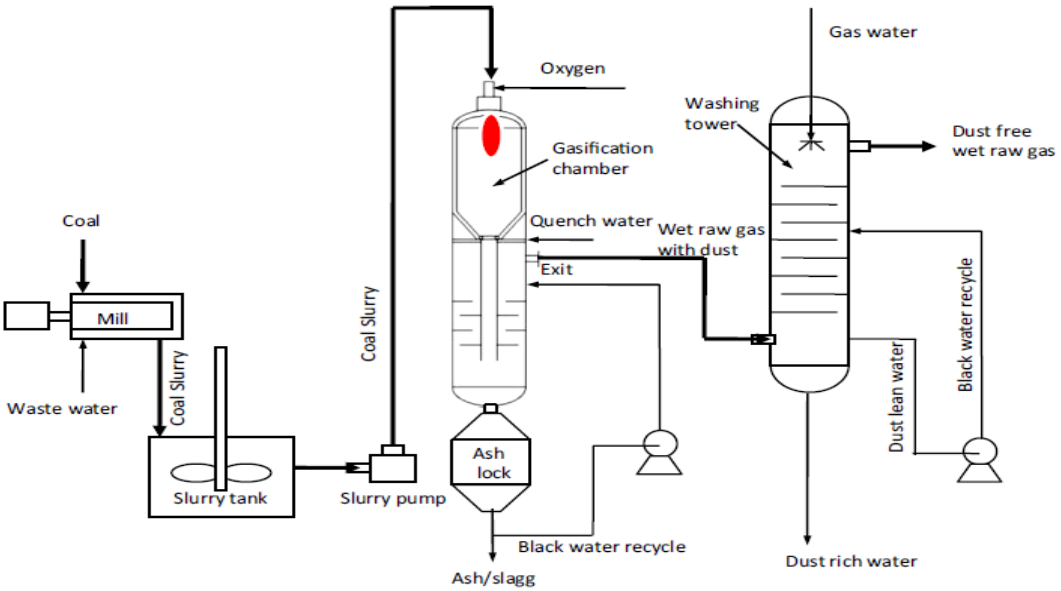

Figure 1.6 Entrained flow gasification with coal-water slurry [35]. (Reprinted with permission from Ref. [35]).

1.3 Two-stage gasification

1.3.1 Decoupling gasification

Macroscopically, the thermochemical conversion process of gasification essentially contains a complex reaction network as shown in **Figure 1.7**. Fuel drying/pyrolysis provides reactants for other reactions and produces steam as a gasification agent and reactant for char gasification and pyrolysis gas/tar reforming. The pyrolysis gas/tar may further occur cracking or decomposition or reforming and the char produced by pyrolysis, in which the contained metal species could catalyze the reforming and decomposition/cracking of tar and pyrolysis gas [7]. The combustible components in the final product gas by reactions such as pyrolysis, char gasification, decomposition/cracking and reforming, including H_2, CO, C_mH_n, etc., can also affect

other sub-reactions, such as suppressing the gasification of char or fuel. The reaction heat required for endothermic reactions such as char gasification is provided by the combustion of combustible components and char, and the CO_2 produced by combustion (a large amount of N_2 when air is used) can cause the dilution of the product gas. The traditional gasification process coupled all the sub-reactions together, and it is difficult to use the various interactions that occur in the reaction network and the intermediate products generated from the sub-reactions.

In other words, the performance of gasification process can be potentially optimized by controlling individual reactions and their engaged interactions. These benefits possibly include the increase in fuel conversion efficiency, low pollution, low consumption, high product quality and product polygeneration in the gasification process. By separating one or some sub-reactions, the coupling of the sub-reactions occurring in the coupling conversion process is decoupled, and the decoupled sub-reactions are reorganized according to the need to enhance or inhibit the interaction of some intermediates and final products with the sub-reactions. The "decoupling gasification (DCG)" is proposed by Zhang *et al.* [7] which is featured with "control of the reaction and its related interactions". **Figure 1.7** shows how these reactions are interrelated based on the sequence of occurrence and the products from the upstream reaction to determine the occurrence of a downstream reaction indicated by the solid line arrow. This implies the coupling of each pair of the adjacent linked reactions. Theoretically, the decoupling of each arrow-linked reaction could be realized by

breaking the linkage in a possibly suitable way. As illustrated by the star between pyrolysis and gasification in **Figure 1.8**, after the breakage of reaction linkage, two approaches can be employed to reorganize the decoupled reactions.

The method of "isolating" decoupling usually integrates two reactors (reacting independently), which are used to isolate the products to inhibit the inter-effects between the products of decoupled reactions and also achieve polygeneration. In the approach of "synergizing" decoupling, the promotion of favorable interactions or the inhibition of undesired interactions among the linked reactions are realized through the re-organization of decoupled reactions. Through this kind of decoupling, the gasification process is expected to improve fuel conversion efficiency and product quality, reduce pollutant formation, and/or enable fuel adaptability. These decoupling effects indicate that it is potentially reduce tar production, improve fuels adaptability as well as product quality by synergizing method, thus innovating advanced technologies of gasification [7]. Based on the synergizing method, the two-stage gasification (TSG) is formed through decoupling pyrolysis reaction from the other reactions.

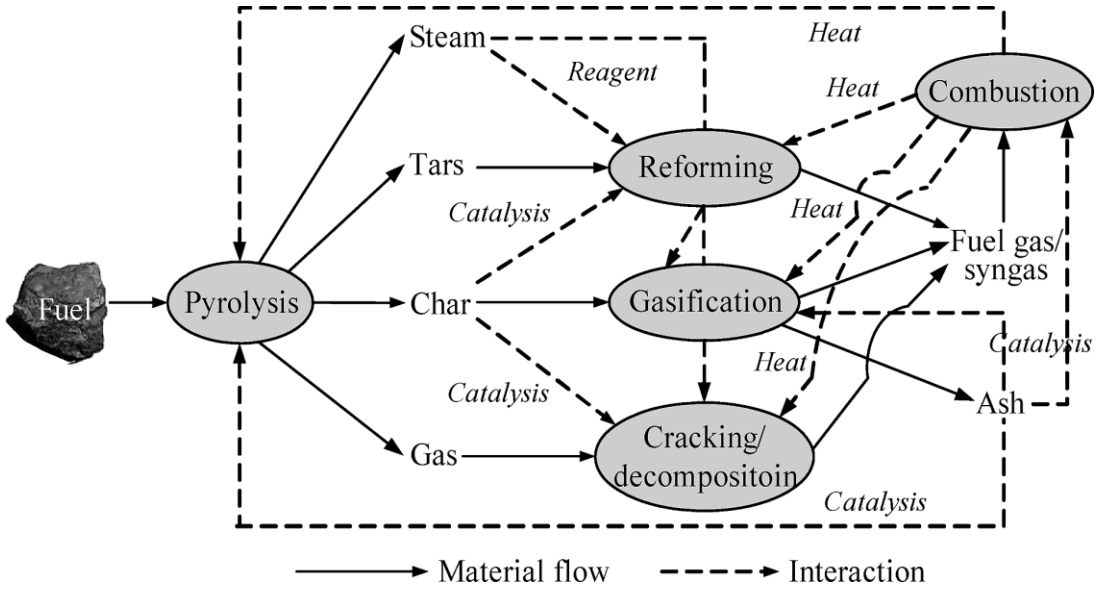

Figure 1.7 Reaction network in the gasification process of carbonaceous solid fuels. (Reprinted with permission from Ref. [7]).

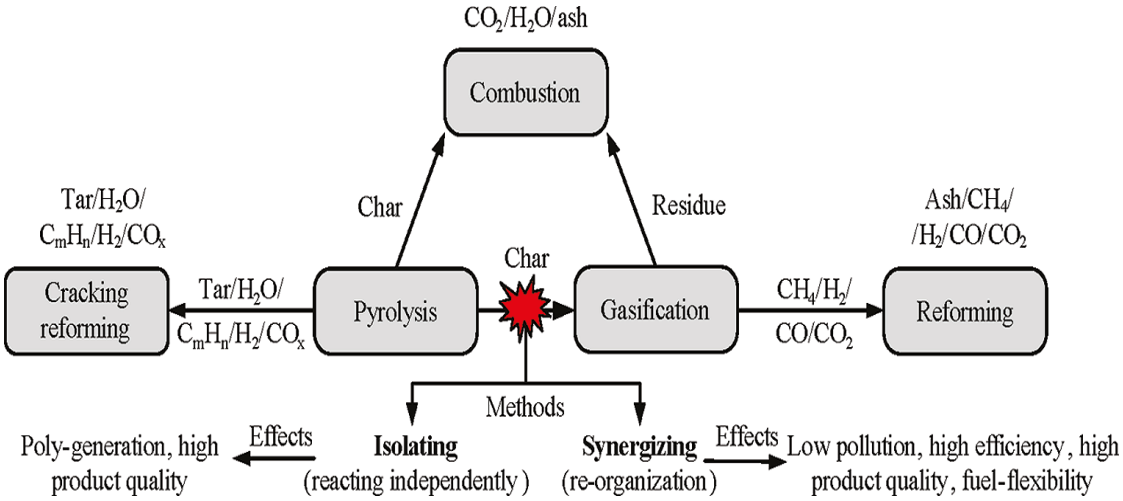

Figure 1.8 Two decoupling approaches applied in developing DCG technologies. (Reprinted with permission from Ref. [7]).

The TSG technology uses the char-catalysis effects for reforming/cracking of tar related substances to realize the removal of tar produced by pyrolysis inside the process. As shown in **Figure 1.9**, fuel first conducts the pyrolysis reaction in a pyrolytic zone (the first stage), then the pyrolysis products including gas, tar, and char are fed to a

gasification/reforming zone (the second stage). As such, char can be employed as the bed material for gasification zone to realize its catalysis for tar cracking/reforming over high-temperature char particles during the process of gasifying char in a gasifier. The produced gas with a very low tar content can be obtained, consequently achieving the decoupling effect [7]. **Table 1.1** presents the summary of typical TSG technologies.

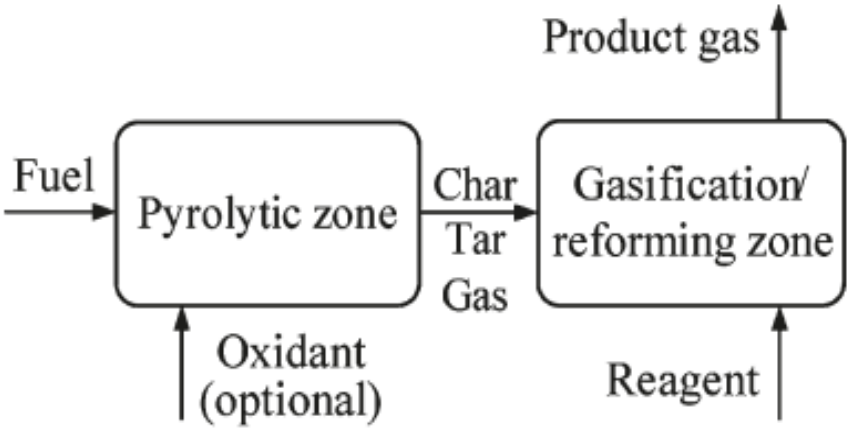

Figuer 1.9 Principle diagram of the two-stage gasifier. (Reprinted with permission from Ref. [7]).

Table 1.1 Summary of typical two-stage gasification technologies.

Technologies	Parts in the two-stage gasifier	Developer	Feedstock	Tar content in fuel gas (mg/Nm^3_{db})	Current state	Ref.
Throatless downdraft fixed bed gasifier	Two DD-FBs for pyrolyzer and gasifier, respectively.	Asian Institute of Technology, Thailand	Wood chips	<50	Pilot	[36]
Viking gasifier	A screw conveyer as pyrolyzer and a DD-FB as gasifier.	Technical University, Denmark	Wood chips	<50-80	Demonstration	[37,38]
Fraunhofer ISE gasifier	A DD-FB for pyrolyzer and a UD-FB for gasifier	Fraunhofer Institute for Solar Energy Systems, Germany	Wood chips	10-50	Pilot	[39]
Two-stage gasifier	A fluidized bed as pyrolyzer and a DD-FB as gasifier	IPE, China	Coal	84	Pilot	[32,40]
Fluidized bed two-stage gasifier	A fluidized bed pyrolyzer and a transport fluidized bed gasifier	IPE, China	Herb residue	400	Demonstration	[41,42]
Fluidized bed two-stage gasifier	A fluidized bed pyrolyzer and a transport fluidized bed gasifier	IPE, China	Low-rank coal	365	Pilot	[43]

1.3.2 Fixed bed TSG

(1) Throatless downdraft gasifier

Throatless downdraft gasifier was designed by the Asian Institute of Technology in 1992. It is a multi-stage reactor that consisted of two DD-FBs. The flaming-pyrolysis zone is separated from the reduction zone. In this gasifier, the two air feedings including the primary and secondary air are employed. The secondary air is introduced in the middle of gasifier for the partial oxidation to raise the temperature of reduction zone, leading to the occurrence of tar cracking at high temperature. As such, the tar concentration in produced fuel gas can be reduced to below 50 mg/Nm^3_{db} with a treating rate of 600 kg/(m^2·h), which is 40 times lower than that from a single-stage gasifier under the same condition [36].

(2) Viking gasifier

In 1999, Peder Brandt from Technical University of Denmark developed a 100-kW_{th} TSG (named "Viking") with a screw conveyer as the pyrolyzer and a DD-FB as the gasifier. As shown in **Figure 1.10**, the pyrolysis products together with the gasifying agent (air and steam) are transported into the gasification section from the top of downdraft reactor. The obtained fuel gas contains a low tar concentration of about 10-40 mg/kg when the wood was used [37,38]. Currently, this Viking technology reaches an industrial scale of 1.5 MW after it has been scaled up several times.

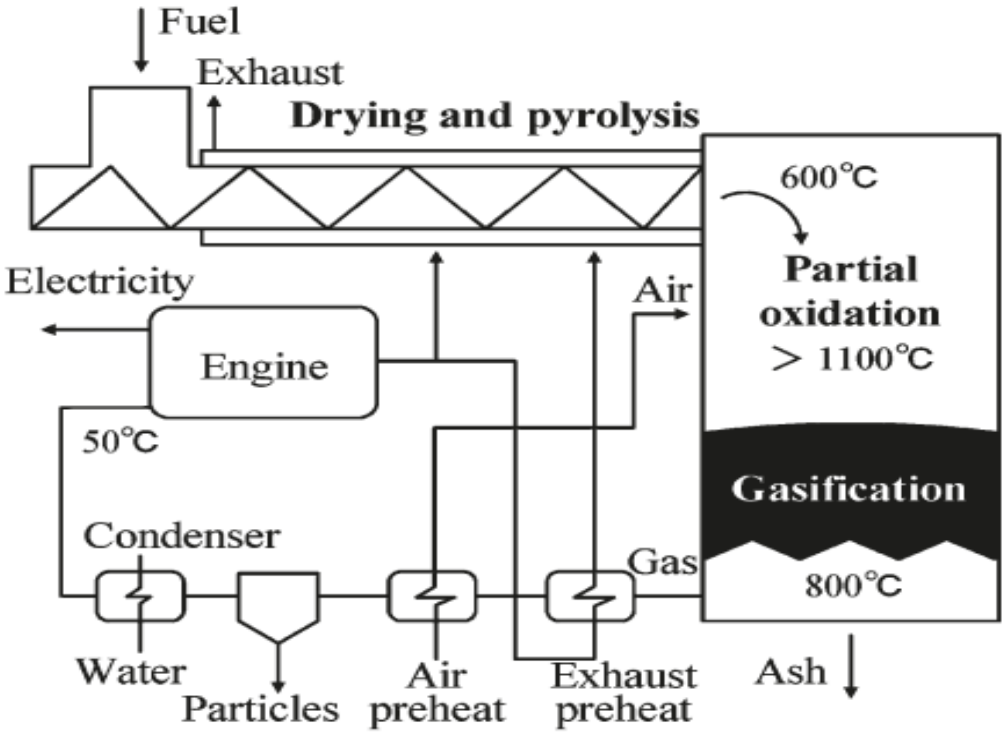

Figure 1.10 A schematic diagram of the Viking gasification plant. (Reprinted with permission from Ref. [7]).

(3) Fraunhofer ISE gasifier

The Fraunhofer Institute for Solar Energy Systems developed the Fraunhofer ISE gasifier in 2013. It is composed of a DD-FB for pyrolysis and a UD-FB for gasification featured with four isolated zones in gasifier for pyrolysis and gasification, partial combustion, tar cracking, and reduction and oxidation to be arranged respectively from the top to the bottom of reactor, thereby achieving a quite low tar concentration of 10–50 mg/Nm^3 db in the produced gas [39].

1.3.3 Fluidized bed TSG

(1) Two-stage gasifier

The two-stage gasifier, which was firstly adopted fluidized bed to the TSG process,

was developed by the Institute of Process Engineering (IPE, CAS) in 2010. As shown in **Figure. 1.11**, it consists of a fluidized bed pyrolyzer and a DD-FB gasifier [40]. After the fuel is pyrolyzed in the fluidized bed, all the products are further introduced into a DD-FB gasifier. and then all the pyrolysis products are forwarded into the downdraft fixed bed gasifier, where the gasification of char occurs and the tar is further cracked and/or reformed to gas through the catalysis effect of high-temperature char. As such, the advantages of high mass and heat transfers in the fluidized bed and high tar removal rate in the DD-FB are well combined. Especially, tar can be more easily cracked and/or reformed in the downstream gasifier with the steam containing atmosphere. In 2012, an auto-thermal pilot-scale plant with a capability of about 50 kg/h based on this technology was built. A low tar content (84 mg/Nm^3_{db}) in the product gas with a heating value of 4.186 MJ/Nm^3_{db} was achieved [32]. However, the obvious disadvantages of DD-FB including difficulty in high pressure drop, poor fuel adaptability of powder raw materials as well as scaling up, still restrict its large-scale industrial applications.

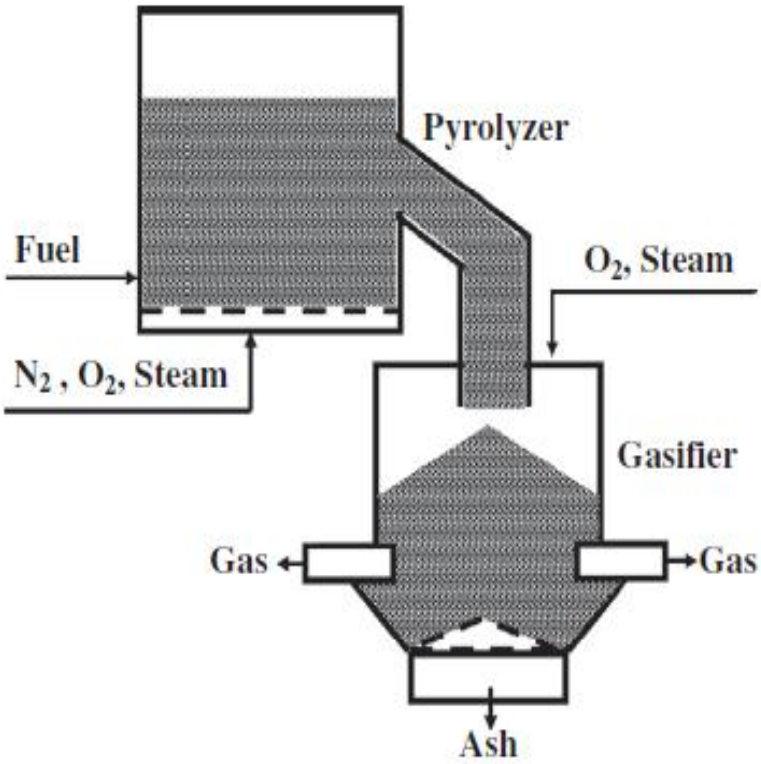

Figure 1.11 A conceptual diagram of the proposed new two-stage gasification process. (Reprinted with permission from Ref. [32]).

(2) Fluidized bed two-stage gasifier

A new technology of fluidized bed two-stage gasifier was developed by IPE in 2015, which employs a fluidized bed type pyrolyzer and a transport fluidized bed type gasifier [42]. As shown in **Figure 1.12**, fuel is autothermally pyrolyzed or partially oxidized in the first-stage fluidized bed reactor. And all the pyrolysis products are forwarded into the second-stage transport bed reactor to perform the gasification of char, the reforming/cracking of tar and the upgrading of gas products. The feasibility of this new technology was proved by the pilot test and then it was further scaled up to a larger capacity (600 kg/h) for the gasification of herb residue using air as the gasification agent to produce fuel gas. The results from this demonstration running showed that the

temperatures of gasifier and pyrolyzer respectively held at about 850 °C and 700 °C, and the compositions of produced gas were 17.6 vol.% CO, 8.6 vol.% H_2, 4.4 vol.% CH_4, and 10.3 vol.% CO_2 as well as 58.8 vol.% N_2 calculated on dry basis with a heating value of 1250 kcal/Nm^3_{db}. The corresponding tar content was reduced to 0.4 g/Nm^3 db f, which was much lower than the tar concentration of 5-12 g/Nm^3 db from the gasification in CFB, demonstrating the effectiveness of fluidized bed two-stage for tar removal [42]. In 2018, Zeng *et al.* [32] extended this technique to low-rank coal gasification technology with a processing capacity of 100 kg/h. When the temperatures in the gasifier and pyrolyzer were 1000 and 840 ºC, respectively, the tar contents detected from the pyrolyzer and gasifier were 1.127 g/Nm^3_{db} and 0.365 g/Nm^3_{db} respectively. In the steady state, the compositions of CO, H_2, CH_4 and CO_2 in the final product gas were 14.4 vol.%, 8.3 vol.%, 3.4 vol.% and 11.3 vol.%, respectively with a heating value of around 1100 kcal/Nm^3_{db}.

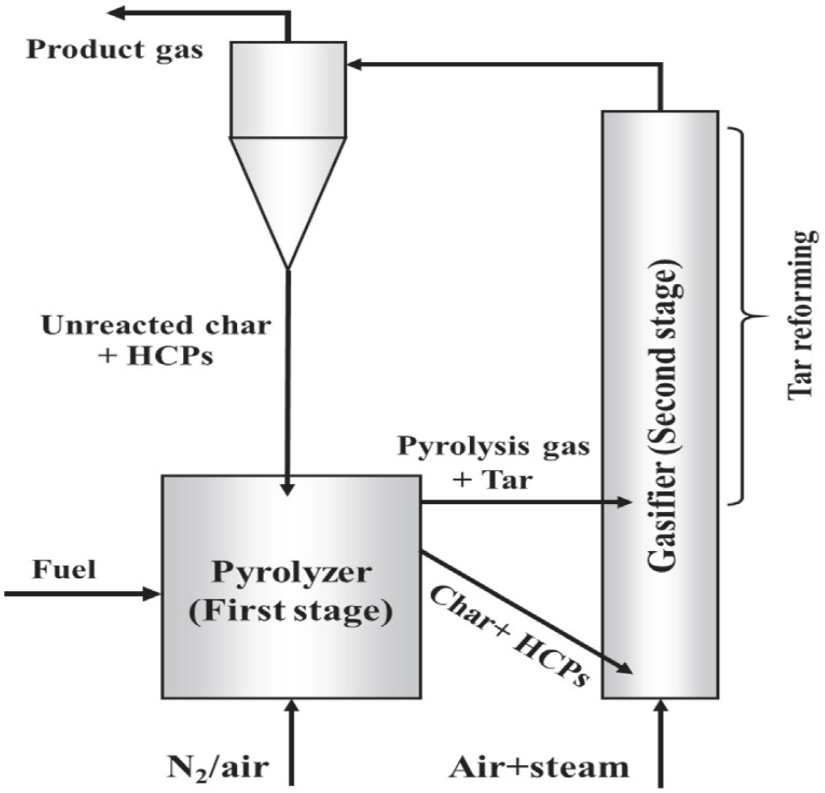

Figure 1.12 A process diagram of fluidized bed two-stage gasification [18].

1.4 MgO-based industry

Magnesium ranks eighth in the Earth's crust, weighting about 2.3 %, and exists in rock formations of magnesite and dolomite. Magnesium ranks third in the seawater with a concentration of about 1300 ppm. Similar to the lime production from limestone, magnesia (MgO or magnesium oxide) is mainly produced by the magnesite calcination. Only a small part magnesia in the world produces from seawater as well as brine, or other sources [44]. Magnesia has been widely used in the field of fire-resistant materials, construction materials, chemical industry, environmental protection, pharmaceuticals industry, agriculture, magnesium metal and magnesium alloys. The favorable properties of magnesia include its high melting point (2800°C), high thermal conductivity,

electrical resistance, excellent resistance to alkali sand, as well as high lime content of flakes formed in steel melting furnaces [45]. Moreover, it is non-toxic and doesn't suffer from hydration problem such as lime [46].

1.4.1 Magnesite

For MgO production, due to the higher energy consumption for the wet route, the most commonly used method is the calcination of magnesite, which is a common natural mineral in the carbonate group. Magnesite is mainly distributed in China, North Korea and Russia, from a global perspective. In recent years, the world's production of magnesite mine has been increasing gradually [47]. China is rich in magnesite with reserves of about 3.1 billion tons, most of which are first- and second-grade magnesite, making it the world's leading source of this strategic mineral. As shown in **Figure 1.13**, about 90% of them are distributed in Liaoning province, where world-class large to super large magnesite processing and production facilities have been developed. In 1913, the first magnesite deposit in China was discovered in Zhuanzishan, Gaixian county, Liaoning province. In the following years, more deposits were discovered in Yingkou and Haicheng (Liaoning), Dahe (Hebei) and Basha (Tibet). The Haicheng-Dashiqiao deposit in Liaoning is the best quality of sparry magnesite in large scale [2].

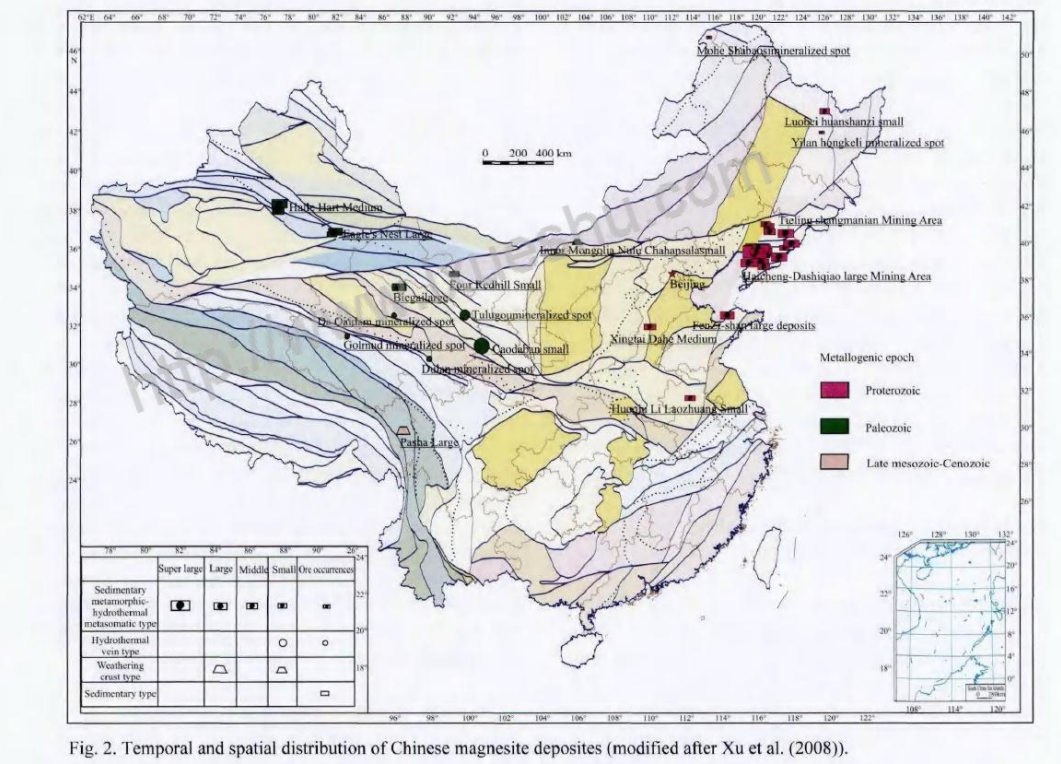

Fig. 2. Temporal and spatial distribution of Chinese magnesite deposites (modified after Xu et al. (2008)).

Figure 1.13 Distribution of Chinese magnesite deposits. (Reprinted with permission from Ref. [2]).

The representative gangue minerals including the silicates and carbonates are usually related to the magnesite in natural deposits. Among them, the calcium- and magnesium-bearing minerals are the most common ones which are present in large amounts. The theoretical composition of magnesite is 47.7% of MgO and 52.3% of CO_2 with traces of Fe, Ca, Co, Mn, N as well as organic compounds. The principal impurities of a magnesite from a chemical analysis include CaO (lime); SiO_2 (silica); Fe_2O_3 (iron oxide); Al_2O_3 (alumina); and B_2O_3 (boric oxide). Magnesite usually appears to be white or yellowish in three different textures in nature including MgO-rich macrocrystalline (MgO content over 43%), dolomite-containing microcrystalline (MgO content ranging 39-43%) and macrocrystalline but containing many impurities (MgO content below

39%) [48]. According to the nature of magnesite and the texture of the minerals accompanying magnesite, the used technologies for magnesite enrichment include magnetic separation, optical or manual sorting, flotation and gravity. Treatments have shown that the obtained concentrate could have the low content of impurity as well as a good quality with the high content of MgO (over 47%) [48]. The magnesite calcination involves a decarbonisation reaction of $MgCO_3$, as described by the following reaction equation (1.6):

$$MgCO_3 \rightarrow MgO + CO_2 \quad (1.6)$$

Generally, the products from $MgCO_3$ decomposition are high catalytic activity. The "caustic" magnesia refers to a brittle material with high reactivity and quite large surface area, which are produced directly from thermal decomposition. Its properties mainly depend on the temperature as well as the time of calcination [49]. The main technologies for CCM production from magnesite calcination are presented in detail in the section of 1.5.

1.4.2 Dolomite

The total proven reserves of dolomite resources for the extraction of magnesium in China exceed 3 billion tonnes [2]. As a carbonate sedimentary rock, dolomite contains over 50% of carbonate, at least half of which is double carbonate of calcium and magnesium $(Ca, Mg)(CO_3)_2$. The content of CaO is 30.4% and MgO occupies 21.7%. The traces of Mn, Fe, Pb and Zn are the most common metals accompanying

magnesium and calcium. Dolomitic rock mainly contains dolomite mineral as well as the appreciable amount of antigorite mineral, quartz, calcite, and pyrite [48]. Compared with limestone, the effervescence in dilute hydrochloric acid cannot occur for dolomite. Dolomite is usually light-colored and grainy with the density around 2.8-2.9 g/cm^3, and the mechanical properties are quite similar to those of limestone. Dolomite decomposes from the temperature of 900 °C losing the CO_2 [50] and the amounts and types of impurities present in it may have a great influence on the extent of densification [48]. Dolomite can be used as refractories bricks in basic soil converters (electric furnaces) after its calcination and sintering at the temperature of 1600-1700 °C. Their disadvantage is that they present an irregular expansion curve which is associated with the calcium flux content. It can be also applied in the glass to prevent devitrification and increase weather resistance. Dolomite can also employ as a good flux for steel manufacturing and an excellent building material for concrete production as well as reconstituted products [50].

Carbonization is a traditional method for the production of activated MgO from dolomite. As shown in **Figure 1.14**, the process of preparing active MgO by carbonating dolomite includes the calcination of dolomite, the slaking of CaO and MgO, the carbonating of $Ca(OH)_2$ and $Mg(OH)_2$, the filtration of $CaCO_3$ and Pyrogenation of $Mg(HCO_3)_2$, the calcination of basic magnesium carbonate. This technology and its related equipment have been well developed for large-scale production. However, the separation of calcium and magnesium is difficult and the purity of product is not high.

In addition, the dissolution rate of magnesium in the processes of carbonization and slaking needs to be further improved. Some scholars have adopted the pressurized carbonization method and twice-carbonization method [51] to increase the recovery rate of magnesium. This undoubtedly results in an increase in production cost although certain effects have been achieved.

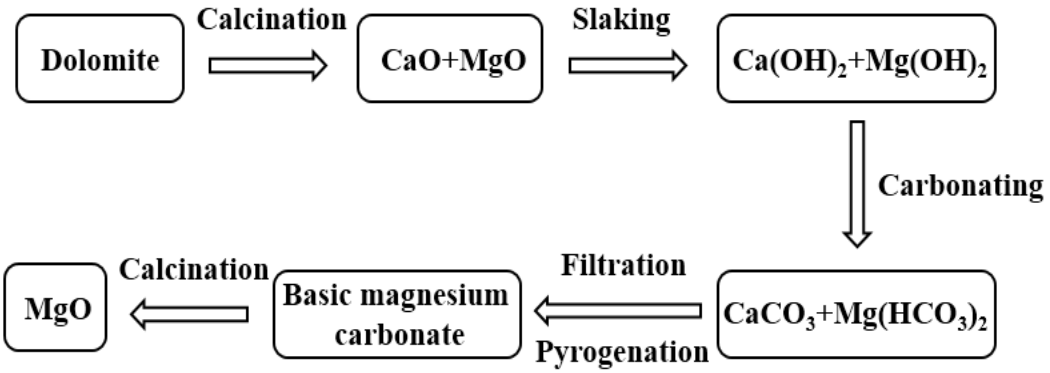

Figure 1.14 Flow chart of preparing active MgO by carbonating dolomite.

1.4.3 Seawater and brine

MgO may also be obtained by the alkaline precipitation of brucite (consisting of $Mg(OH)_2$) which can come from seawater and Mg-rich brine, as shown in **Figure 1.15**. In order to remove the carbonates, the seawater needs to be pretreated using the sulphuric acid in order to decrease its pH to about 4 (equation 1.7). Then, an alkali (sodium hydroxide or lime) is used to increase its pH above the brucite precipitation point of 10.5. To produce MgO with a low content of Ca, the sodium hydroxide is usually used (equation 1.8). And lime, which generally comes from dolomitic limestone, is employed to decrease the amounts of additive required (equation 1.9). After the

brucite slurry is filtered, the obtained filter cake starts to decompose at 350°C and the decomposition rate rapidly rises above this temperature, which requires the higher consumption of energy than that of the calcination of magnesite. The calcination of $Mg(OH)_2$ involves heating a filter cake which contains the $Mg(OH)_2$ solids content of 50-72% (equation 1.10). Several inconsequential processes would take place during this calcination, including filter cake dehydration, dry $Mg(OH)_2$ decomposition as well as MgO sintering. A critical step in this process is to calcinate $Mg(OH)_2$ at the temperatures of 700-1000 °C to produce MgO. Then the produced reactive MgO powder can be either briquetted before firing at 1900 °C for obtaining a refractory grade material, or employed as a raw material to produce magnesium chemicals. The properties of MgO are greatly influenced by the calcining time, temperature, atmosphere, impurity and $Mg(OH)_2$ morphology. Hence, the economics and performance of the calcining process as well as the product quality can be significantly affected by a number of variables [52]. In additional, it is difficult to remove the chemically bound water from $Mg(OH)_2$ without raising the temperature above 1000 °C [53].

$$Ca(HCO_3)_2 + H_2SO_4 \rightarrow CaSO_4 + 2CO_2 \uparrow + 2H_2O \quad (1.7)$$

$$CaO + H_2O + MgCl_2 \rightarrow Mg(OH)_2 \downarrow + CaCl_2 \quad (1.8)$$

$$CaO + MgO + 2H_2O + MgCl_2 \rightarrow 2Mg(OH)_2 \downarrow + CaCl_2 \quad (1.9)$$

$$Mg(OH)_2 + Heat \rightarrow MgO + H_2O \quad (1.10)$$

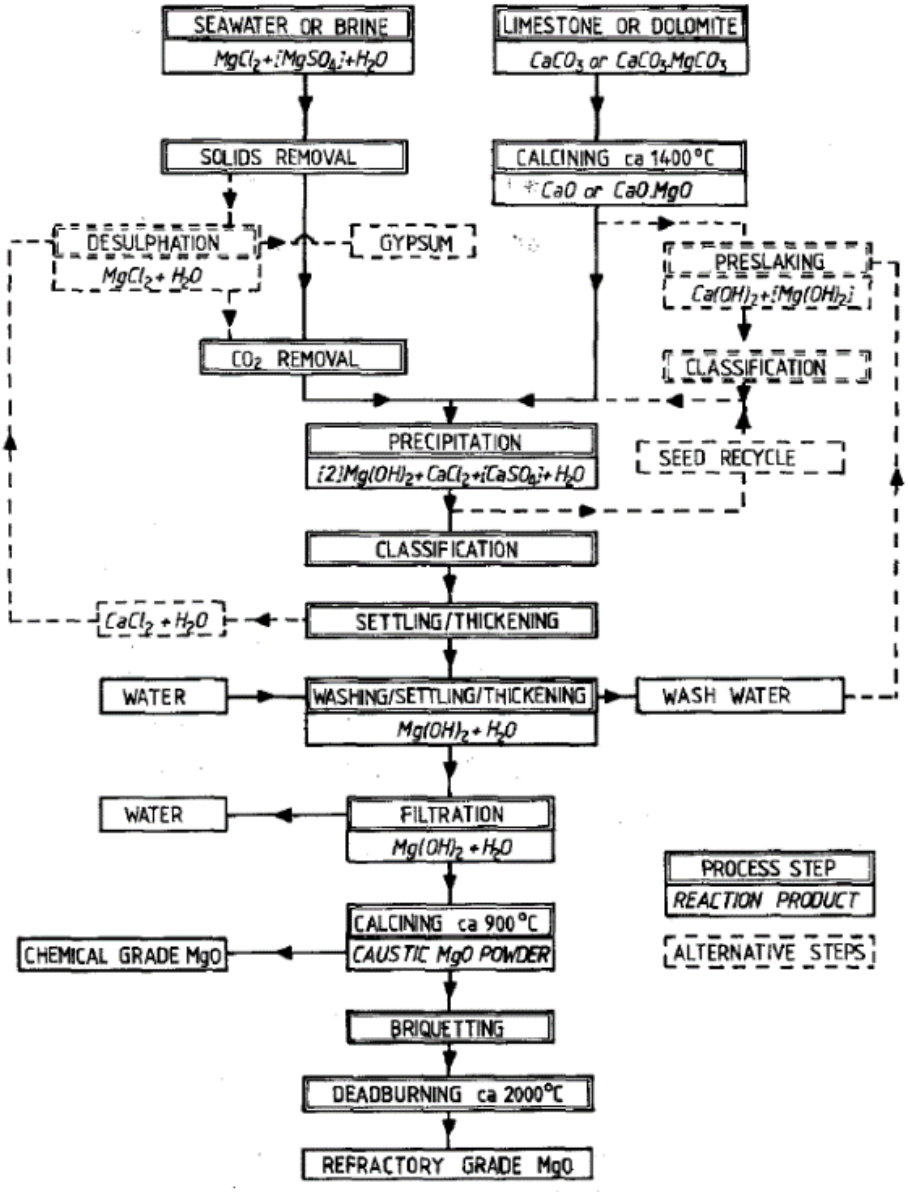

Figure 1.15 A flowscheme for the production of high quality chemical and refractory grade MgO from seawater or $MgCl_2$ brine. (Reprinted with permission from Ref. [52]).

1.4.4 MgO applications

According to the sintering temperature used, MgO is generally divided into three categories: light-burned MgO or CCM (about 800-1000 °C) with the highest reactivity and largest surface area, dead burned MgO or periclase or dead burned magnesia (DBM)

(about 1400-1800 °C) with the very low surface area and almost non-reactive, and fused magnesia (FM) or fused MgO (about 2800 °C) usually with the lowest reactivity. The MgO can also be classified into the refractory grade and chemical grade based on its use. The main properties [47] of MgO are shown in **Table 1.2**. Due to the favorable properties of MgO, including its high thermal conductivity, mechanical strength, electrical resistance, excellent resistance to corrosion as well as fire, nontoxicity and antibacterial activity, low susceptibility to hydration [49], it is widely used in a wide range of fields, which are shown in **Figure 1.16**.

Table 1.2 Physical properties of magnesia.

Item	Value
Melting point (°C)	2800
Boiling point (°C)	3600
Density (g/cm^3)	3.8 (25°C)
Thermal conductivity (cal s^{-1} cm^{-2} °C^{-1} cm)	0.03 -0.1 (sintered)
Thermal expansion coeffcient (×10^{-6}/°C)	12-16 (sintered)
Specific heat capacity (J K^{-1} mol^{-1})	37-61
Specific electrical resistance (Ω)	9×10^7 (900°C)

As the most essential raw material, MgO is used to produce refractory materials, such as bricks, crucibles and furnace linings. MgO can also be applied to the bottoms and walls of electrical furnaces and open-hearth, as well as in magnesium bricks for oxygen converters in the steel industry [54]. MgO is also widely applied in construction materials especially in the cement materials. The use of MgO can decrease the thermal

shrinkage [55], speed up construction process through continuously casting concrete as requiring less cold-joints, and reduce the concrete cost by decreasing cooling measures which are quite costly. This leads to a rapid increase in interest in the field of MgO-based cements [56]. The dielectric properties of MgO make it very suitable to produce the insulating materials in ceramic industry. MgO may also be employed as a raw material to produce magnesium salt compounds (such as $MgSO_4$) in the chemical industry and as a desulfurizer or neutraliser in the field of environmental protection [57]. Due to its nontoxicity, MgO can be used in the pharmaceuticals industry, such as an acid neutraliser for the treatment of stomach ulcers, increased intestinal fermentation as well as gastric hyperacidity. Moreover, it can also be used for the production of fertilizers in agriculture as well as magnesium metal and alloys and other fields [49].

Currently, high-purity, high-density, high-strength magnesia refractories are the key development direction. The relevant researches have been widely and deeply investigated in the world. The LTV Steel Corporation in the United States adopted slag splashing technology with magnesia-carbon bricks and the lining lives reached a record of 25,000 heats in 1998. The Mitsubishi Steel Corporation in Japan not only used magnesia-carbon bricks in the hot spot and slag line of AC electric furnaces to double its service life, but also in the bottom of DC electric furnaces with the highest lining lives of 8746 times [58,59].

Figure 1.16 Main applications of magnesia.

1.5 Technologies for light calcination of magnesite

As reviewed above, light calcination of magnesite is the first step and the most commonly used method for MgO production in the MgO-based industry to obtain the CCM. The main technologies for light calcination of magnesite are reviewed as follows.

1.5.1 Reverberatory furnace

As mentioned earlier, the most widely used technology, for decades, is the reverberatory furnace. It has high energy consumption, long reaction time, poor feedstock adaptability, unsteady product quality and serious environmental pollution [3]. As shown in **Figure 1.17**, the reverberatory furnace is a fixed bed calcination reactor [60], in which the high-temperature flue gas generated from fuel gas combustion passes through the magnesite bed from bottom to top to perform the light calcination of magnesite. In order to ensure the gas permeability of bed and reduce the pressure drop, the reverberatory furnace can only use large-size magnesite particles in 30-80 mm. As

a result, massive small-size magnesite produced in mining and processing are difficult to be used. The large-size feedstock also makes the reaction time in RF even up to 3-5 h and a low production capacity of about 30 t/d for one furnace. It also causes the so-called phenomena of over-burning on surface and insufficient-burning in inner part, leading to the unstable quality of CCM and the low activity of products [61].

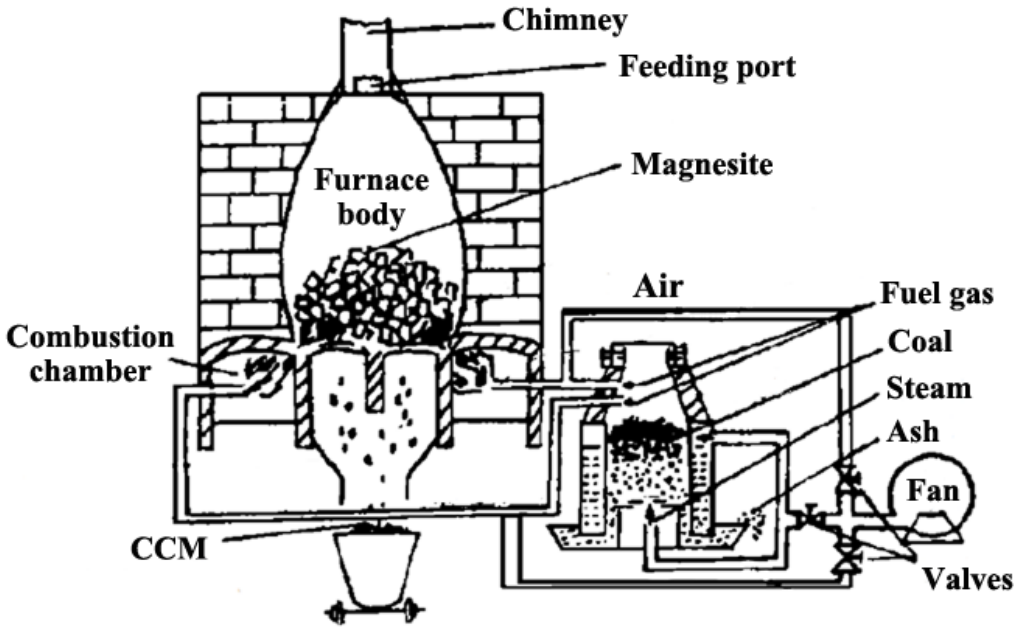

Figure 1.17 Schematic process-flow diagrams of reverberatory furnace [60].

1.5.2 Rotary kiln

The center of rotary kiln is a cylindrical reaction tube, and the outside of reaction tube is a combustion chamber which is used to provide energy for the magnesite calcination by fuel combustion through uniformly heating the reaction tube. In a rotary kiln, the feedstock is forced to move axially through kiln rotation. The raw material is fed at one end of the kiln and consecutively passes through the zones of heating, combustion/calcination, cooling. The heat required is provided through fuel

combustion in the combustion zone. The quality of final product (usually the density, determined by analysis in a laboratory) can be manually controlled by human operators in fixed time intervals. In addition, for a given fuel supply, it is the responsibility of operators to adjust the speed of rotation. The continuous operation ensures uniform filling in the kiln throughout the process [62].

Luan *et.al.* modified the rotary kiln through external heating and heat recovery to produce CCM from waste magnesite ore [63]. The calcination of magnesite in the rotary kiln is accompanied by the formation of a large amount of flue dust entrained by the combustion gases. A self-regulating feeder with a radial diffusive burner has been developed for the rotary kiln by Jan Spisak *et.al.* Flue dust reduction has been realized through increasing the thickness of the layer of the material passing through the kiln and raising the intensity of process using radial diffusive burner [64]. Compared with the reverberatory furnace, the rotary kiln occupies the obvious superiority such as large capacity, high mechanization level, simple maintenance operation, high product activity. However, it still exists the problems of sticking and high energy consumption in the industrial calcination process.

1.5.3 Fluidized bed furnace

Fluidized bed furnace has the characteristics of fast heat transfer, mass transfer and reaction, high-efficiency production, uniform product quality, also suitable for powder materials. As shown in **Figure 1.18**, the fluidized bed furnace system is mainly

composed of feeding equipment, furnace body for reaction, heat exchanger, separators for product recovery and product storage tank. Through a series of laboratory research and small-scale and semi-industrial tests, its industrial demonstration was carried out in Liaoning Magnesium Mine Company in 1984. Compared with the rotary kiln, the fluidized bed furnace has not only good product quality, but also the superiorities of low investment, simple structure, low fuel consumption, stable and easy operation [65]. Since there is no further heat recovery of the high-temperature flue gas (about 650 °C), the energy consumption is still high.

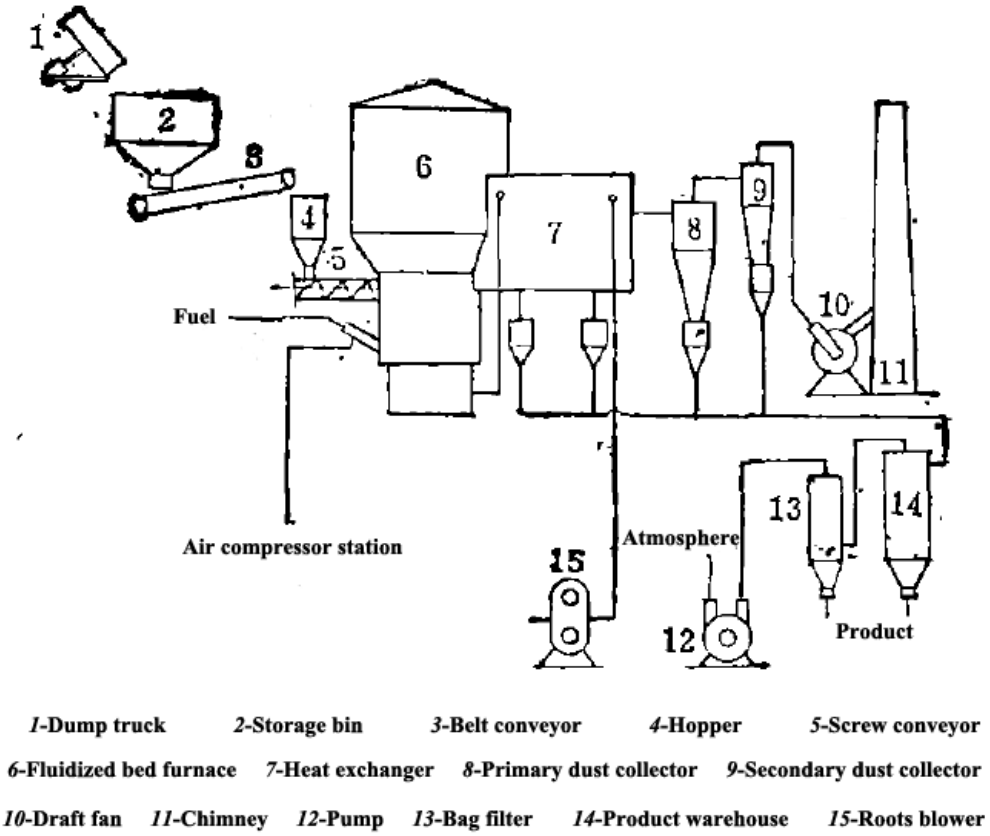

Figure 1.18 Scheme of the fluidized bed furnace system [65].

1.5.4 Suspension furnace

In the suspension furnace system, small-size magnesite particles are blown into the reactor by the gas heat carrier and remained a suspending state. The heat and mass transfer in the suspension furnace is much greater than that in the fixed bed and fluidized bed. A scheme of suspension furnace system is shown in **Figure 1.19**. A MgO plant with a production capacity of 50,000 ton per year has been in operation at Veitscher Magnesitwerke AG in Austria since 1984. A flotation concentrate of natural magnesite with a moisture content of about 7% and an average particle size of 100 μm was used as a feedstock. The production of a calcine with a residual loss on ignition of less than 0.6% required the energy consumptions of about 4,400-4,600 kJ/kg product depending on the discharge temperature of 500-700 °C. The plant has five stages in the heating system while only one cooling cyclone is equipped since the calcined product is then hot-briquet ted. The calcined briquettes are sent to a shaft kiln to produce high-quality MgO sinter [66].

In 1987, Xu *et al.* designed a dilute phase reactor (i.e., magnesite flash calciner, MFC) for the light calcination of magnesite. It is composed of a two-stage cyclone preheater, a suspension calciner and a one-stage cyclone cooler. Compared to those fixed bed calciners, MFC can produce higher active CCM within a shorter reaction time [67]. In 1988, the Liaoning Magnesite Corporation introduced a 150 t/d light-burned magnesite suspension furnace from Europe. The raw material is flotation concentrate with particle size below 200 μm, and heavy oil is employed as fuel. The designed

temperature of light calcination is 800-1000 °C, and the corresponding energy consumption is 4180-5016 kJ/kg-CCM. Although the suspension furnace is very suitable for powder magnesite calcination, it also has shortcomings such as difficult adjustment of production parameters, poor raw material adaptability, material blocking and high energy consumption. Currently, there are more than 20 suspension furnaces built and planned in Liaoning province, but only some of them can be produced continuously and stably [68].

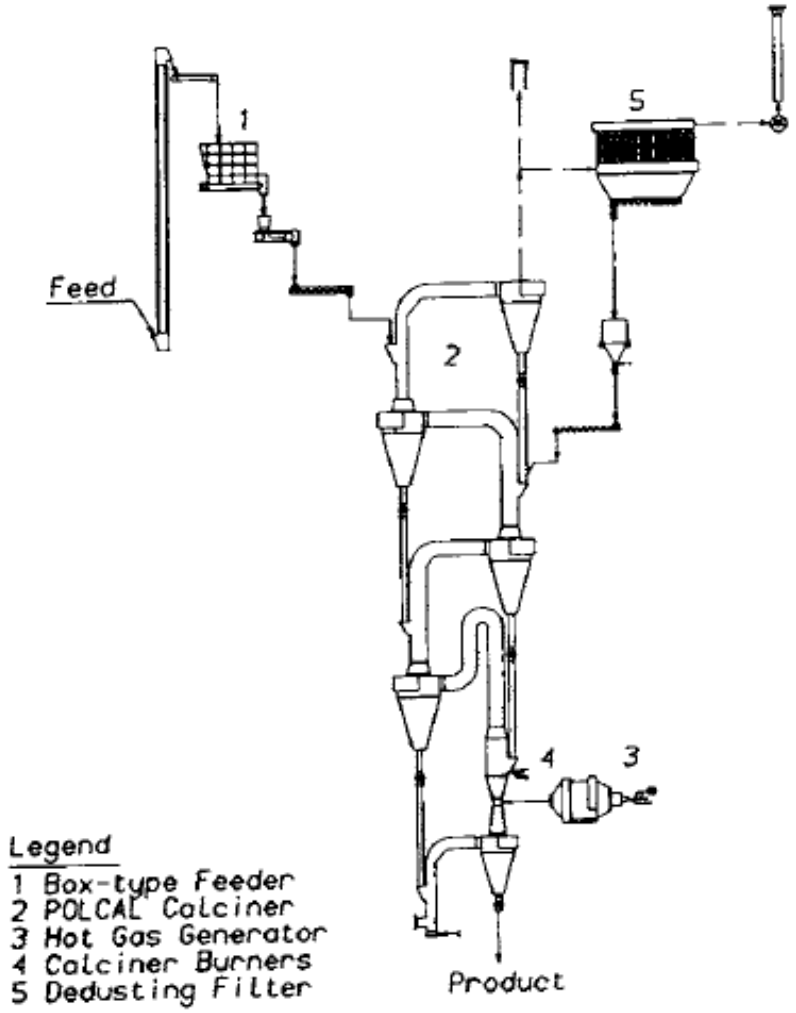

Figure 1.19 Scheme of the suspension furnace system. (Reprinted with permission from Ref. [66]).

1.5.5 Multiple hearth furnace

The multiple hearth furnace is a thermal equipment that employs multi-hearth for continuous production, as shown in **Figure 1.20**. In a multiple hearth furnace, the slow-turning rake guarantees the radial movement in a zigzag pattern to continuously lower the hearths through ports on the floor of each hearth. Simultaneously, the hot gas generated from fuel combustion is fitted to each hearth and passes through the materials. In generally, an electroprecipitator is adopted to remove the dust entrained with exhaust or rising gas before venting the gas. Then, it is circulated to the furnace either to the perimeter of one of the lower hearths whose operation temperature is higher than exhaust gas or with the normal feeding. The materials radially move towards the rake shaft to avoid short circuiting when materials flow to the next lower hearth. Through a screw conveyor, the active MgO is usually separated from the circumference of the lowest hearth [52].

In the 1970s, multiple hearth furnaces were used to produce CCM in Japan, North Korea, Greece, and Brazil. In the 1980s, China Metallurgical Coking Resistant Engineering Technology Co., Ltd. (formerly Anshan Coking Resistant Fire Material Design and Research Institute) carried out magnesite calcination test in the multiple hearth furnace. After 2000, Liaoning Aoding Magnesium Industry Co., Ltd. and Haicheng Haiming Mining Co., Ltd. successively introduced European equipment for magnesia production. The size and number of hearths are determined according to the requirements of capacity and thermal efficiency. Multiple hearth furnace can handle

raw materials in 0-40 mm and its annual output is generally about 100,000 tons CCM. The temperature and reaction time in each hearth can be controlled to ensure uniform calcination, good product quality and high activity. Its energy consumption is usually 5400-6200 kJ/kg-CCM. Automatic production can be realized, and the exhaust gas can be collected and treated in a centralized way [68]. However, the heavy equipment and high investment of multiple hearth furnace restrict its industrial applications.

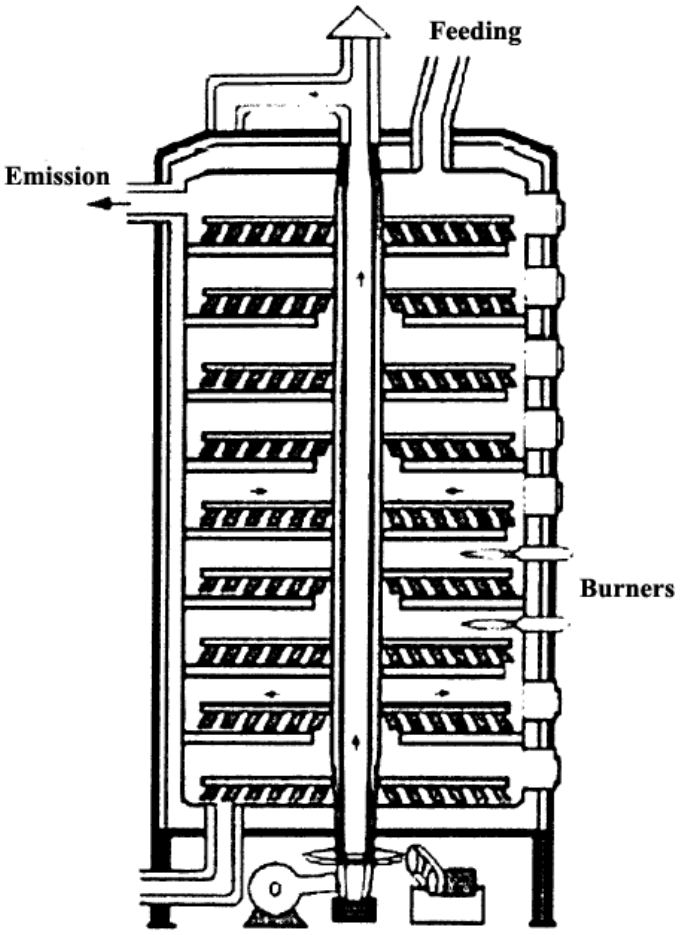

Figure 1.20 A scheme of the multiple hearth furnace [69].

1.5.6 Transport bed flash calciner

Jiang *et al.* [70] explored the feasibility of fluidization calcination for magnesite

using a micro fluidized bed, and found that the light calcination process can be finished in a few seconds. Based on this innovative concept, Shenyang University of Chemical Technology proposed a transport bed flash calcination process for CCM production, as shown in **Figure 1.21**. A transport bed calciner is employed to substitute the traditional reverberatory furnace, for which small magnesite powder can also be effectively used as a raw material. In this transport bed reactor, the high-temperature flue gas generated from fuel gas combustion is rapidly mixed with magnesite powder so that the production efficiency and product stability are greatly improved. Sun *et al.* [71] investigated the calcination of magnesite in a laboratory-scale transport bed, and found that the conversion of magnesite powder (<150 μm) reached 98% in only 1-2 seconds with significantly higher activity of product compared with that from fixed bed calciner, corroborating the feasibility of transport bed flash calcination for high-efficiency calcination magnesite.

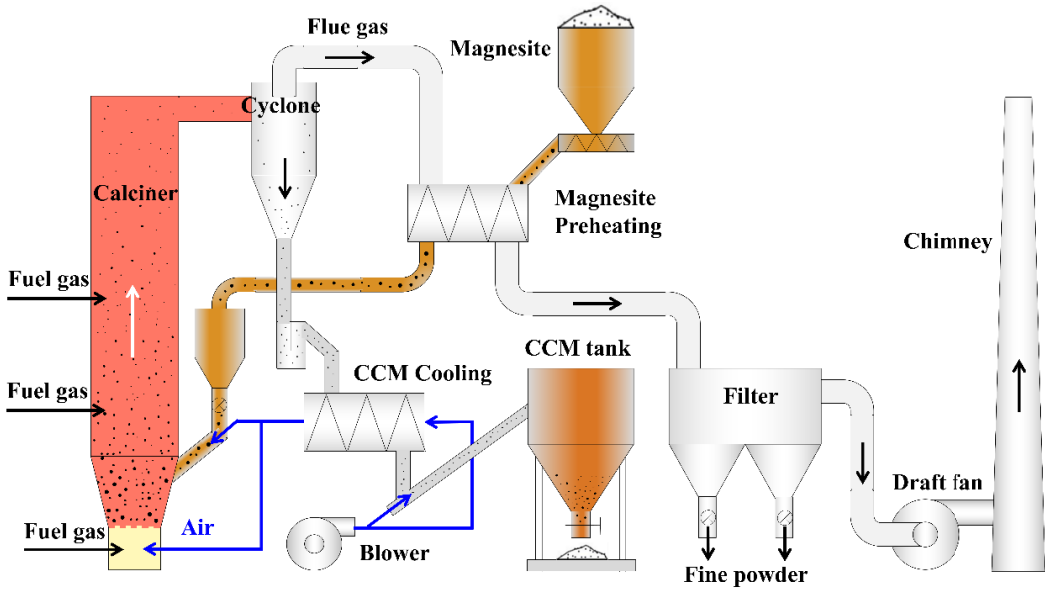

Figure 1.21 A schematic diagram of transport bed flash calcination process.

1.6 Objectives and scope of this dissertation

As reviewed above, CCM is traditionally produced by the combination of water gas generator and reverberatory furnace. It has high energy consumption, bad feedstock adaptability, long reaction time, unsteady product quality and serious environmental pollution. The need of upgrading for CCM production technology is urgent. Two-stage fluidized bed gasification is more attractive and economical for fuel gas production in mid- and small-scale plants due to excellent heat/mass transfer, adaptability to low rank fuels with a very low tar content and no phenolic waste water. Meanwhile, transport bed flash calcination can adopt small magnesite powder as the feedstock for CCM production with high efficiency and product stability. Hence, the objectives of this study focus on obtaining the high energy efficiency for light calcination of magnesite in the CCM production through a two-stage fluidized bed gasification system with a transport bed flash calcination process.

The introduction is considered as **Chapter 1**, in which the gasification technology, two-stage gasification, MgO-based industry and light calcination technology of magnesite are reviewed. It presents several typical two-stage gasification technologies and main technologies for light calcination of magnesite.

Chapter 2 presents a two-stage fluidized bed gasification system of coal with high water content simulated by Aspen Plus to identify the effect of pre-drying for coal on gasification performance, particularly energy efficiency. The analysis of energy allocations is conducted to further illustrate the effect of the pre-drying of coal on

energy efficiency.

Chapter 3 focuses on a transport bed flash calcination process applied to magnesite, in which the process performance and energy efficiency is systematically investigated by varying with the number of heat-exchange stages and residence time of particles in preheaters through a process simulation. Pre-decomposition of magnesite during preheating is considered on basis of the kinetics measured using a micro fluidized bed reaction analyzer that allows the minimized effect of external diffusion on reaction. The acquired results for the transport bed flash calcination process are also compared with those of reverberatory furnaces and magnesite flash calciner processes.

In **chapter 3**, the kinetic parameters obtained by measuring magnesite calcination in air using a micro fluidized bed reaction analyzer (MFBRA) are adopted. While, due to fuel gas combustion, the magnesite calcination actually occurs under the product gas containing inhibited atmosphere. However, the difficulties arose as how to distinguish between product gas CO_2 and fluidized gas CO_2 because the reaction kinetics data are determined based on the measurement of time-series of product gas species in MFBRA. Liu *et al.* [72] introduced the isotope-tagging method while the $Mg^{13}CO_3$ was not available and the similar carbonate $Ca^{13}CO_3$ was available. Thus, the kinetics of $Ca^{13}CO_3$ decomposition in the presence of CO_2 by MFBRA were obtained and results showed that the initial temperatures of $CaCO_3$ decomposition under thermal equilibrium simulation are very close to that of MFBRA, indicating that MFBRA is indeed approaching to the real reaction kinetics in the product gas strongly inhibited

atmospheres [72]. Following this, in **Chapter 4**, the detailed $CaCO_3$ decompositions under different flue gas atmospheres and different pressures through simulation are performed to provide more fundamental and complete information for the reaction in the product gas strongly inhibited atmospheres and certain reference values for industrial applications.

Finally, the general conclusions of this research and outlook for future work are summarized and discussed in **Chapter 5**.

References

1. L. Wang, P. Tai, C. Jia, X. Li, P. Li, X. Xiong, Magnesium contamination in soil at a magnesite mining region of Liaoning province, China, Bull Environ. Contam. Toxicol. 2015, 95, 90-96.
2. Z. Zhao, X. Cui, D. Wang, Y. Chen, G. Bai, J. Li, X. Liu, Review of the Metallogenie Regularity of Magnesite Deposits in China, Acta Geol. Sin-Engl. 2015, 89, 1747-1761.
3. H. Ba, L. Bai, W. Zhao, Y. Ma, X. Yin, Review on preparation and processing of caustic calcined magnesite (in Chinese), Conserv. Util. Miner. Resour. 2017, 1, 84-89.
4. H.D. Matthews, N.P. Gillet, P.A. Stott, K. Zickfeld, The proportionality of global warming to cumulative carbon emissions, Nature 2009, 459,829-832.
5. N. Mahinpey, A. Gomez, Review of gasification fundamentals and new findings: Reactors, feedstock, and kinetic studies, Chem. Eng. Sci. 2016, 148, 14-31.

6. L. Su, S. Feng, P. Li, Y. Zhang, Z. Liu, Z. Li, Study on Simulation of Pulverized Coal Gasification Process in the GSP Gasifier, Can. J. Chem. Eng. 2017, 95, 688-697.

7. J. Zhang, Y. Wang, L. Dong, S. Gao, G. Xu, Decoupling Gasification: Approach Principle and Technology Justification, Energy Fuels 2010, 24, 6223–6232.

8. J. Ruiz, M. Juarez, M. Morales, P. Munoz, M. Mendivil, Biomass gasification for electricity generation: review of current technology barriers, Renew. Sust. Energy Rev. 2013, 18, 174-183.

9. R. Warnecke, Gasification of biomass: comparison of fixed bed and fluidized bed gasifier, Biomass Bioenergy 2000, 18, 489-497.

10. S.H. Aljbour, K. Kawamoto, Bench-scale gasification of cedar wood - Part I: Effect of operational conditions on product gas characteristics, Chemosphere, 2013, 90, 1495-1500.

11. W. Chen, K. Annamalai, R.J. Ansley, M. Mirik, Updraft fixed bed gasification of mesquite and juniper wood samples, Energy, 2012, 41, 454-461.

12. C.A. Jordan, G. Akay, Occurrence, composition and dew point of tars produced during gasification of fuel cane bagasse in a downdraft gasifier, Biomass Bioenergy 2012, 42, 51-58.

13. J.H. Kihedu, R. Yoshiie, Y. Nunome, Y. Ueki, I. Naruse, Counter-flow air gasification of woody biomass pellets in the auto-thermal packed bed reactor, Fuel 2014, 117, 1242-1247.

14. H. Beohar, B. Gupta, V. Sethi, M. Pandey, Parametric Study of Fixed Bed Biomass Gasifier: A review, Int. J. of Thermal Technol. Vol.2, No.1 (March 2012), 2 (2012) 134-140.

15. V. Krishnamoorthy, S.V. Pisupati, A critical review of mineral matter related issues during gasification of coal in fixed, fluidized, and entrained flow gasifiers, Energies, 2015, 8, 10430-10463.

16. S. Kern, C. Pfeifer, H. Hofbauer, Gasification of lignite in a dual fluidized bed gasifier - influence of bed material particle size and the amount of steam, Fuel Process. Technol. 2013, 111, 1-13.

17. D.L. Li, M. Tamura, Y. Nakagawa, K. Tomishige, Metal catalysts for steam reforming of tar derived from the gasification of lignocellulosic biomass, Bioresour. Technol. 2015, 178, 53-64.

18. Z. Han, S. Geng, X. Zeng, S. Xu, P. An, J. Cheng, J. Yang, F. Li, S. Zhang, M. Liu, G. Guan, G. Xu, Reaction decoupling in thermochemical fuel conversion and technical progress based on decoupling using fluidized bed, Carbon Resour. Convers. 2018, 1, 109-125.

19. F. Miccio, A. Picarelli, G. Ruoppolo, Increasing tar and hydrocarbons conversion by catalysis in bubbling fluidized bed gasifiers, Fuel Process. Technol. 2016, 1, 31-37.

20. A. Molino, V. Larocca, S. Chianese, D. Musmarra, Biofuels Production by Biomass Gasification:A Review, Energies 2018, 11, 811.

21. P. Basu, Combustion and Gasification in Fluidized Beds, CRC Press: Boca Raton, FL, USA, 2006.

22. T. Lu, K. Li, R. Zhang, J. Bi, Addition of ash to prevent agglomeration during catalytic coal gasification in a pressurized fluidized bed, Fuel Process. Technol. 2015, 134, 414-423.

23. S. Tao, J. Wu, L. Shen, J. Xiao, Experimental investigation on hydrogen production from biomass gasification in interconnected fluidized beds, Biomass Bioenergy, 2012, 36, 258-267.

24. J. Yu, C. B. Yao, X. Zeng, S. Geng, L. Dong, Y. Wang, S. Q. Gao, G. W. Xu, Biomass pyrolysis in a micro fluidized bed reactor: characterization and kinetics, Chem. Eng. J. 2011, 168, 839-847.

25. J. A. Moulijn, F. Kapteijn, Towards a unified theory of reactions of carbon with oxygen-containing molecules, Carbon 1995, 33, 1155-1165.

26. G. W. Xu, T. Murakami, T. Suda, Y. Matsuzawa, H. Tani, The superior technical choice for dual fluidized bed gasification, Ind. Eng. Chem. Res. 2006, 45, 2281-2286.

27. J. Zhang, R. Wu, G. Zhang, C. Yao, Y. Zhang, Y. Wang, G. Xu, Recent studies on chemical engineering fundamentals for fuel pyrolysis and gasification in dual fluidized bed. Ind. Eng. Chem. Res, 2013, 52, 6283-6302.

28. H.H. Lowry, Chemistry of coal utilization, New York:John Wiley and Sons, 1963, 949-965.

29. F. Wang, Coal gasification technologies in China: Review and prospect (in Chinese), Clean Coal Technol. 10.13226/j.issn.1006-6772.20101820.

30. M. M. Papic, Technology and Economics of Coal Gasification, Can. J. Chem. Eng. 1976, 54, 413-420.

31. A.G. Collot, Matching gasification technologies to coal properties, Int. J. Coal Geol. 2006, 65,191-212.

32. X. Zeng, F. Wang, H. Li, Y. Wang, L. Dong, J. Yu, G. Xu, Pilot verification of a low-tar two-stage coal gasification process with a fluidized bed pyrolyzer and fixed bed gasifier, Applied Energy 2014, 115, 9-16.

33. Y. He, Handbook of modern coal chemical engineering technology, Beijing: Chemical Industry Press, 2003.

34. Z. Dai, X. Gong, X. Guo, H. Liu, F. Wang, Z. Yu, Pilot-trial and modeling of a new type of pressurized entrained-flow pulverized coal gasification technology, Fuel 2008, 87, 2304-2313.

35. J. Xu, Y. Yang, Y. W. Li, Recent development in converting coal to clean fuels in China, Fuel, 2015, 152, 122-130.

36. T. Bui, R. Loof, S.C. Bhattacharya, Multi-stage reactor for thermal gasification of wood, Energy, 1994, 19, 397-404.

37. P. Brandt, E. Larsen, U. Henriksen, High tar reduction in a two-stage gasifier, Energy Fuels, 2000, 14, 816-819.

38. U. Henriksen, J. Ahrenfeldt, T. K. Jensen, B. Gøbel, J. D. Bentzen, C. Hindsgaul, L. H. Sørensen, The design, construction and operation of a 75kW two-stage gasifier, Energy, 2006, 31, 1542-1553.

39. L. Burhenne, L. Rochlitz, C. Lintner, T. Aicher, Technical demonstration of the novel Fraunhofer ISE biomass gasification process for the production of a tar-free synthesis gas, Fuel Process. Technol. 2013, 106, 751-760.

40. X. Zeng, Y. Wang, J. Yu, S. Wu, M. Zhong, S. Xu, G. Xu, Coal pyrolysis in a fluidized bed for adapting to a two-stage gasification process, Energy Fuels, 2011, 25, 1092-1098.

41. X. Zeng, Y. Dong, F. Wang, P. Xu, R. Shao, P. Dong, G. Xu, L. Dong, Fluidized Bed Two-Stage Gasification Process for Clean Fuel Gas Production from Herb Residue: Fundamentals and Demonstration, Energy Fuels, 2016, 30, 7277-7283.

42. X. Zeng, R. Shao, F. Wang, P.W. Dong, J. Yu, G.W. Xu, Industrial demonstration plant for the gasification of herb residue by fluidized bed two-stage process, Bioresour. Technol. 2016, 206, 93-98.

43. X. Zeng, F. Wang, Z. Han, Y. Sun, Y. Cui, G. Xu, Characterization and pilot scale test of a fluidized bed two-stage gasification process for the production of clean industrial fuel gas from low-rank coal, Carbon Resour. Convers. 2018, 1, 73-80.

44. A. Al-Tabbaa, Chapter 19: Reactive magnesia cement, In Eco-Ecient Concrete; F. Pacheco-Torgal, S. Jalali, J. Labrincha, V. John, Eds.;Woodhead Publishing Limited: Cambridge, UK, 2013; pp. 523–543.

45. J.D. Smith, W.G. Fahrenholtz, in Refractory Oxides in Ceramic and GlassMaterials: Structure, Properties and Processing, Ed. by J.F. Shackelford and R.H. Doremus, 2008, pp. 87-110.

46. S. C.Bhattacharya, H. L. Pham, A study on a multi-stage hybrid gasifier-engine system. Biomass Bioenergy, 2001, 21, 445-460.

47. W. Z. Yin, Y. Tang, Interactive effect of minerals on complex ore flotation: A brief review, Int. J. Min. Met. Mater. 2020, 27, 571-583.

48. C. Sadik, O. Moudden, A. El Bouari, I. E. El Amrani, Review on the elaboration and characterization of ceramics refractories based on magnesite and dolomite. J. Asian Ceram. Soc. 2016, 4, 219-233.

49. A. A. Pilarska, Ł. Klapiszewski, T. Jesionowski, Recent development in the synthesis, modification and application of Mg $(OH)_2$ and MgO: A review, Powder Technol. 2017, 319, 373-407.

50. R.A. Landy, in Refractories Handbook, Ed. by C.A. Schacht, 2004, pp. 109–149.

51. Q. Hu, X. Hu, X. Hu, L. Song, New technology for the production of activated magnesium oxide from dolomite by carbonization, Inorg. Chem. Ind. 2004, 36, 36-38.

52. J. Green, Calcination of precipitated Mg $(OH)_2$ to active MgO in the production of refractory and chemical grade MgO, J. Mater. Sci. 1983, 18, 637-651.

53. S.J. Gregg, R.K. Packer, The production of active solids by thermal decomposition. Part VI. The calcinationof magnesium hydroxide, J. Chem. Soc. 1955, 51-55.

54. B. Cubukcuoglu, S.K. Ouki, Solidification/stabilisation of electric arc furnace waste using low grade MgO, Chemosphere 2011, 86, 789-796.

55. M. Yuan, M. Tang, Study on the mechanism of autogenous expansion of concrete used in Baishan Dam (In Chinese), J. Nanjing Inst. Chem. Technol. 1984, 2, 15-18.

56. N. José, H. Ahmed, B. Miguel, E. Luís, D. B. Jorge, Magnesia (MgO) Production and Characterization, and Its Influence on the Performance of Cementitious Materials: A Review, Materials, 2020, 13,4752.

57. T. Ohira, O. Yamamoto, Correlation between antibacterial activity and crystallite size on ceramics, Chem. Eng. Sci. 2012, 68, 355-361.

58. H. Hirota, N. Okabayashi, K. Toyoda, Characterization and sintering of reactive MgO, Mater. Res. Bull. 1992, 27, 319-326.

59. Q. Hu, X. Hu, L. Song, development status and suggestions of special magnesium oxide in China, Chem. Ind. Eng. Prog. 2005, 24, 28-31.

60. H. Li, M. Li, The choice and application of pollution control technique on flue dust from light sintering magnesium kiln (in Chinese), Environ. Prot. Sci. 1997, 2, 8-10.

61. Z. Li, Thoughts on magnesia refractory raw materials of Liaoning Province (in Chinese), Refractories 45 (2011) 382-385, 389.

62. M. Mariška, I. Taufer, I. Koštial, P. Doležel, P. Palička, Simulation of predictive control algorithm for rotary furnace producing magnesite sinter. Int. J. Eng. Res. Afr. 2015, 18, 36-43.

63. J. Luan, Y. Wang, M. Yao, C. Wang, Analysis on the Green Development of Liaoning Light Burnt Magnesium Production Enterprises-Take Liaoning Clean Magnesite Technology Co., Ltd. as an example, Proceedings of the 2017 National Refractory Materials Academic Conference, 2017, 155-157.

64. J. Spisak, D. Nascak, E. Oravcova, Increasing dust-chamber efficiency of rotary furnace for magnesite treatment, Eur. Sci. J. 2015, 11, 77-84.

65. Z. Xu, Q. L, Study on Light calcination of Magnesite in Fluidized Bed Furnace, Metal Mine 1985, 10, 31-35.

66. P W. Böhm, POLCAL-A gas suspension calciner for pyroprocessing of minerals, Production and Processing of Fine Particles, Pergamon, 1988, 751-760.

67. D. Xu, Q. Jia, Study on the residence time distribution of powder in magnesite flash calciner (in Chinese), J. Xi'an U. Archit. Technol. 1987, 4, 95-100.

68. J. Liu, Application status of magnesite light calcination equipment, Proceedings of the 2019 National Refractory Materials Academic Conference, 2019, 38-40.

69. T. Wei, Q. Chen, Energy saving and emission reduction in Liaoning light burned magnesia production process, 2010 National Magnesium Salt Industry Annual Conference/Energy Saving, Emission Reduction and Development Seminar, 2010, 25-32.

70. W. Jiang, W. Hao, X. Liu, Z. Han, J. Yue, G. Xu, Characteristic and kinetics of light calcination of magnesite in micro fluidized bed reaction analyzer (in Chinese), CIESC J. 2019, 70, 2928-2937.

71. C. Sun, B. Yan, C. Cai, Z. Han, G. Xu, Characteristics of reaction and product microstructure during light calcination of magnesite in transport bed (in Chinese), CIESC J. 2020, 71, 5735-5744.

72. X. Liu, W. Hao, K. Wang, Y. Wang, P. An, H. Zhang, J. Yue, D. Bai, G. Xu, Acquiring real kinetics of reactions in inhibitory atmosphere containing product gases using micro fluidized bed, AIChE J. 2021, e17325.

CHAPTER 2

Process analysis of a two-stage fluidized bed gasification system with and without pre-drying of high-water content coal

2.1 Introduction

As the most abundantly reserved fossil fuel, coal remains an important energy and carbonaceous material source today and will be for the foreseeable future. Compared to other fossil fuels such as crude oil and natural gas, coal is more carbon intensive,[1] and therefore determining how to utilize the vast reserves more efficiently and less carbon emission has been a challenge. Gasification technology has been developed worldwide for more efficient and clean use of coal as a feedstock and energy resource.[2] Compared to direct combustion, gasification provides opportunities for coal to be used more efficiently and cleanly with significant carbon emission reduction, since the produced gas (fuel gas or syngas) from gasification can be used not only for the generation of heat and power but also manufacturing of value-added chemical products.[3,4]

Several types of gasifiers, including fixed bed, fluidized bed, and entrained bed, have been developed for the gasification of coal.[5-7] For fuel gas production, fluidized bed gasifiers are more attractive and economical for applications in mid- and small-

scale plants due to excellent heat/mass transfer, adaptability to low rank and wider particle size distribution of solid fuels.[8,9]

Two-stage fluidized bed gasification (TSFBG) is an advanced gasification technology that consists of two subprocesses, namely, fuel pyrolysis and pyrolysis products gasification. By employing such a two-stage gasification technology, tars on the surfaces of chars produced in the pyrolysis process can be catalytically and/or thermally cracked in the high temperature gasification process; therefore, a fuel gas with a very low tar content can be produced, which is vital for industrial processes. In addition, TSFBG has attracted an increased amount of attention because it can use powdered coals (eg, below 10 mm) and no phenolic waste water is produced. To promote the TSFBG technology, a demonstration plant with a processing capacity of 600 kg/h of herb residues was designed and built by the Institute of Process Engineering, Chinese Academy of Sciences, China. The operation of this demonstration plant yielded fuel gas with a tar content below 100 mg/Nm^3 (dry basis), which is significantly lower than that of 5 g/Nm^3-12 g/Nm^3 (dry basis) in the product gas that is typically produced from circulating fluidized bed gasifiers.[10]

In addition, TSFBG can effectively reduce the need for steam as a gasification agent due to its ability to handle fuels with high water content, in which water contained in the fuels can substitute some of the steam. As a result, a lower energy consumption or a higher energy utilization efficiency is realized, which is technologically and economically critical for industrial applications. Process simulation plays an important

role in the development of new technologies in the processes of design and optimization.[11,12] Numerous simulation works have been carried out to investigate gasification processes in entrained beds,[12-14] fixed beds,[15-17] and fluidized beds.[18-21] These works focused mainly on understanding effects of process parameters such as temperature, equivalence ratio (ER), and steam to coal ratio (S/C) on the gasification performance commonly characterized by the composition and lower heating value (LHV) of the produced gas, carbon conversion, cold gas efficiency (CGE), and thermal efficiency. However, to the best of our knowledge, a limited amount of research has been conducted to gain an understanding of the effect of pre-drying fuels with high water contents on the gasification process. This study presents a comprehensive TSFBG process simulation, focusing on quantifying the effect of pre-drying fuels on the gasification performance, especially on the overall energy efficiency. The results can provide vital information that can serve as a guide for the industrial design and application of the TSFBG technology.

2.2 Methods and models

2.2.1 Process description

A schematic process flow diagram of the TSFBG system is shown in **Figure 2.1**. The system can be operated with/without fuel pre-drying. In cases of fuel pre-drying, coal is fed to a dryer and then is brought into a fluidized bed pyrolyzer (ie, the first stage). During this stage, coal with a certain water content is autothermally pyrolyzed

or partially oxidized. Then, all the pyrolysis products overflow to the next gasification reactor (the second stage of the TSFBG), in which the pyrolysis gas and char produced in the first stage are gasified and reformed. In the second stage, tars are catalytically and thermally cracked at a high temperature so low-tar fuel gas is produced. After exiting the gasifier, the fuel gas is separated from ash by a cyclone separator and then is directed into a heat exchanger to generate a preheated air or oxygen-steam mixture as the gasification agent. Next, the fuel gas is supplied to a boiler for steam generation. A part of the produced steam is directed to the heat exchanger to be utilized as the gasification agent, and a portion of the produced steam is supplied to the dryer for drying of the fuel. The rest of the produced steam is outputted as a by-product. After passing through the boiler, the fuel gas product is obtained by removing the fly ash further using a bag filter.[22] In cases without fuel pre-drying, the coal with an original water content is directly fed into the pyrolyzer. The steam, that is used for fuel drying in the pre-drying operations is outputted as a by-product.

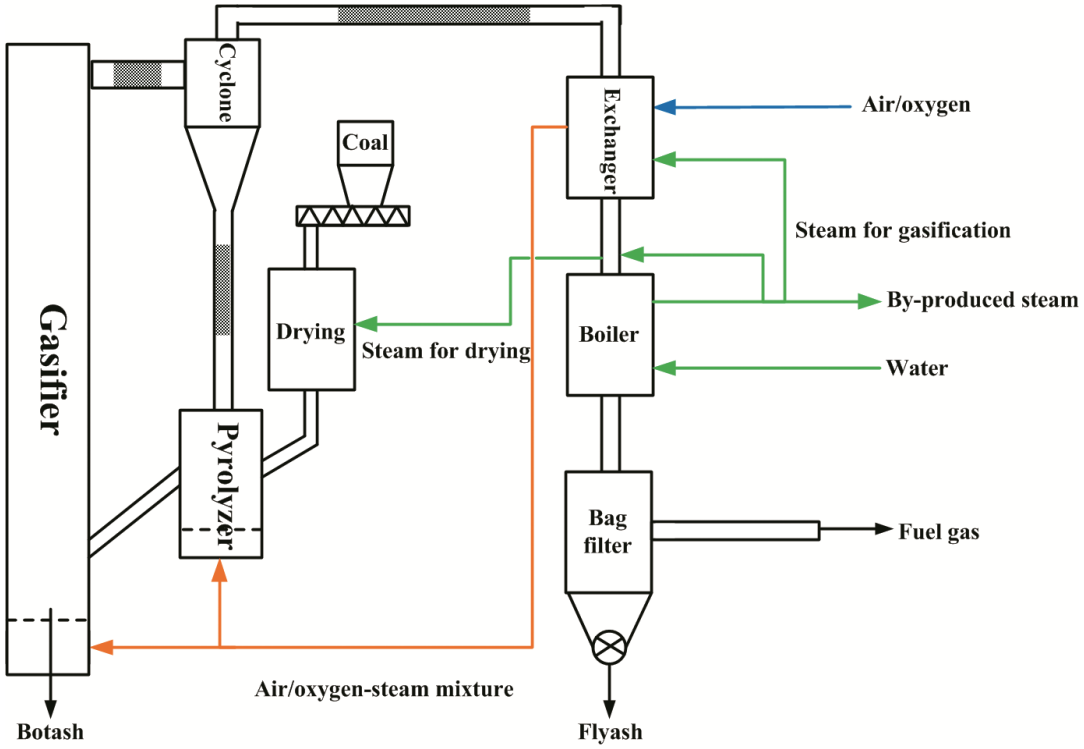

Figure 2.1 Schematic process flow diagram of two-stage fluidized bed gasification with pre-drying of coal.

2.2.2 Simulation approach

The TSFBG system is simulated by the commercial process simulator Aspen Plus. Coal, with the properties shown in **Table 2.1**, is employed as the representative fuel in the simulation. The representative unit and corresponding Aspen Plus models used in the simulation are outlined in **Table 2.2**.

For all simulations of the TSFBG system with and without fuel pre-drying, the temperature of gasification and the carbon conversion are set at 900°C and 90%, respectively. The temperature of gasification is attained by adjusting the flowrate of air/oxygen. The system is operated at around atmospheric pressure, except for the steam

that is set at a pressure of 1 MPa. In this work, the S/C is defined in the following equation:

$$S/C = \frac{m_w + m_s}{m_c} \quad (2.1)$$

where m_w and m_s are the mass of water in the coal and steam into the gasifier, respectively; and m_c is the mass of coal into gasifier based on dry basis.

In this study, the TSFBG performances with mixtures of air/steam and oxygen/steam as gasification agents respectively are investigated. The corresponding S/C ratios are set from 0.35-0.55. If the water contained in the coal is not enough to attain the preset S/C ratio, a supplementary steam is added into the gasifier. On the other hand, when the water contained in coal meets or exceeds the requirement, no additional steam is required, and the simulation is conducted under the corresponding S/C ratio.

Figure 2.2 depicts the Aspen Plus flow chart of the TSFBG system with the pre-drying of coal. The coal feedstocks with the same dry mass are dried from the initial water contents of 15 wt.%-65 wt.% to 10 wt.% by steam in the dryer at 80°C with a heat efficiency of 90%. Then, the coals dried at ambient temperature around 25°C after storage in a silo are fed to the pyrolyzer where the coal is decomposed to various elements using the RYield model. The pyrolysis products (except the unconverted carbon of 10%) are transported into the gasifier and gasified at 900°C. From the gasifier, 30 wt.% of ash is taken as the bottom ash, which is discharged by the model SEP2. The remaining gasification products, with the unconverted carbon from the pyrolyzer, are directed to the heat exchangers to preheat the gasification agents of the air/oxygen-

steam mixture to 500°C and the air or oxygen to 300°C. The gasification products are cooled to 120°C after the boiler for steam production. The fuel gas is obtained as the final product after removing the fly ash, including the unconverted carbon, through a bag filter. The volumetric flowrate of air/oxygen is adjusted to attain a gasification temperature of 900°C. The produced steam is split into three streams, one as gasification agent, another as drying medium, and the rest as by-product output.

In the cases of no fuel pre-drying, the Aspen Plus flow chart is similar to **Figure 2.2** but with no dryer shown in the dotted line box. The coal feedstocks with original water contents of 10 wt.%-65 wt.% are directly fed into the pyrolyzer. The steam, which is used for coal drying in the pre-drying operations, is also outputted as a by-product. The main parameters of the TSFBG system simulations with and without the pre-drying of coal are tabulated in **Table 2.3**.

Table 2.1 Proximate analysis and ultimate analysis of coal used in the simulation.

Proximate analysis (wt.%, dry basis)	
VM	39.84
ASH	22.43
FC	37.73
Ultimate analysis (wt.%, dry ash free basis)	
C	78.68
H	5.53
N	0.63
S	2.71
O (by difference)	12.45

Table 2.2 Representative unit and corresponding models used in the simulation.

Unit	Name in flow chart	Aspen Plus model	Specification
Drying	DRYREACT	RYield	Drying coal
Separation	SEP	Sep	Separating dried coal and steam
Pyrolysis	DECOMPOS	RYield	Decomposing coal to elements
Separation	SEP1	Sep	Separating lost carbon
Gasification	GASIFIER	RGibbs	Gibbs gasifier
Cyclone	SEP2	SSplit	Separating bottom ash and fuel gas
Heater exchanger	HEAT-1	HeatX	Between fuel gas and air/oxygen-steam mixture
Heater exchanger	HEAT-2	HeatX	Between fuel gas and air/oxygen
Heater exchanger	HEAT-3	HeatX	Between fuel gas and water for steam
Bag filter	SEP3	SSplit	Separating fly ash and produced gas

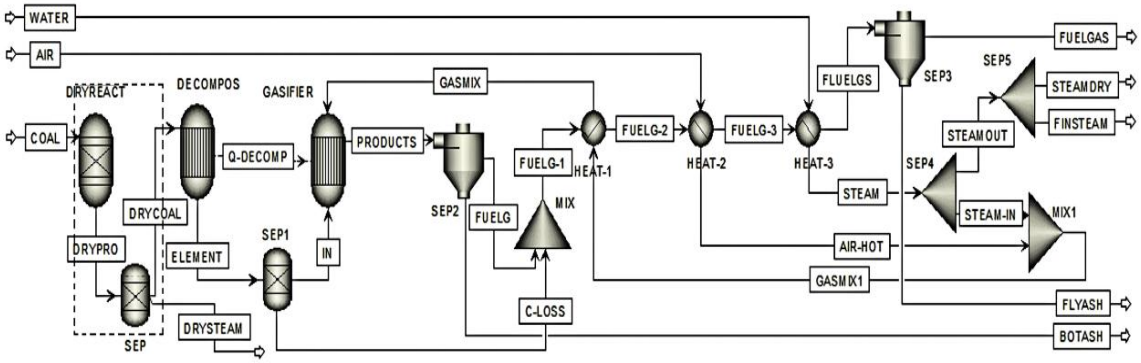

Figure 2.2 Aspen Plus flow chart of two-stage fluidized bed gasification with coal pre-drying.

Table 2.3 The main parameters of the two-stage fluidized bed gasification system simulations.

Process parameter	Value
Temperature of gasification (°C)	900
Carbon conversion	90%
Pressure of produced steam (MPa)	1
Temperature of agent into gasifier (°C)	500
Temperature of produced gas (°C)	120
Temperature of dryer (°C)	80
Heat efficiency of dryer	90%
Initial water contents of coal	10-65 wt.%
Water content after pre-drying	10 wt.%

2.2.3 Energy analysis

To quantitively characterize the fuel gas production by the TSFBG using coals with and without pre-drying, the following parameters are calculated:

ER: $$ER = \frac{R_a}{R_s} \quad (2.2)$$

where R_a is the actual air/oxygen to fuel ratio and R_s the stoichiometric air/oxygen to fuel ratio. ER > 1 represents a lean fuel process, while ER < 1 indicates a fuel rich process or incomplete combustion. ER = 1 indicates stoichiometric combustion, where all the fuel in the gasifier is completely oxidized and transformed into H_2O and CO_2.[13]

CGE: $$CGE\ \% = \frac{Q_{gas\ LHV}}{Q_{gc\ LHV} + Q_{gs}} \times 100\% \quad (2.3)$$

where $Q_{gas\ LHV}$ is the LHV of the produced fuel gas, $Q_{gc\ LHV}$ and Q_{gs} are the energy inputs to gasifier from the coal based on LHV and the steam, respectively.

Energy efficiency: $$\eta_{LHV}\ \% = \frac{Q_{gas\ LHV} + Q_{bp}}{Q_{sc\ LHV} + Q_{es}} \times 100\% \quad (2.4)$$

$$\eta_{HHV}\ \% = \frac{Q_{gas\ LHV} + Q_{bp}}{Q_{sc\ HHV} + Q_{es}} \times 100\% \quad (2.5)$$

where Q_{bp} is the energy of by-produced steam and Q_{es} is the energy of extra steam if the produced steam is not enough for drying; $Q_{sc\ LHV}$ and $Q_{sc\ HHV}$ are the energy inputs to the system of coals based on LHV and higher heating value (HHV), respectively. $\Delta\eta$ is the subtraction of energy efficiency (η_{LHV}/η_{HHV}) without and with pre-drying.

In order to illustrate and compare the influence of the fuel pre-drying on the gasification performance, especially on the system energy efficiency, the energy allocations are also conducted, which will be discussed below.

2.3 Results and discussion

2.3.1 ER and surplus steam for gasification with air

For the TSFBG systems with and without pre-drying, the required ER values and steam supply rates are calculated as functions of the initial water content of coal. The results are shown in **Table 2.4**. In the cases without pre-drying, when the initial water content is increased from 10 wt.% to 65 wt.%, the ER changes from 0.307 to 0.555 in order to maintain the gasifier at the preset temperature, which corresponds to the air consumptions of 1.948 Nm^3/kg to 3.527 Nm^3/kg dry coal. When the initial water contents are 10 wt.%, 15 wt.%, and 20 wt.%, the water contained in the coal alone

cannot meet the requirement of S/C= 0.35, and thus, an additional 0.24 kg-steam/kg dry coal, 0.17 kg-steam/kg dry coal, and 0.10 kg-steam/kg dry coal are needed to make up the shortages. For the water content of 26 wt.% and above, the water in the coal is more than what is required to maintain S/C=0.35, no additional steam is added into the gasifier, and the corresponding steam is produced as a by-product. For the TSFBG system with pre-drying, the coal with the initial water contents ranging from 15 wt.%-65 wt.% is dried to 10 wt.% of the final water content in the dryer. For the coal pyrolyzer and gasifier, this is equivalent to receiving a coal feed with an initial water content of 10 wt.%, thus, the required ERs and air consumptions are the same as when an initial water content of 10 wt.% of coal is used in the case of no pre-drying. However, the amount of the steam for drying is required to be increased from 0.14 kg/kg to 2.50 kg/kg dry coal when the initial water content is increased from 15 wt.% to 65 wt.%. Accordingly, the by-produced steam is reduced. Note that for the initial water contents of 50 wt.% and 65 wt.%, the water contained in the coal is too high and some extra steam supplements are required for drying, which is reflected by the negative values of the by-produced steam.

Table 2.4 Results of equivalence ratio (ER) and surplus steam with gasification agent of air/steam.

Initial water content of coal		ER	Consumed air (Nm^3/kg^a)	Steam (kg/kg^a)		
				To gasifier	For drying	By-product
Without pre-drying	10 wt.%	0.307	1.948	0.24	0.00	0.69
	15 wt.%	0.314	1.998	0.17	0.00	0.78
	20 wt.%	0.323	2.055	0.10	0.00	0.88
	26 wt.%	0.336	2.132	0.00	0.00	1.01
	35 wt.%	0.361	2.292	0.00	0.00	1.16
	50 wt.%	0.426	2.706	0.00	0.00	1.52
	65 wt.%	0.555	3.527	0.00	0.00	2.18
With pre-drying to 10 wt.%	15 wt.%	0.307	1.948	0.24	0.14	0.55
	20 wt.%	0.307	1.948	0.24	0.25	0.44
	26 wt.%	0.307	1.948	0.24	0.39	0.30
	35 wt.%	0.307	1.948	0.24	0.65	0.04
	50 wt.%	0.307	1.948	0.24	1.30	-0.61
	65 wt.%	0.307	1.948	0.24	2.50	-1.81

[a] Results calculated on dry basis of coal.

2.3.2 Gas composition and yield for gasification with air

Figure 2.3A shows variations in the concentrations of CO, CO_2, and H_2 in fuel gas with the initial water content of coal fed directly to the pyrolyzer without drying. When the initial water content of the coal is increased from 10 wt.% to 26 wt.%, the concentrations of CO and H_2 decrease gradually along with an increase in CO_2

concentration. This is because with the higher water content of coal, more cold water is added to the gasifier and more CO and H_2 need to be combusted in order to maintain the temperature of gasification. When the initial water content is greater than 26 wt.%, the water supplied to the gasifier is supplied entirely from the water of the coal, and thus an increased amount of combustion of CO and H_2 is required to maintain the gasification temperature. As a result, the decrease in CO and the increase in CO_2 become sharper. However, the H_2 concentration increases slightly and is followed by another gradual decrease. When there is higher water content in the coal, which leads to higher S/C ratios, both the H_2 consumption by combustion and production by water-gas shift reaction, which is shown by the increase in the H_2 yield shown in **Figure 2.3**B, are simultaneously enhanced. When the initial water content of the coal is gradually increased from 26 wt.% to 50 wt.%, the H_2 production by the water-gas shift reaction exceeds the consumption by combustion, and consequently leads to gradual increases in H_2 yields. Further increasing the water content from 50 wt.% to 65 wt.%, due to too much water brought into the gasifier, causes the H_2 to start declination since the combustion plays a controlling role. Note that the maximum H_2 concentration and yield appear at different initial water contents, one at 35 wt.% and the other at 50 wt.%. This may be due to the difference in the relative extent of N_2 dilution introduced with air. More N_2 added to the gasifier may lead to an increase in the total produced gas when the initial water content of the coal is increased. As stated earlier, for the gasification with initial water contents from 15 wt.%-65 wt.% drying to 10 wt.%, the results of the

corresponding gas composition and yield are the same as the gasification without pre-drying with an initial water content of 10 wt.%.

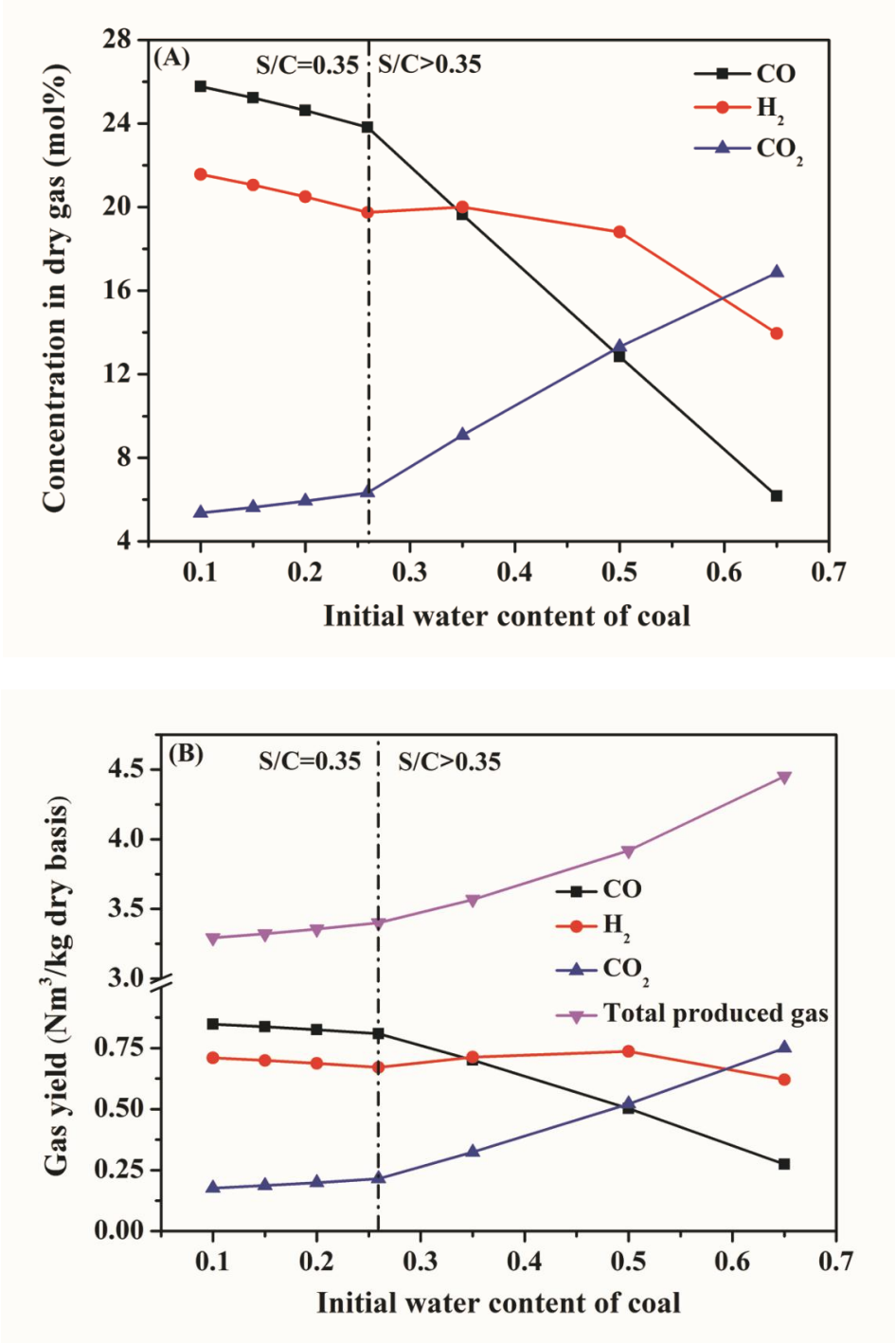

Figure 2.3 Influence of initial water content of coal on: A, fuel gas composition; and B, yield with air/steam as gasification agent and without the pre-drying of coal.

2.3.3 LHV and CGE for TSFBG with air

The influences of the initial water content of coal on the LHV and CGE are shown in **Figure 2.4**. For the TSFBG without pre-drying, the LHV of the produced fuel gas reduces gradually as the initial water content of the coal is increased from 10 wt.% to 26 wt.%, owing to the diluting effect of N_2 and reductions in H_2 and CO due to combustion. Although there is a slight increase in H_2 production between 26 wt.% and 50 wt.% of the initial water content, a more drastic reduction in the CO production and increasingly enhanced N_2 dilution yield an accelerated declination in LHV of the produced gas when the initial water content of the coal is continuously increased above 26 wt.%. With the increase in the initial water content, the CGE increases gradually to a maximum of about 79% at an initial water content of 26 wt.% and then decreases remarkably. A gradual increase in CGE from 10 wt.% to 26 wt.% of the initial water content of the coal contributes to the increase in gas yield and the reduction of steam into gasifier. When the initial water content of the coal is increased from 26 wt.% to 65 wt.%, the reduction in LHV of the produced gas mainly leads to a decrease in CGE from about 79% to 55%. As stated earlier, for the TSFBG with initial water contents from 15 wt.% to 65 wt.% drying to 10 wt.%, the results of the corresponding LHV and CGE are the same as that of gasification without pre-drying with an initial water content of 10 wt.%.

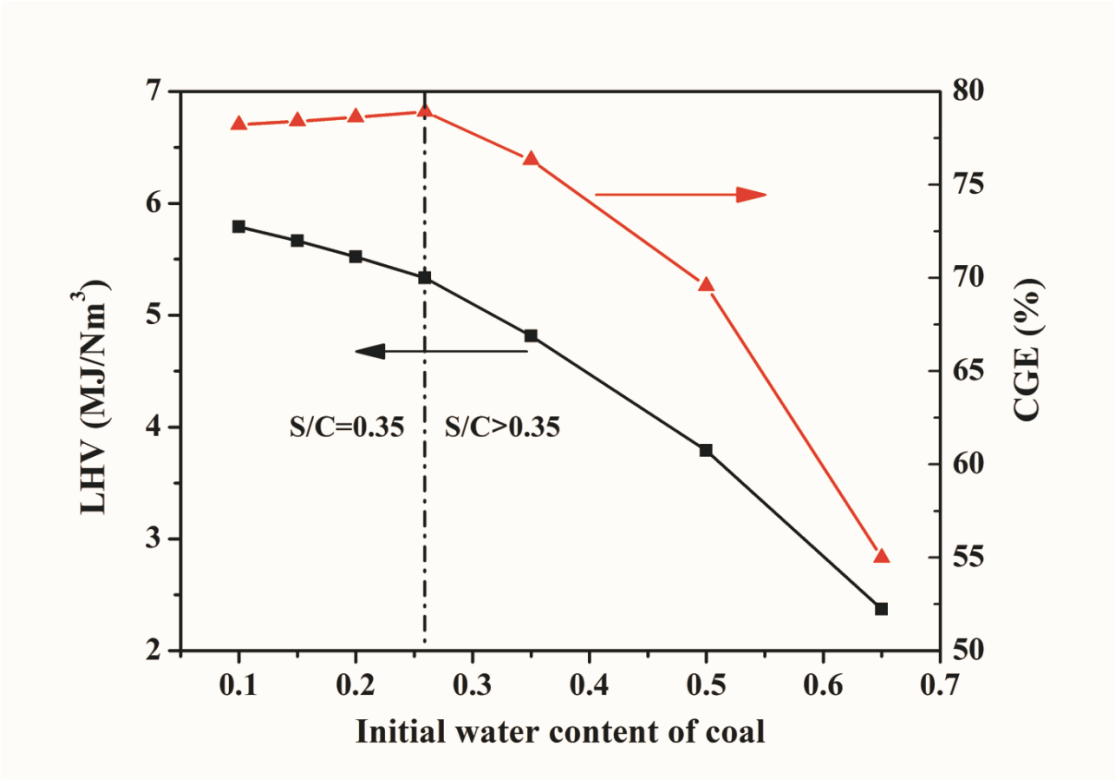

Figure 2.4 Influences of initial water content of coal on lower heating value and cold gas efficiency with air/steam as gasification agent and without the pre-drying of coal.

2.3.4 Effect of gasification agent on performance

The influences of gasification agents including oxygen/steam and air/steam on ER, produced gas, and surplus steam are presented in **Table 2.5**. For gasification without the pre-drying of coal with an initial water content from 10 wt.% to 65 wt.%, the ER values are 0.279-0.501 with oxygen/steam as gasification agent, which are lower than 0.308-0.555 with air/steam. This indicates that even for the gasification of the same feeding coal, to attain the same and constant temperature of gasification, the use of air/steam as gasifying agent requires higher ER to make up the heat loss of N_2 introduced with air. Different from the progressive increase in the total produced gas

yields with air/steam as gasification agent, the total produced gas yields with oxygen /steam show an overall downward trend, except for an increase at an initial water content of 50 wt.%. For the gasification with oxygen/steam, since there is no introduction of N_2, the increase and decrease of the total produced gas yield can be attributed to the controlling role of the water-gas shift reaction and CO and H_2 consumptions by combustion, respectively. The LHV of the produced gas with oxygen/steam decreases from 10.52 MJ/Nm^3 to 6.93 MJ/Nm^3 when the initial water content of coal is increased from 10 wt.% to 65 wt.%, which is much higher than that from 5.56 MJ/Nm^3 to 2.37 MJ/Nm^3 with air/steam. Table 5 also shows that the by-produced steam of gasification with oxygen/steam is about 0.2 kg/kg-0.5 kg/kg lower than that with air/steam. **Figure 2.5** shows that the CGE of gasification using oxygen/steam is about 3%-9% higher than that using air/steam due to the higher LHV of the produced gas and reaches a maximum of about 81%, compared to 76% using air/steam, both at 35 wt.% of initial water content of coal.

Table 2.5 Results of equivalence ratio (ER), produced gas, and surplus steam using different gasification agents.

Initial water content of coal		Gasification agent	ER	Consumed air/oxygen (Nm^3/kg^a)	TPGY (Nm^3/kg^a)	LHV (MJ/Nm^3)	Steam (kg/kg^a)		
							To gasifier	For drying	By-product
Without pre-drying	10 wt.%	air/steam	0.308	1.960	3.39	5.56	0.44	0.00	0.58
	20 wt.%	air/steam	0.325	2.068	3.45	5.31	0.30	0.00	0.77
	35 wt.%	air/steam	0.361	2.293	3.57	4.80	0.01	0.00	1.16
	50 wt.%	air/steam	0.426	2.706	3.92	3.79	0.00	0.00	1.52
	65 wt.%	air/steam	0.555	3.527	4.45	2.37	0.00	0.00	2.18
With pre-drying to 10 wt.%	20 wt.%	air/steam	0.308	1.960	3.39	5.56	0.44	0.25	0.33
	35 wt.%	air/steam	0.308	1.960	3.39	5.56	0.44	0.65	-0.07
	50 wt.%	air/steam	0.308	1.960	3.39	5.56	0.44	1.30	-0.72
	65 wt.%	air/steam	0.308	1.960	3.39	5.56	0.44	2.50	-1.92
Without pre-drying	10 wt.%	oxygen/steam	0.279	0.372	1.88	10.52	0.44	0.00	0.31
	20 wt.%	oxygen/steam	0.294	0.393	1.86	10.38	0.30	0.00	0.49
	35 wt.%	oxygen/steam	0.326	0.436	1.81	10.09	0.01	0.00	0.85

	50 wt.%	oxygen/steam	0.385	0.514	1.85	8.74	0.00	0.00	1.16
	65 wt.%	oxygen/steam	0.501	0.669	1.77	6.93	0.00	0.00	1.71
With pre-drying to 10 wt.%	20 wt.%	oxygen/steam	0.279	0.372	1.88	10.52	0.44	0.25	0.06
	35 wt.%	oxygen/steam	0.279	0.372	1.88	10.52	0.44	0.65	-0.34
	50 wt.%	oxygen/steam	0.279	0.372	1.88	10.52	0.44	1.30	-0.99
	65 wt.%	oxygen/steam	0.279	0.372	1.88	10.52	0.44	2.50	-2.19

Abbreviations: TPGY, total produced gas yield; LVH: lower heating value.

[a] Results calculated on dry basis of coal.

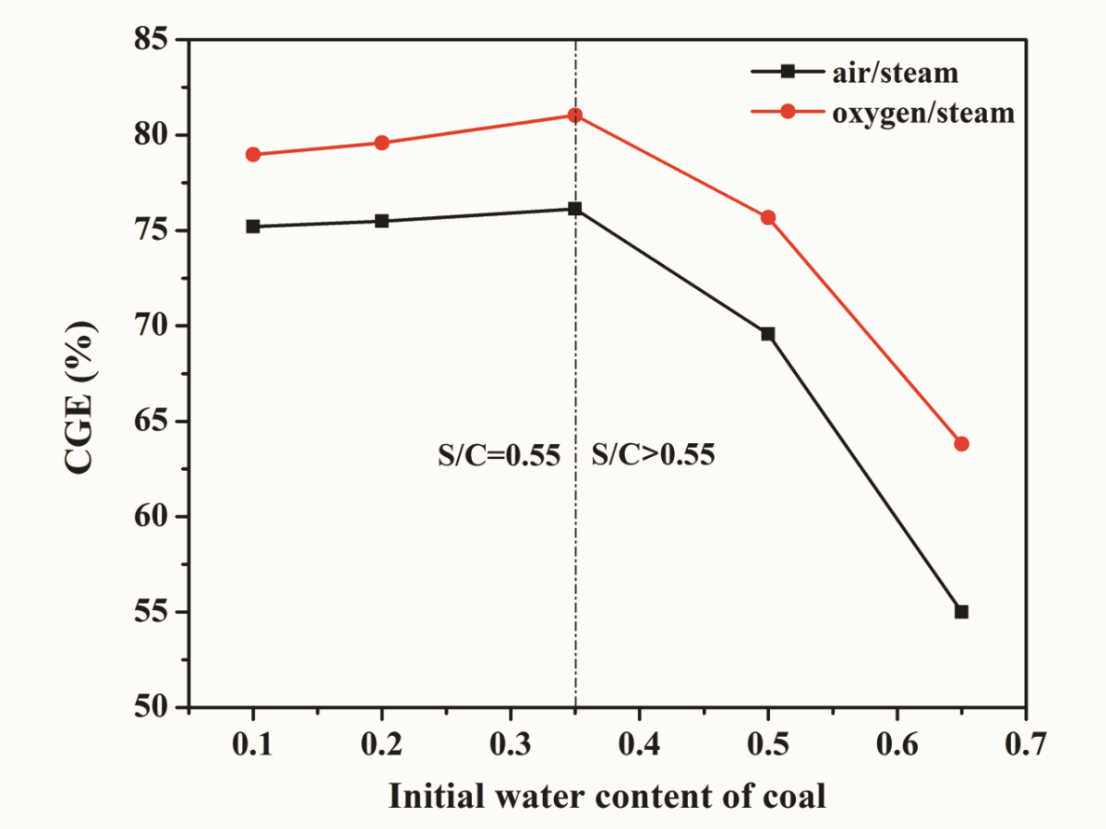

Figure 2.5 Influence of gasification agent on cold gas efficiency.

2.3.5 Energy efficiency of TSFBG with air

The effect of pre-drying of coal on energy efficiency η_{LHV} at different initial water contents is illustrated in **Figure 2.6**A. Without the pre-drying of coal, η_{LHV} gradually increases from about 89% to 91% when the initial water content increases from 10 wt.% to 26 wt.%, and then gradually reduces to 86% when the initial water content of the coal continuously increases to 65 wt.%. With the pre-drying of coal, η_{LHV} decreases continuously as the initial water content increases from 15 wt.% to 65 wt.%. The result of $\Delta\eta_{LHV}$ in Figure 6A shows clearly how the lack of pre-drying increases the η_{LHV} of gasification system. The η_{LHV} increases by about 1.5%-7% when the initial water

contents of coal are in the range of 15 wt.%-65 wt.%. The higher the water content, the greater the increased energy efficiency without the pre-drying. When the initial water content is below 26 wt.%, $\Delta\eta_{LHV}$ increases by about 1.4% with every 5% increase in water content. The $\Delta\eta_{LHV}$ further increases from about 4.4% to 6.9% when the initial water content of coal is increased from 26 wt.% to 65 wt.%. For the industrial application, the energy efficiency and quality of fuel gas are the highest concerns. The LHV of the produced fuel gas in **Figure 2.4** is the indicator of the quality of the fuel gas. The dashed line in Figure 6A clearly indicates that without the pre-drying the η_{LHV} with high initial water content of 50 wt.% is still comparable with that of a low initial water content of 10 wt.% with an acceptable LHV of fuel gas. Although the η_{LHV} of TSFBG without the pre-drying of the initial water content of 65 wt.% is still about 86%, the corresponding LHV of the fuel gas is lower than 3.0 MJ/Nm^3. This indicates that such a high water content may not be recommended in the practical process. Hence, for TSFBG using air/steam without the pre-drying, the preferred initial water content of coal is below 50 wt.%.

The effects of the pre-drying of coal on energy efficiency η_{HHV} and $\Delta\eta_{HHV}$ at different initial water contents are illustrated in **Figure 2.6**B. In the case without the pre-drying of coal, η_{HHV} changes little between initial water contents of coal from 10 wt.% to 26 wt.%; however, this reduces noticeably when the initial water content of coal is beyond 26 wt.%. With the pre-drying of coal, η_{HHV} decreases continuously with the increase in the initial water content of coal from 15 wt.% to 65 wt.%. Similar to

η_{LHV}, the pre-drying of coal reduces the η_{HHV} of the TSFBG system by about 1.5%-5%. These results indicate that the TSFBG system without the pre-drying of coal is superior in energy efficiency compared to the system with the pre-drying of coal.

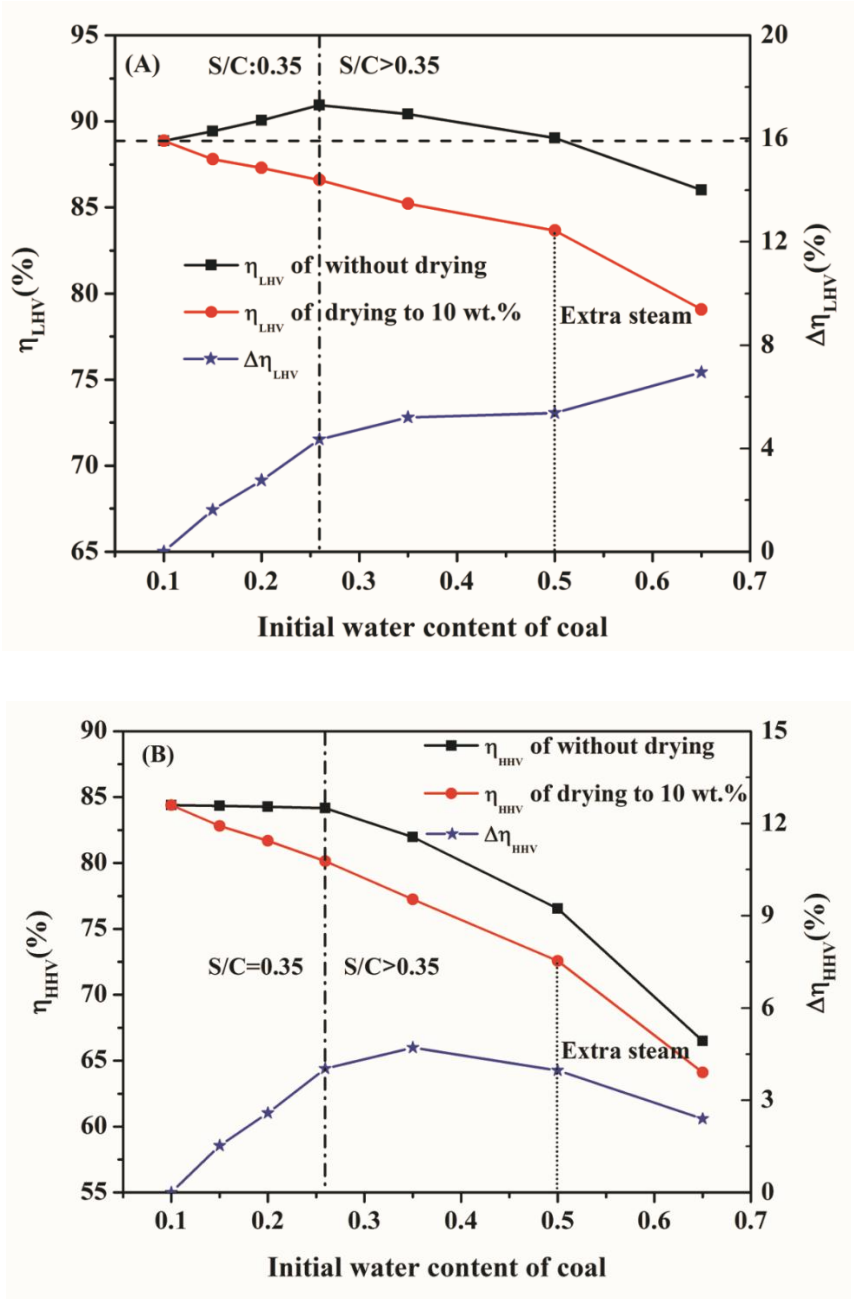

Figure 2.6 Influence of pre-drying of coal on: A, η_{LHV} and $\Delta\eta_{LHV}$; and B, η_{HHV} and $\Delta\eta_{HHV}$ with air/steam as gasification agent at different initial water contents of coal.

2.3.6 Energy allocations of TSFBG with air

To further illustrate the effect of the pre-drying of coal on energy efficiency, an analysis of energy allocations is conducted. Taking 26 wt.% of the initial water content of coal as an example, the energy allocations of TSFBG systems without and with the pre-drying of coal are comparatively shown in **Figure 2.7**A and B, respectively. It shows that the pre-drying of coal increases the energy allocation of the fuel gas HHV by about 4% but reduces the energy of by-produced steam by about 7.8%. Due to the higher yield of produced fuel gas as mentioned earlier, the energy allocation of the sensible heat of fuel gas of TSFBG without the pre-drying is about 0.4% higher than that with the pre-drying. However, the energy allocation of heat loss due to the drying of coal is about 4.2% of TSFBG with the pre-drying, mainly leading to the decrease in the total system energy efficiency. Additionally, since the feed coals on a dry basis are the same and the carbon conversion is considered as constant, energy allocation of the chemical energy of lost carbon and heat loss of ash are the same as about 8.0% and 0.8%, respectively, in these processes.

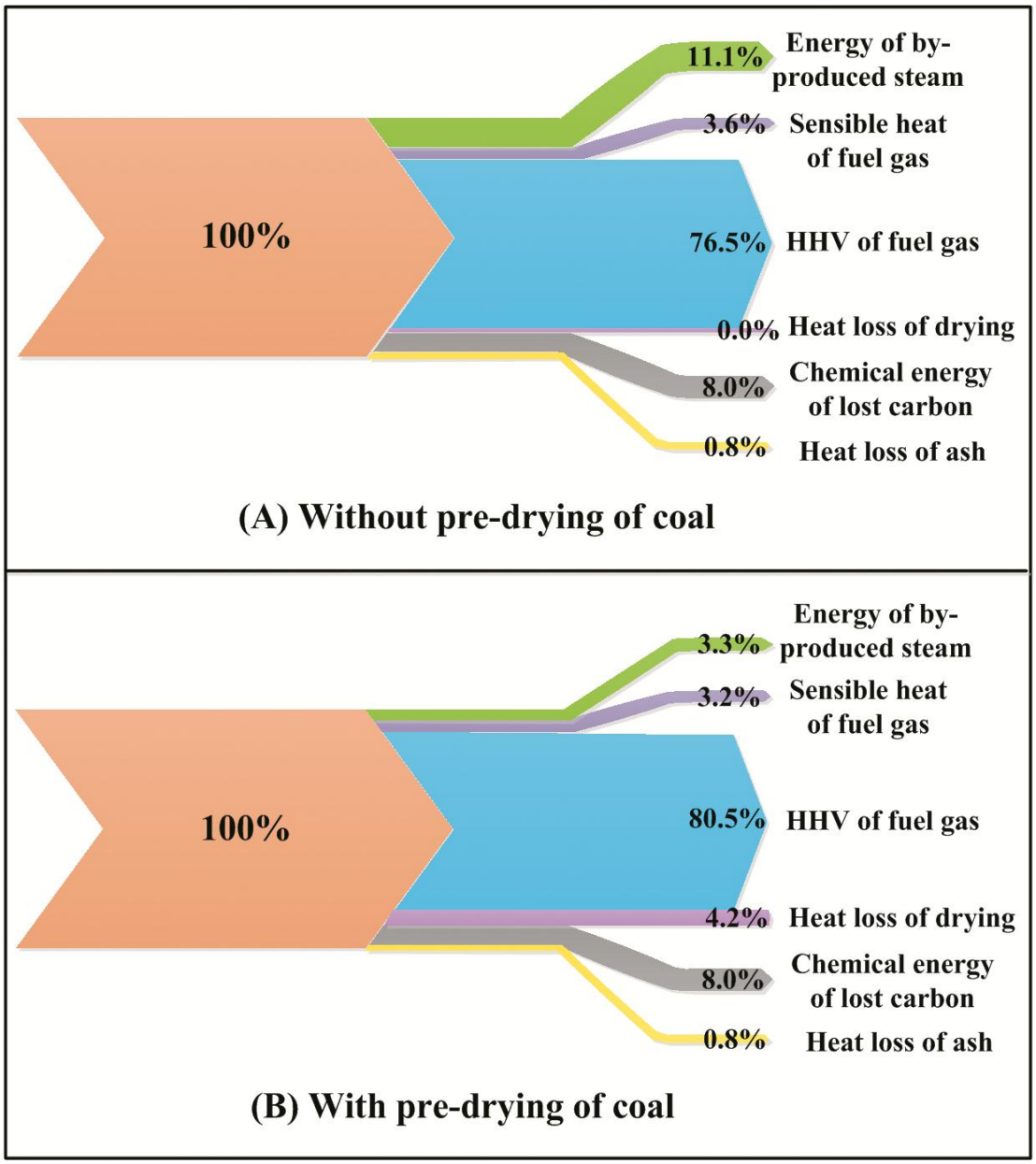

Figure 2.7 Effect of pre-drying of coal in energy allocations with an initial water content of 26 wt.%.

2.3.7 Effect of gasification agent on efficiency

Figure 2.8 shows that variations in η_{LHV} and η_{HHV} of the TSFBG systems with the initial water content of coal using oxygen/steam as the gasification agent are similar to those with air/steam. Replacing air with oxygen increases energy efficiency for both

η_{LHV} and η_{HHV} by about 1% to 2% for both TSFBG systems with and without the pre-drying of coal under all initial water contents simulated. For the TSFBG system without the pre-drying of coal using oxygen/steam, η_{LHV} reaches a maximum of about 91%, compared to about 90% using air/steam, both at 35 wt.% initial water content of coal. The value of η_{LHV} of gasification using oxygen/steam at 65 wt.% of initial water content of coal is about 0.6% higher than that at 10 wt.% of initial water content of coal, while the η_{LHV} of the same system using air/steam at 65 wt.% initial water content of coal is below that at 10 wt.% of initial water content of coal. From **Table 2.5**, we can see that the LHV of the fuel gas of the TSFBG system without the pre-drying of coal at an initial water content of 65 wt.% using oxygen/steam is still about 6.93 MJ/Nm^3, which is much higher than 2.37 MJ/Nm^3 when the air/steam is used. This indicates that the initial water content of 65 wt.% for TSFBG without the pre-drying using oxygen/steam can still be conducted. The result of $\Delta\eta_{LHV}$ in **Figure 2.9** shows clearly that the increase in the energy efficiency without the pre-drying of coal at 65 wt.% initial water content using oxygen/steam is greater than that using the air/steam. These results suggest that TSFBG without the pre-drying of coal using the oxygen /steam possesses certain advantages over using air/steam, especially at a high water content.

Allocations of energy for the TSFBG without the pre-drying of coal at an initial water content of 35 wt.% are shown in **Figure 2.10** for the oxygen/steam and air/steam used respectively as gasification agents. It is obvious that the use of oxygen to replace air increases the heating value of the product gas by about 4.7% since there is no

dilution effect of N_2 introduced with air. The energy of the by-produced steam when oxygen is used instead of air accounts for about 9.3% and is about 3.3% lower than that with the air/steam. It is worth noting that energy allocation of the sensible heat of the product gas with oxygen/steam as the gasification agent is about 1.4% lower than that with the air/steam, which is mainly responsible for the increase in energy efficiency.

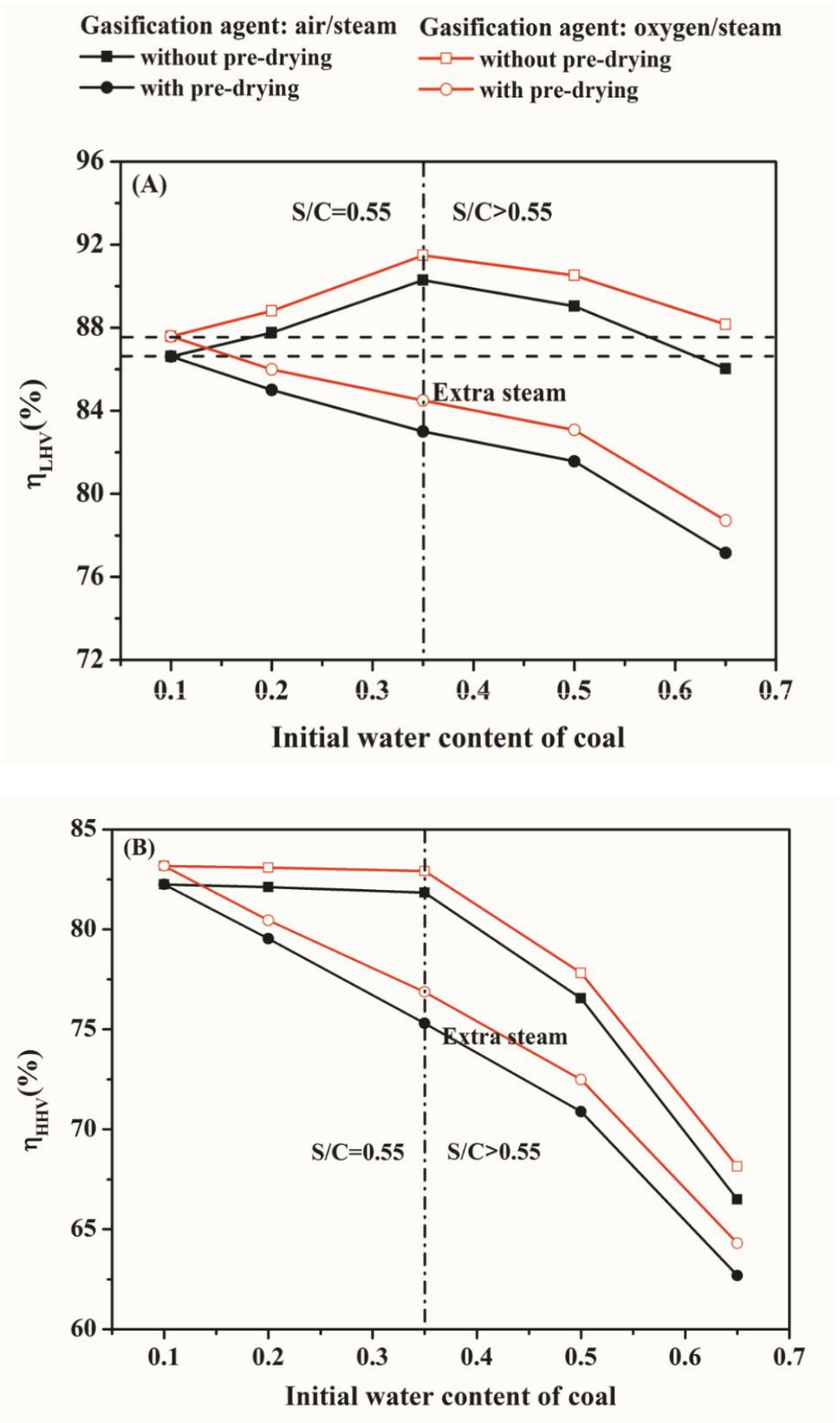

Figure 2.8 Influence of gasification agent on: A, η_{LHV}; and B, η_{HHV}.

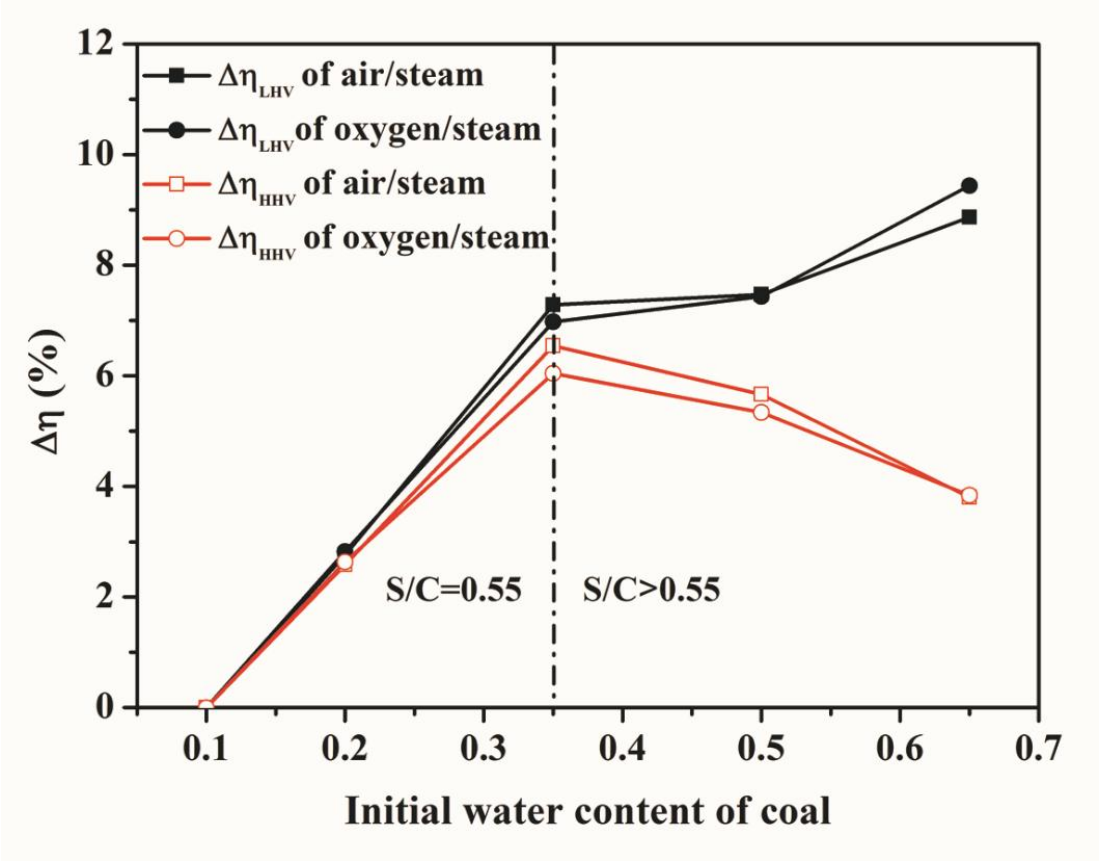

Figure 2.9 Influence of gasification agent on Δη.

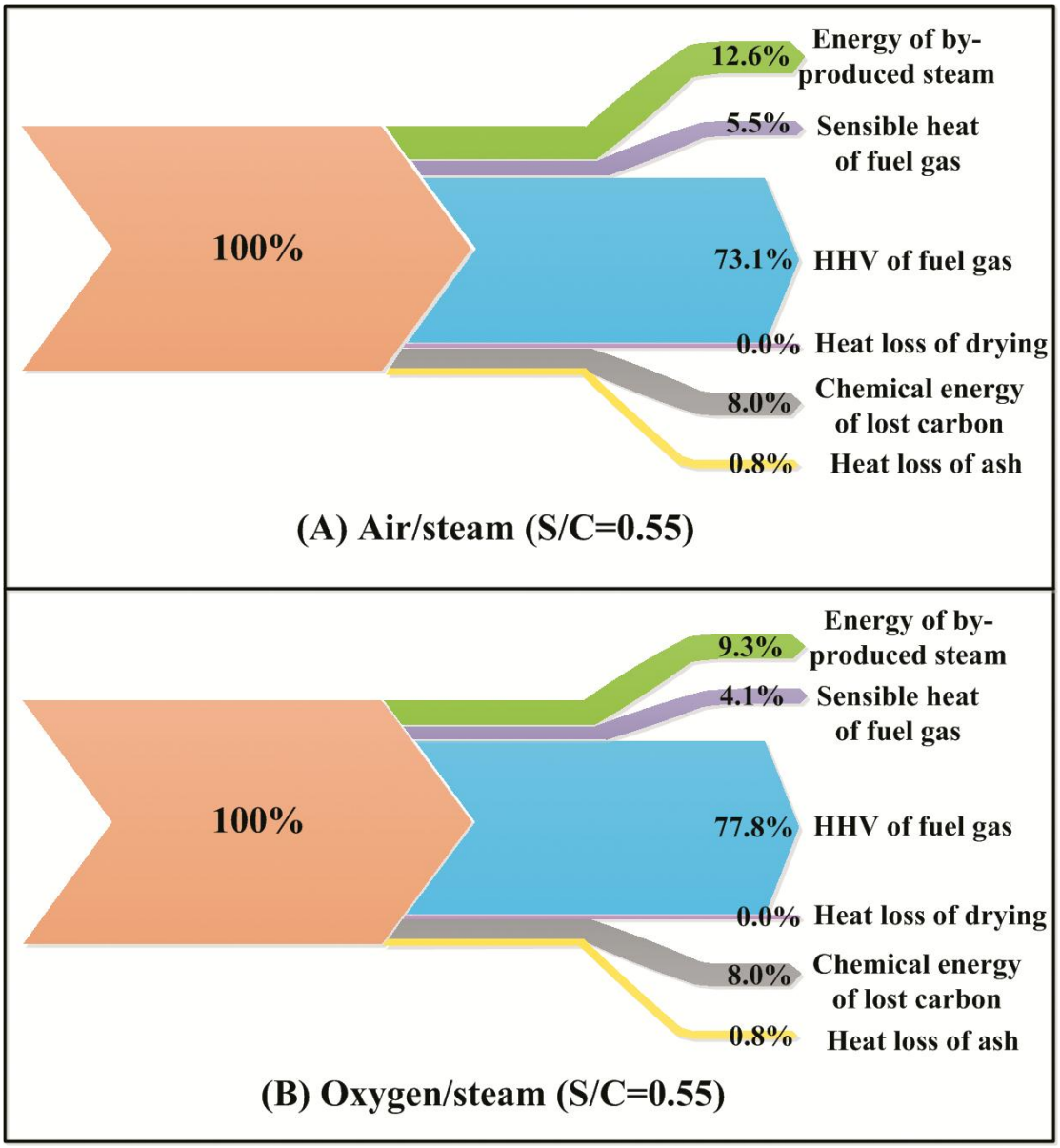

Figure 2.10 Allocations of energy for the two-stage fluidized bed gasification system without pre-drying of coal at 35 wt.% initial water content of coal.

2.4 Conclusions

The TSFBG process has been investigated based on the Aspen Plus process simulation with a focus on examining the effect of coal pre-drying on gasification performance, especially on the overall energy efficiency. It shows clearly how pre-

drying reduces the gasification system energy efficiency. Through a comprehensive analysis of the simulation results, the following conclusions can be obtained.

- For the TSFBG system, the higher the water content, the greater the reduced energy efficiency through the pre-drying of coal. When the initial water content is below 26 wt.%, $\Delta\eta_{LHV}$ increases by about 1.4% with every 5 wt.% increase in water content. The $\Delta\eta_{LHV}$ further increases from about 4.4% to 6.9% when the initial water content of coal is increased from 26 wt.% to 65 wt.%. An analysis of energy allocations demonstrates that the heat loss due to the pre-drying of coal is mainly responsible for the reduction in energy efficiency.
- The η_{LHV} of the TSFBG system without the pre-drying of coal using the air/steam as gasification agent reaches its maximum of about 91% at an initial water content of 26 wt.%. The η_{LHV} at a high initial water content of 50 wt.% is comparable with that at a low initial water content of 10 wt.%. For TSFBG using the air/steam without the pre-drying, the preferred initial water content of coal is below 50 wt.%.
- Replacing air with oxygen increases energy efficiency by about 1% to 2% for the TSFBG systems with and without the pre-drying of coal when the initial water content of coal is between 10 wt.%-65 wt.%. Variation in the sensible heat of the product gas is responsible for this difference in energy efficiency. The TSFBG without the pre-drying using the oxygen/steam as the gasification agent shows advantages over using air/steam, especially at a high water content.

These findings suggest that the TSFBG system without the pre-drying of coal is more energy efficient and it is recommended as the better choice in practical gasification operations when a higher water content of coal is used.

References

1. F. Li, L. Zeng, L.-S. Fan, Techno-Economic Analysis of Coal-Based Hydrogen and Electricity Cogeneration Processes with CO_2 Capture, Ind. Eng. Chem. Res. 2010, 49, 11018-11028.
2. F. Qian, X. Kong, H. Cheng, W. Du, W. Zhong, Development of a Kinetic Model for Industrial Entrained Flow Coal Gasifiers, Ind. Eng. Chem. Res. 2013, 52, 1819-1828.
3. Q. Li, M. Zhang, W. Zhong, X. Wang, R. Xiao, B. Jin, Simulation of Coal Gasification in a Pressurized Spout-Fluid Bed Gasifier, Can. J. Chem. Eng. 2009, 87, 169-176.
4. L. Su, S. Feng, P. Li, Y. Zhang, Z. Liu, Z. Li, Study on Simulation of Pulverized Coal Gasification Process in the GSP Gasifier, Can. J. Chem. Eng. 2017, 95, 688-697.
5. E. Biagini, A. Bardi, G. Pannocchia, L. Tognotti, Development of an Entrained Flow Gasifier Model for Process Optimization Study, Ind. Eng. Chem. Res. 2009, 48, 9028-9033.
6. N. Mahinpey, A. Gomez, Review of gasification fundamentals and new findings: Reactors, feedstock, and kinetic studies, Chem. Eng. Sci. 2016, 148, 14-31.

7. M. M. Papic, Technology and Economics of Coal Gasification, Can. J. Chem. Eng. 1976, 54, 413-420.
8. P. K. Chatterjee, A. B. Datta, K. M. Kundu, Fluidized Bed Gasification of Coal, Can. J. Chem. Eng. 1995, 73, 204-210.
9. X. Zeng, R. Shao, F. Wang, P. Dong, J. Yu, G. Xu, Industrial demonstration plant for the gasification of herb residue by fluidized bed two-stage process, Bioresource Technol. 2016, 206, 93-98.
10. Z. Han, S. Geng, X. Zeng, S. Xu, P. An, J. Cheng, J. Yang, F. Li, S. Zhang, M. Liu, G. Guan, G. Xu, Reaction decoupling in thermochemical fuel conversion and technical progress based on decoupling using fluidized bed, Carbon Resour. Convers. 2018, 1, 109-125.
11. V. Wilk, H. Hofbauer, Analysis of optimization potential in commercial biomass gasification plants using process simulation, Fuel Process. Technol. 2016, 141, 138-147.
12. B. Dai, L. Zhang, J.-f. Cui, A. Hoadley, L. Zhang, Integration of pyrolysis and entrained-bed gasification for the production of chemicals from Victorian brown coal - Process simulation and exergy analysis, Fuel Process. Technol. 2017, 155, 21-31.
13. R. Barrera, C. Salazar, J. F. Pérez, Thermochemical Equilibrium Model of Synthetic Natural Gas Production from Coal Gasification Using Aspen Plus, Int. J. Chem. Eng. 2014, 2014, 1-18.

14. C. Li, Z.-h. Dai, J. Yang, G.-s.Yu, F.-c.Wang, Modelling and energy analysis of an integrated coal gasification and pyrolysis system for synthetic natural gas, J. Fuel Chem. Technol. 2015, 43, 779-789.
15. C. He, X. Feng, K. H. Chu, A. Li, Y. Liu, Industrial-scale Fixed-bed Coal Gasification: Modeling, Simulation and Thermodynamic Analysis, Chinese J. Chem. Eng. 2014, 22, 522-530.
16. C. He, X. Feng, K. H. Chu, Process modeling and thermodynamic analysis of Lurgi fixed-bed coal gasifier in an SNG plant, Appl. Energy 2013, 111, 742-757.
17. G. Cau, V. Tola, A. Pettinau, A steady state model for predicting performance of small-scale up-draft coal gasifiers, Fuel 2015, 152, 3-12.
18. Y. Wang, W. Dong, L. Dong, J. Yue, S. Gao, T. Suda, G. Xu, Production of Middle Caloric Fuel Gas from Coal by Dual-Bed Gasification Technology, Energy Fuels 2010, 24, 2985-2990.
19. C. Sánchez, E. Arenas, F. Chejne, C. A. Londoño, S. Cisneros, J. C. Quintana, A new model for coal gasification on pressurized bubbling fluidized bed gasifiers, Energy Convers. Manage. 2016, 126, 717-723.
20. Y. Furusawa, H. Taguchi, S. N. Ismail, S. Thangavel, K. Matsuoka, C. Fushimi, Estimation of cold gas efficiency and reactor size of low-temperature gasifier for advanced-integrated coal gasification combined cycle systems, Fuel Process. Technol. 2019, 193, 304-316.

21. Y. Wang, J. Yang, Z. Zhang, X. Ma, P. Li, X. Hao, G. Guan, TBCFB system simulation and optimization for pyrolysis-gasification-combustion of low rank coal (in Chinese), CIESC J. 2018, 69, 3596-3604.

22. X. Zeng, Y. Dong, F. Wang, P. Xu, R. Shao, P. Dong, G. Xu, L. Dong, Fluidized Bed Two-Stage Gasification Process for Clean Fuel Gas Production from Herb Residue: Fundamentals and Demonstration, Energy Fuels 2016, 30, 7277-7283.

CHAPTER 3

Energy-saving strategy for a transport bed flash calcination process applied to magnesite

3.1 Introduction

Magnesite is one of the most important raw material source in the world for magnesia refractory production [1]. China has abundant magnesite resources (mainly composed of $MgCO_3$) with a proved reserve of approximately 3.1 billion tons, nearly 90% of which is distributed in Liaoning province [2]. Relying on its resource and good industry basis, Liaoning province has formed a particular industry chain for exploitation and utilization of magnesite and been the world's largest production and exportation site of magnesium-based raw and some functional materials [3-5]. In the magnesite-based industry, light calcination of magnesite is the first step, which occurs at about 1000 °C to obtain the caustic calcined magnesia (CCM, mainly composed of MgO) based on the reaction shown below [6-9]. Here, the term "light" means at relatively low temperatures. CCM is the feedstock for the production of downstream high-value products, such as silicon-steel magnesium oxide, magnesium hydroxide and magnesium cement [10-16].

$$MgCO_3\ (s) \rightarrow MgO\ (s) + CO_2\ (g) \qquad \Delta H = +99.66\ kJ/mol \qquad (3.1)$$

There are more than 1,500 light-calcined furnaces in Liaoning province with a production capacity of CCM over 10 million tons per year. However, the most widely used technology, for decades, is the reverberatory furnace (RF) that has high energy consumption, bad feedstock adaptability, long reaction time, unsteady product quality

and serious environmental pollution [17,18]. As shown in **Figure 3.1**A, the RF is a fixed bed calcination reactor [19], in which the high-temperature flue gas produced by fuel gas combustion passes through the magnesite bed from bottom to top for implementing the calcination of magnesite. In order to ensure the gas permeability of bed and reduce the pressure drop, the RF can only adopt large-size magnesite particles in 30-80 mm. As a result, massive small-size magnesite generated in mining and processing are difficult to be used. The large-size feedstock also makes the reaction time in RF is even up to 3-5 h and a low production capacity of about 30 t/d for a furnace. It also causes the so-called phenomena of over-burning on surface and insufficient-burning in inner part, making the quality of CCM unstable and the products have low activity [20].

Xu *et al.*[21] designed a dilute phase reactor (i.e., magnesite flash calciner, MFC) for the calcination of magnesite as shown in **Figure 3.1**B. Compared to those fixed bed calciners, MFC can produce higher active CCM within a shorter reaction time. Jiang *et al*.[22] explored the feasibility of fluidization calcination for the magnesite using a micro fluidized bed, and found that the calcination process can finish in a few seconds. Based on this innovative concept, Shenyang University of Chemical Technology proposed a transport bed flash calcination (TBFC) process for CCM production. A transport bed reactor is employed to substitute the traditional RF, for which small magnesite powder can also be effectively used as the feedstock. In this transport bed reactor, the high-temperature flue gas from fuel gas combustion is rapidly mixed with magnesite powder so that the production efficiency and product stability are greatly improved. Sun *et al.*[23]

investigated the calcination of magnesite in a laboratory-scale transport bed, and found that the conversion of magnesite powder (<150 μm) reached 98% in only 1-2 seconds with obviously higher activity of product when compared to the products from the fixed bed calciner, corroborating the feasibility of TBFC for high-efficiency calcination of magnesite.

Due to the high operation temperature in the light calcination process, the heat recovery and reutilization is vital for the improvement of system energy efficiency. In this work, the TBFC process is systematically investigated through process simulation considering the pre-decomposition of magnesite during preheating, aiming at optimizing the energy-saving strategy for the process, an essential need for its industrial design as well as operation.

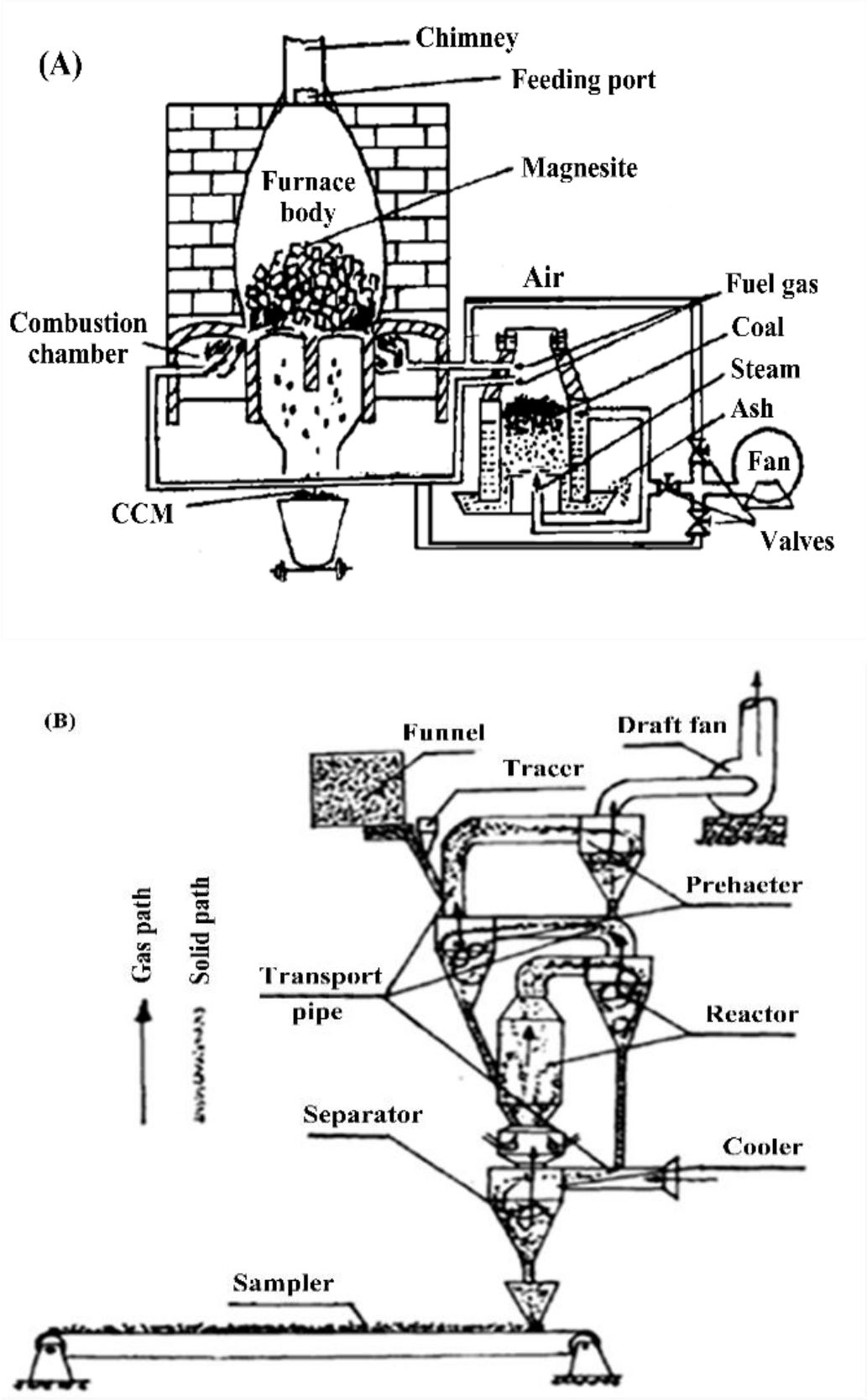

Figure 3.1 Schematic process-flow diagrams of (A) RF [19] and (B) MFC [21].

3.2 Methods and models

3.2.1 Process description

The TBFC process is mainly composed of a calciner implementing the light calcination of magnesite, a magnesite preheating system and a CCM cooling system. In the preheating system, the fed magnesite is heated by flue gas from the high-temperature calciner. While, in the cooling system, the high-temperature CCM is cooled down by air sent to the calciner. Herein, the TBFC process with two-stage cooling and four-stage preheating is taken as an example and shown in **Figure 3.2**. The magnesite with a certain water content is first fed to a dryer (i.e., the 4^{th}-stage preheater) and dried by the flue gas from the 3^{rd}-stage preheater. The flue gas from the exit of the dryer is directed into a bag filter to remove its entrained fine powder and finally brought into a chimney. The dried magnesite from the 4^{th}-stage preheater, mixing with the flue gas from the 2^{nd}-stage preheater goes into the 3^{rd}-stage preheater to preheat magnesite further by the sensible heat with the flue gas. Similarly, the magnesite from the 3^{rd}-stage and 2^{nd}-stage preheaters is preheated by the flue gas from the 1^{st}-stage preheater in the 2^{nd}-stage preheater and from the calciner in the 1^{st}-stage preheater, respectively. The preheated magnesite from the 1^{st}-stage preheater goes into the calciner as the feed of calcination, and the energy required comes from the fuel gas combustion by air preheated in cooling the CCM product. A staged combustion is employed to better maintain a uniform temperature distribution along the calciner. At the exit of the calciner, the produced CCM is separated from flue gas by a cyclone. Then, the high-

temperature CCM is cooled, successively, by the air recovered in the 2nd-stage cooler and blown into the 1st-stage cooler. The preheated air from the 2nd-stage cooler is directed into the calciner to support the fuel gas combustion. The final CCM product from the 1st-stage cooler is forwarded to a CCM tank. The compositions of magnesite and fuel gas considered in this study are presented in **Table 3.1**.

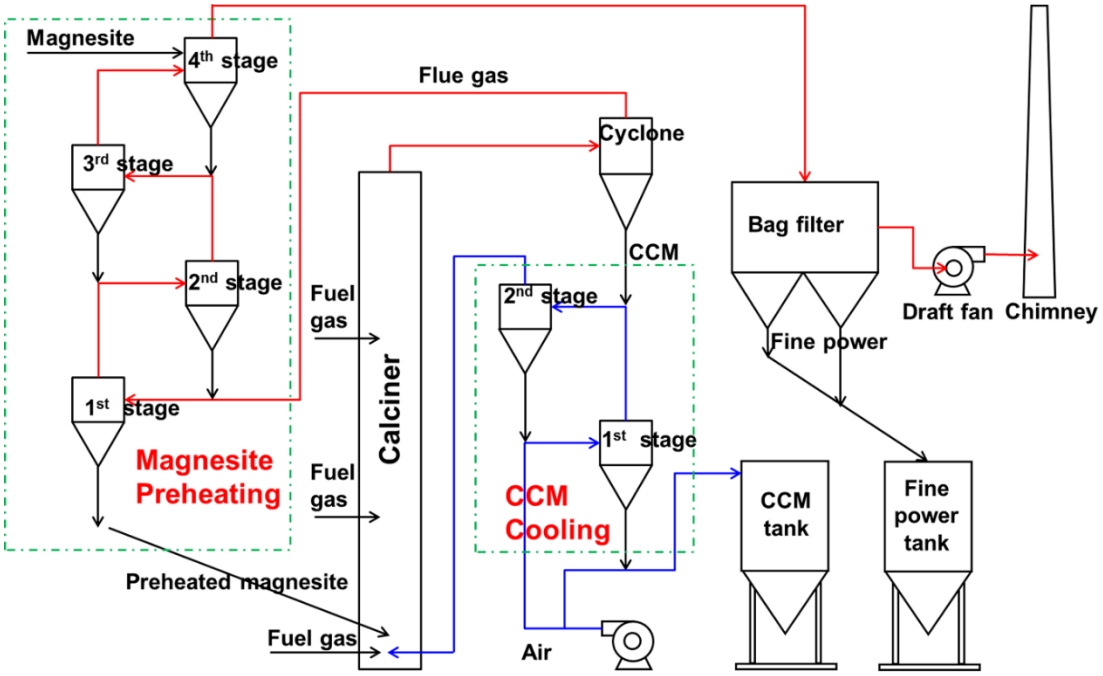

Figure 3.2 A schematic diagram of the TBFC process with two-stage cooling and four-stage preheating.

Table 3.1 Compositions of magnesite and fuel gas used in this study.

Magnesite composition (wt.%)	
$MgCO_3$	90
Water	10
Fuel gas composition (mol.%)	
CO_2	3.00
CH_4	96.10
N_2	0.34

C_2H_6	0.45
C_3H_8	0.11

3.2.2 Kinetic analysis of magnesite calcination

The work used the micro fluidized bed reaction analyzer (MFBRA) to explore the feasibility of quick magnesite calcination. Besides thermogravimetric analyzer (TGA), it has shown that MFBRA can provide a complementary and reliable way to characterize gas-solid reactions [24-33]. **Figure 3.3** presents the typical results obtained. Magnesite powder in 100-200 μm can be completely decomposed in only about 3 seconds at 900 °C, indicating the nature of flash calcination. While detailed reaction kinetics for magnesite calcination can be found in Jiang *et al.*[22], here we intended to use the kinetic parameters from MFBRA to simulate the kinetics occur in the transport bed calcination process. Because of its minimized effect of external diffusion on reaction, MFBRA would give high-accuracy kinetic data than TGA does. For the TBFC processes imbedded with multi-stage preheating, the temperature of magnesite would surely increase continuously along the process such that the fed magnesite may start to decompose even at 500 °C [22]. Therefore, pre-decomposition of magnesite has to be considered for achieving an accurate process analysis, which in turn requires an input of the kinetic data. In this study, the following kinetic equation obtained by measuring magnesite calcination in air using MFBRA was adopted in performing the process simulation [18].

$$\frac{dx}{dt} = 10^{5.69} exp(-\frac{124160}{RT}) \times (1 - x) \quad (3.2)$$

where x is the conversion for magnesite calcination, t and T are the reaction time and temperature, respectively.

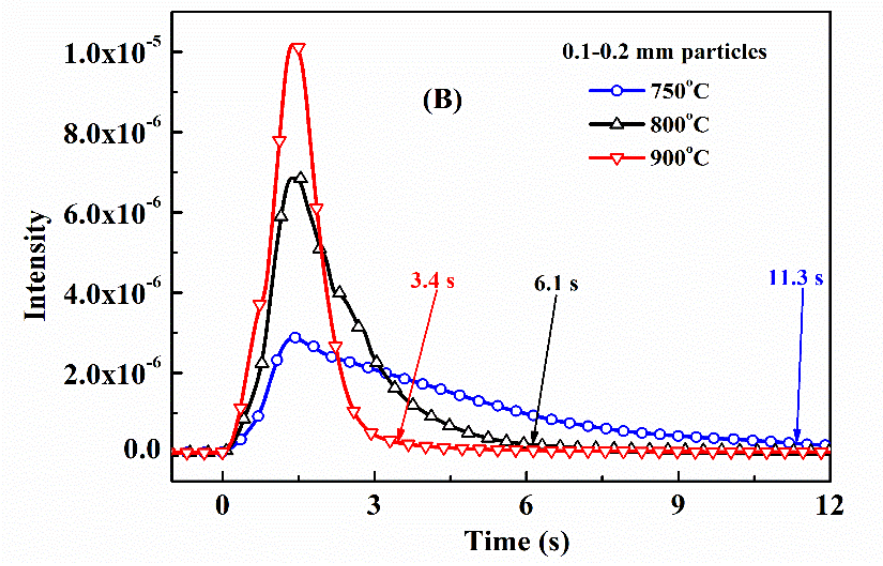

Figure 3.3 Calcination of magnesite in MFBRA: (A) a photo of analyzer and (B) CO_2 formation curve detected using a process mass spectrometer.

3.2.3 Magnesite preheating model

In TBFC process, a cyclone-type preheater, shown in **Figure 3.4**, is adopted to preheat the fed magnesite where the particles and gas first proceed heat transfer in the heat-exchange pipe and then they are separated in the cyclone. Generally, the residence time of particles in the heat-exchange pipe (until the tangential entrance) and cyclone body, even for industrial plants, should not be longer than 0.2 s and be about a few seconds (such as 5 s), respectively. With rise of temperature, the fed magnesite may decompose since reaching 500 °C in the cyclone-type preheater so that pre-decomposition of magnesite needs to be considered in process analysis. As for this study, the results shown in **Table 3.3** indicate that the temperature of all preheaters is in the range of 450 °C to 750 °C. Estimating with the kinetics shown above clarifies that under such temperatures the possible decomposition rate of magnesite in 0.2 s is not over 4.3% (**Figure 3.5**). On the other hand, the separation of gas and solid in the cyclone is very quick, due to the quick segregation of particles to the vicinity of the cyclone wall under the action of centrifugal force. Not only the gas-solid contacting area is quite small but the heat transfer between gas and solid can also be neglected. Accordingly, the magnesite pre-decomposition in the heat-exchange pipe will not be considered, while in the cyclone body it occurs under the adiabatic condition. Consequently, the magnesite preheating model adopted in simulation consists of two subprocesses, the gas-solid heat transfer without magnesite pre-decomposition in the heat-exchange pipe and the gas-solid quick separation with adiabatic pre-

decomposition of magnesite in the cyclone body.

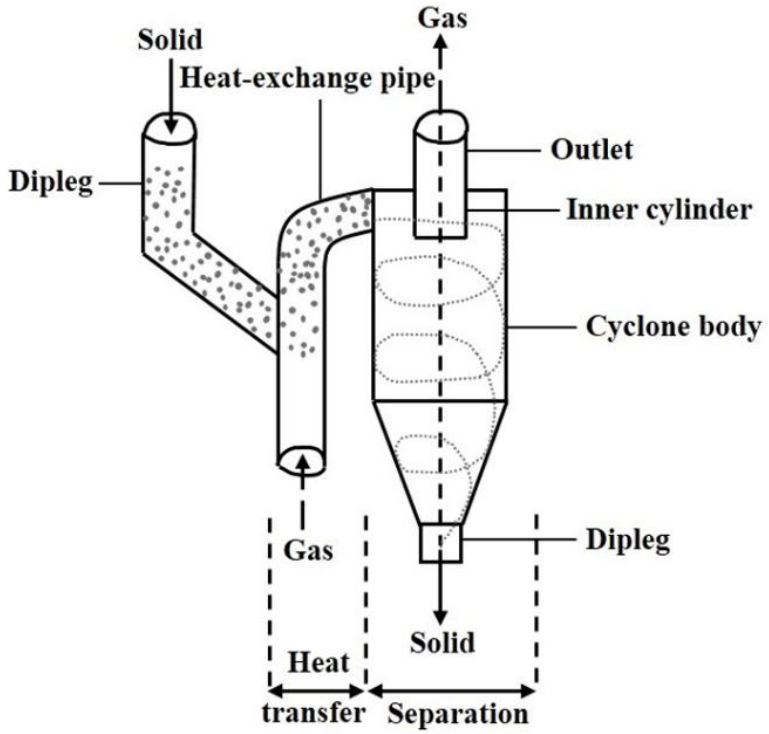

Figure 3.4 A schematic drawing of the cyclone preheater.

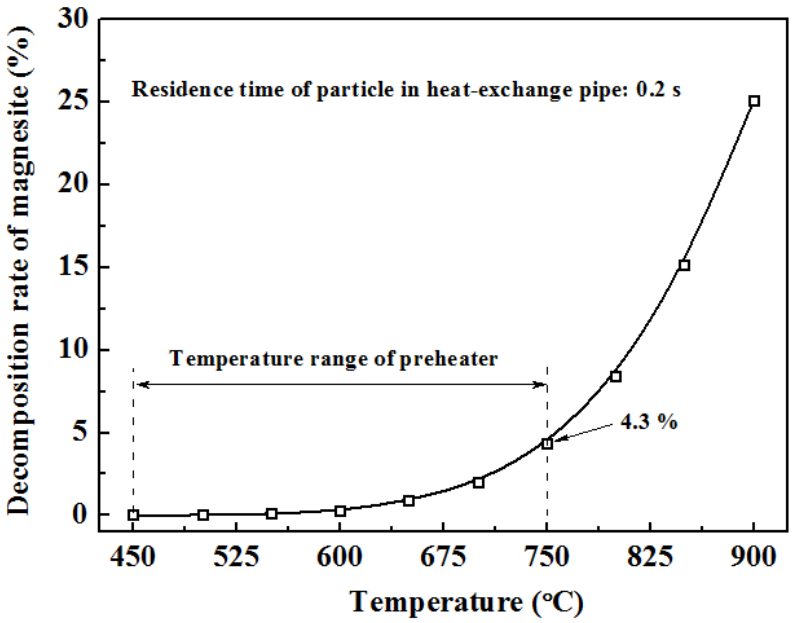

Figure 3.5 Decomposition rate of magnesite in heat-exchange pipe calculated by equation (3.2) at different temperatures.

3.2.4 Simulation approach

The commercial process simulator Aspen Plus is employed for the simulation. **Table 3.2** outlines the representative units and their corresponding Aspen Plus models used in the simulation. In simulations, the temperature of light calcination is set at 900 °C and the equivalence ratio for fuel gas combustion is 1.2. The whole system is operated at around atmosphere pressure. This work investigated the TBFC process performance and energy efficiency varying with the number of heat-exchange stages and residence time of particles in cyclone preheaters. The acquired results for the TBFC process are also compared with those of the RF and MFC processes.

Table 3.2 Representative unit and corresponding models used in the simulation.

Unit	Name in flow chart	Aspen model	Specification	Parameters setting
Calcination	RSTOIC1/2/3	RStoic	Calcination and combustion in TBFC	900 °C
Calcination	RSTOICR	RStoic	Calcination in RF	750 °C
Calcination	RSTOICM	RStoic	Calcination in MFC	900 °C
Combustion	COMBUSTR	RGibbs	Combustion in RF	1200 °C
Combustion	COMBUSTR/M	RGibbs	Combustion in MFC	1300 °C
Pre-decomposition	HEATEXF1/XF2/F1M	RCSTR	Pre-decomposition following kinetics	Residence time in preheater: 1-5 s
Mixing	MIX1/2/3/4/1M/2M	Mixer	Multiple streams mixer	/
Separation	SEP1/2/3/4/5/1M/2M/3M/R	SSplit	Separating gas and solid	/
Heat	HEATEXF3/XF4/XF	RGibbs	Heat exchanging	Preheating

exchanger	5/F2M/XR		between flue gas and magnesite	stages: 1-5
Heat exchanger	HEATEXM1/XM2/XM3/XM4/M1M	RGibbs	Heat exchanging among CCM and air	Cooling stages: 1-4
Heater	HEATERs 1-4, 1M-4M, 1R-4R	Heater	Heating or cooling a single stream	/

Figure 3.6A depicts the Aspen Plus flow chart of the TBFC with four-stage cooling and five-stage preheating. The magnesite feedstock with 10 wt.% water is fed to a RGibbs-mode heat exchanger (i.e., the 5th-stage preheater) where it is dried by the flue gas from the 4th-stage preheater. In turn, the magnesite is separated from the flue gas by the setup "Assign Streams" in the RGibbs model. The flue gas from the 5th-stage preheater is directed to a heater model and cooled to ambient temperature. As such, its sensible heat loss is calculated. Similarly, the RGibbs model arranges the magnesite from the 5th-stage and 4th-stage preheaters to be respectively preheated by the flue gas from the 3rd-stage and 2nd-stage preheaters, which are implemented respectively in the 4th-stage and 3rd-stage preheaters. For the high-temperature 2nd and 1st stages of preheaters, the possible pre-decomposition of magnesite is considered on basis of the kinetics obtained by MFBRA, for which the RCSTR model is adopted. The magnesite from the 3rd-stage preheater is first mixed with the flue gas from the 1st-stage preheater in the Mixer model. Separated from flue gas by the SSplit model, the magnesite goes to the 2nd-stage RCSTR-modeled preheater. Passing through another SSplit model, the CO_2 generated by pre-decomposition is merged into the flue gas from the 2nd-stage

preheater. The possibly partially decomposed magnesite from the 2nd-stage preheater undergoes further a heat exchange by contacting the flue gas from the calciner. This is succeeded by the gas-solid separation and also magnesite pre-decomposition in the RCSTR of the 1st-stage preheater. Its CO_2 product is merged into the flue gas from the 1st-stage preheater.

The final magnesite from preheating is transported into the RStoic reactor to implement calcination. The fuel combustion occurs in three stages and their respective conversions are 30%, 30% and 40%, respectively. Downstream of the gas-solids separation at the calciner exit, the high-temperature CCM is mixed with the air from the 3rd-stage cooler and goes into the 4th-stage RGibbs-mode cooler, another cyclone in fact. The preheated air from the 4th-stage cooler is directed to the RStoic model to combust fuel gas. On the other hand, the CCM from the 4th-stage cooler successively undergoes three stages of cooling (i.e., the 3rd to 1st stages of coolers) by heat exchange with air according to the RGibbs-mode coolers. The CCM finally from the 1st-stage cooler is the product, which is usually cooled down to ambient temperature by the air blowing it into the product tank.

As shown in **Figures 3.6**B and 3.6C, in comparison with the TBFC the RF has not staged combustion and CCM cooling whereas the MFC has two-stage preheating for magnesite and one-stage cooling for CCM although without fuel-staged combustion. The main parameters for simulating RF and MFC are also tabulated in **Table 3.2**. Considering industrial application, the energy efficiency of an entire system becomes

critical. We estimate the following energy efficiency to quantitatively analysis the efficiency of CCM production.

$$\text{Energy efficiency} = (Q_{FG\ HHV} - Q_{fl} - Q_m) / Q_{FG\ HHV} \times 100\% \quad (3.3)$$

where $Q_{FG\ HHV}$ is energy input from fuel gas based on higher heating value, Q_{fl} and Q_m are sensible heat loss of exhausted final flue gas and CCM, respectively. In order to well illustrate the superiority of the TBFC process over RF and MFC, the energy allocation analysis is also performed and discussed in the coming sections of this article.

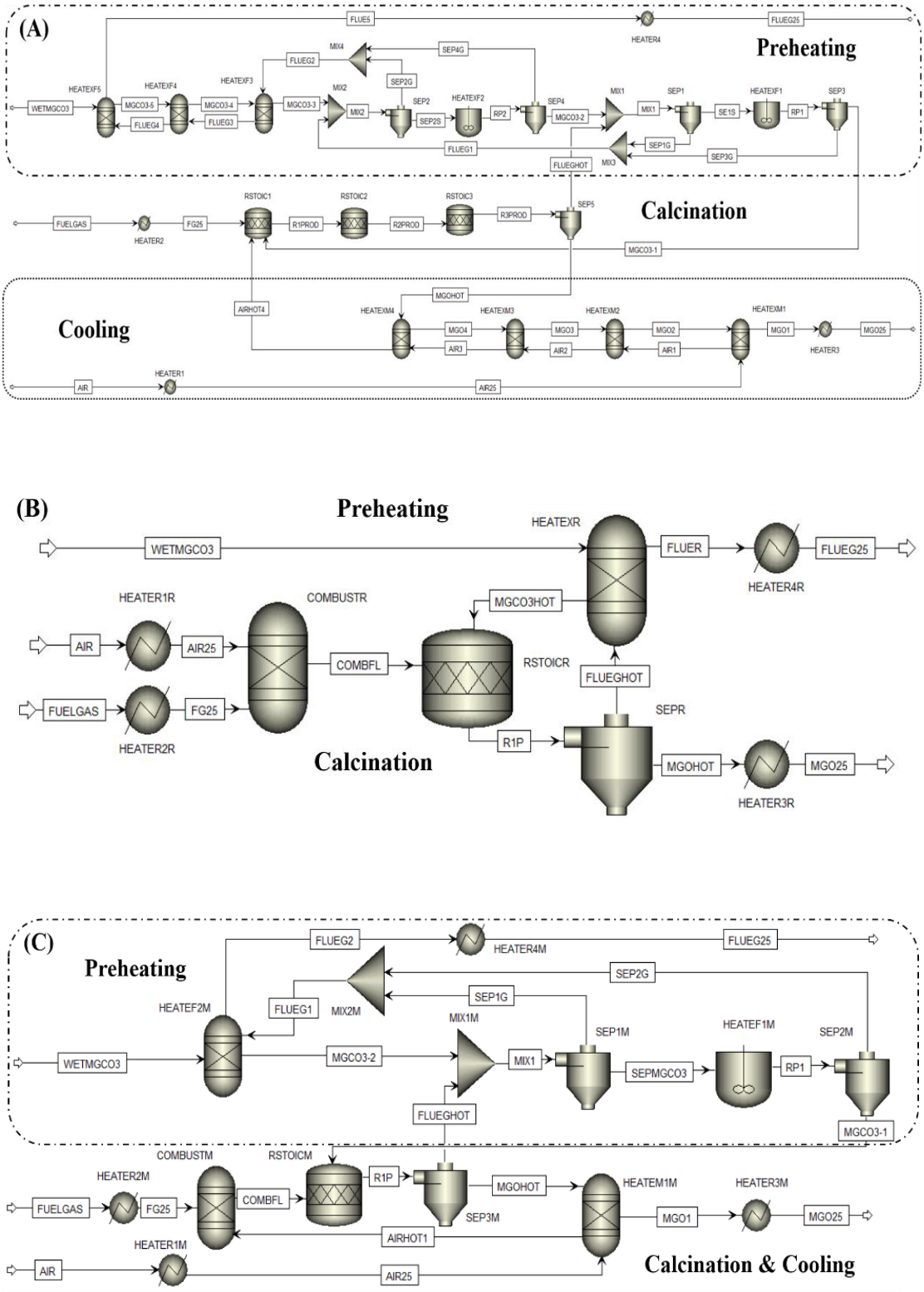

Figure 3.6 Aspen Plus flow charts of (A) TBFC with four-stage cooling and five-stage preheating, (B) RF and (C) MFC.

3.3 Results and discussion

3.3.1 Energy consumption and efficiency

Figure 3.7 illustrates the influences of different stages of cooling and preheating on energy consumption and efficiency of TBFC. The energy consumption decreases with the increase in the number of preheating and cooling stages. In the case of one-stage cooling, the consumption of energy obviously decreases from about 5975 to 4178 kJ/kg-CCM while increasing the preheating stages from 1 to 5. Further increasing the cooling stages from 1 to 2 (at 5 stages of preheating), the energy consumption is reduced to about 3913 kJ/kg-CCM.

Concerning the energy efficiency, it raises from about 49.7% to 72.8% when varying the preheating stages from 1 to 5 at 4 stages of cooling. With five-stage preheating, increasing the cooling stages from 1 to 4 varies the energy efficiency from about 65.0% to 72.8%. However, the more the heat-exchange stages, the lower the increased energy efficiency. When the cooling stages are from 1 to 2, the energy efficiency increase is 2.4%-4.3% corresponding to the preheating stages of 1 to 5. Further having the cooling stages from 2 to 4, the efficiency rise is only 1.4%-3.4%. Thus, 2 stages of cooling are preferred for industrial application. Also, increasing the magnesite-preheating stages is more dominant in raising the energy efficiency than having more CCM-cooling stages does. Correspondingly to cooling stages 1 to 4, the two-stage preheating raises the energy efficiency by 8.5%-10.2% against one preheater does. Varying the preheating stages from 2 to 3, 3 to 4 and 4 to 5, the gained increases

in energy efficiency is 4.8%-5.9%, 3.5%-4.1% and 2.4%-2.8%, respectively. By considering the available efficiency rise, the industrial application thus prefers 4 stages of preheating. These results show that the number of heat-exchange stages has vital influence on the energy consumption and efficiency of the TBFC process.

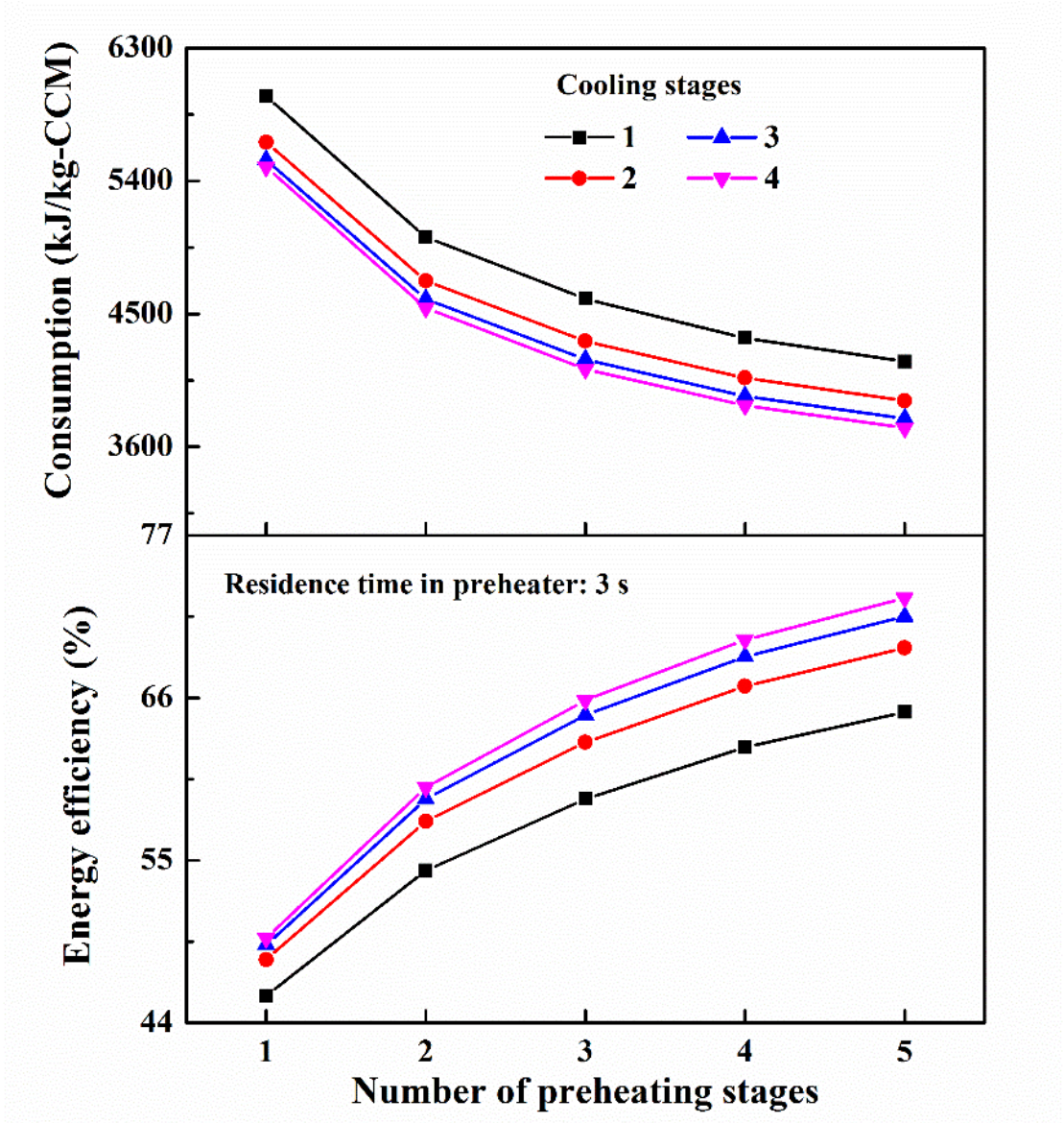

Figure 3.7 Energy consumption and efficiency of TBFC varying with number of preheating and cooling and stages.

3.3.2 Pre-decomposition in preheating

Figures 3.8 and **3.9** show the results of magnesite pre-decomposition and corresponding temperatures of magnesite in the first and second stage of preheaters, respectively. In the 1st-stage preheater, the maximal conversion of pre-decomposition is 12-13% for a five-stage preheating process. Increasing the cooling stages slightly decreases the pre-decomposition conversion of magnesite. Having more cooling stages is good for the sensible heat utilization of CCM, thus lowering the energy consumption. As such, less energy of flue gas can be used in the heat-exchange with magnesite. **Figure 3.8**B shows that the temperatures of magnesite from the 1st-stage preheater slightly decreases with increasing the stages of cooling. The magnesite temperatures in cases of two-stage and three-stage cooling which are not shown are between those of one-stage and four-stage cooling. The pre-decomposition cased obvious decrease in the magnesite temperature (of the 1st-stage preheater). The more the preheating stages, the greater the temperature decrease (in the 1st-stage stage) due to pre-decomposition. When the five-stage preheating is adopted, the maximal temperature reduction is over 150 °C. On the contrary, the increase in pre-decomposition becomes smaller with the more the preheating stages. The pre-decomposition of magnesite cannot occur if only one preheater is installed and the reached temperature of magnesite is below the required least value for occurring decomposition (i.e., about 500 °C). The number of preheating stages plays the controlling role in increasing the energy efficiency than the cooling stage number does. The pre-decomposition of magnesite should be considered

especially in the case with a few of preheaters.

The pre-decomposition of magnesite occurs in the 2nd-stage preheater only for the 4 and 5 stages of preheating since its temperature (shown in **Table 3.3**) can hardly reach the pre-decomposition requirement for the case with fewer preheating stages. **Figure 3.9**A shows the pre-decomposition conversion of magnesite in the 2nd-stage preheater, which increases as more preheating and fewer cooling stages are adopted. This is consistent with the result for the 1st-stage preheater. The conversion of magnesite pre-decomposition in the 2nd-stage preheater is below 3% for the four-stage preheating process and are no more than 5.0% even in the cases with five stages of preheating. In **Figure 3.9**B, the maximal temperature reduction in the 2nd-stage preheater due to pre-decomposition is about 90 °C, suggesting that the effect of pre-decomposition on the 2nd-stage preheater is much smaller than that in the 1st-stage preheater.

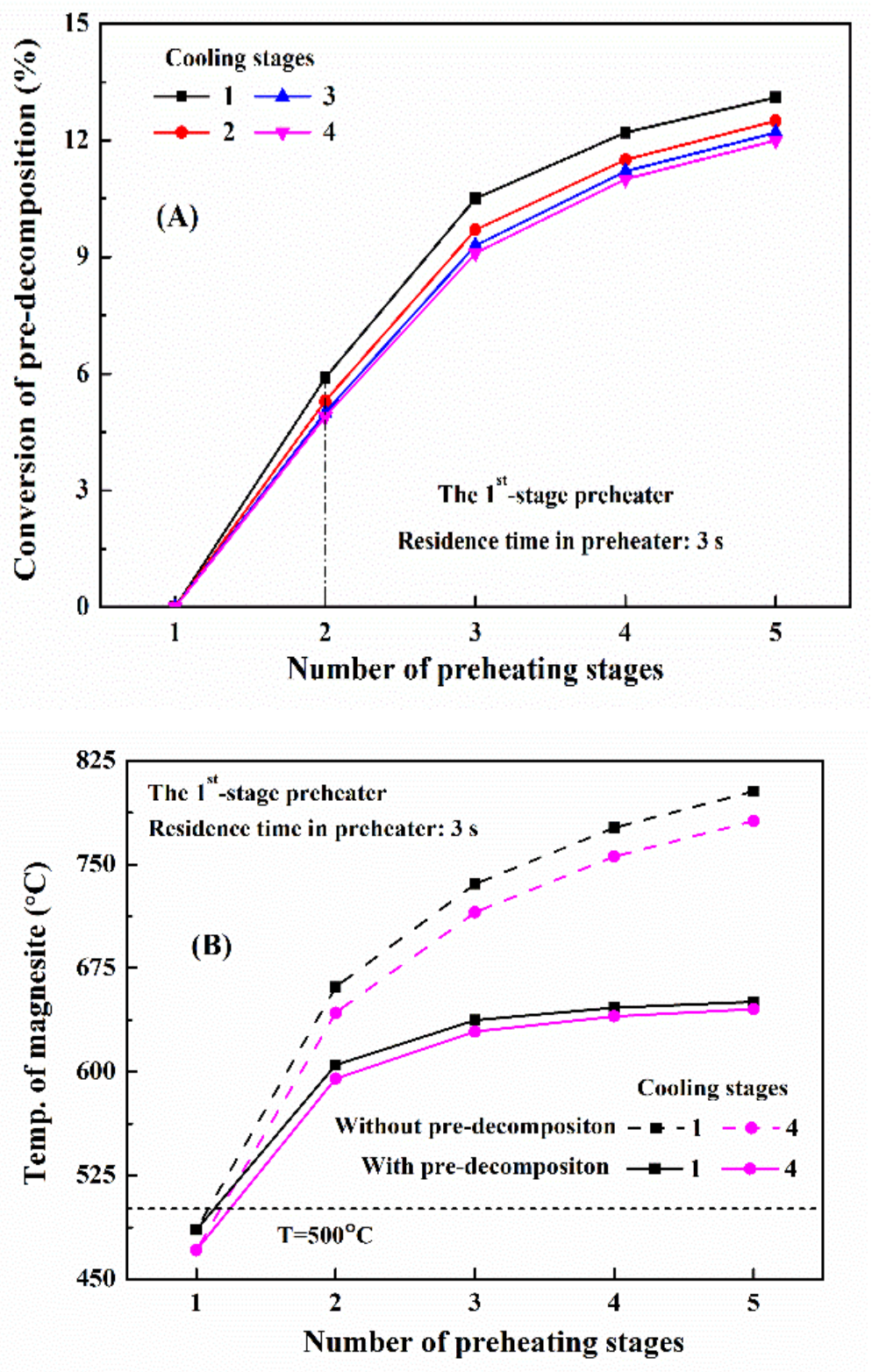

Figure 3.8 Pre-decomposition of magnesite in the 1st-stage preheater at different preheating and cooling stages: (A) conversion and (B) temperature of magnesite.

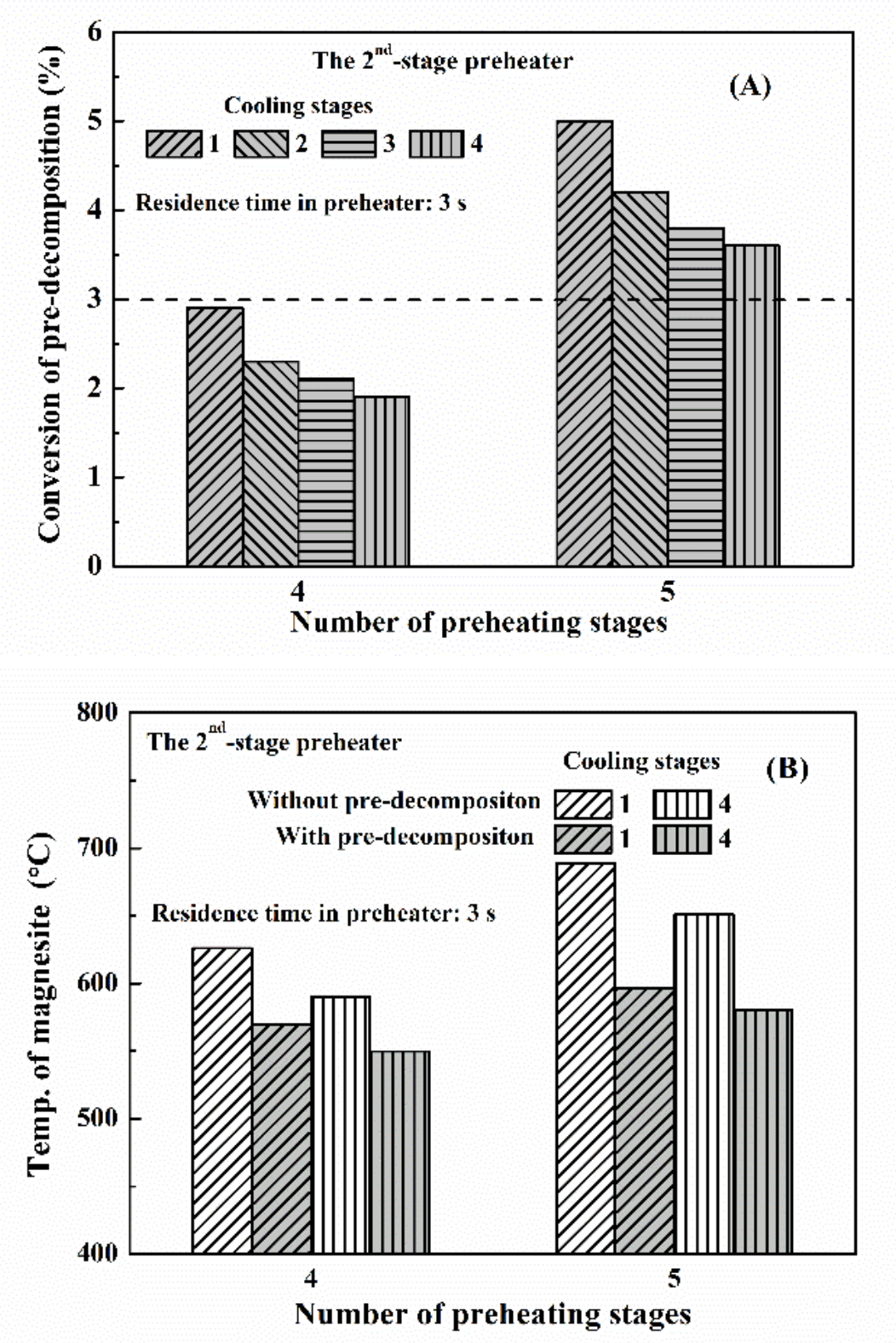

Figure 3.9 Pre-decomposition of magnesite in the 2nd-stage preheater at different preheating and cooling stages: (A) conversion and (B) temperature of magnesite.

3.3.3 Temperature variation in process

Figure 3.10 shows the flue gas temperatures before and after drying and the CCM temperature from the 1st-stage cooler varying with the preheating and cooling stages. With the increase in the preheating and cooling stages, the flue gas temperature shows obvious decrease both before and after the drying to indicate higher energy utilization. For two-stage and three-stage cooling, the corresponding flue gas temperatures before and after drying which are not shown are also between those of one-stage and four-stage cooling with similar trend. The minimal temperature reduction by drying process is about 230 °C. The temperature of dried magnesite in the five-stage preheating system is already below 100 °C. This would be the limit for the industrial application.

On the contrary, the temperature of CCM from the 1st-stage cooler (the final CCM) increases with the increase of preheating stages, while the more the cooling stages lead to lower temperature of the final CCM. The temperature of final CCM is over 300 °C if only one-stage cooling is used, whereas it can be 50-110 °C in the case of four-stage cooling. Thus, the number of cooling stages is mainly responsible for the temperature of final CCM. **Table 3.3** summarizes the temperature of solid in individual stages in various possible strategies of heat recovery and utilization so as to provide useful reference data for industrial design. For applied process of TBFC, the preferred stages for magnesite preheating and CCM cooling would be 4 and 2, respectively.

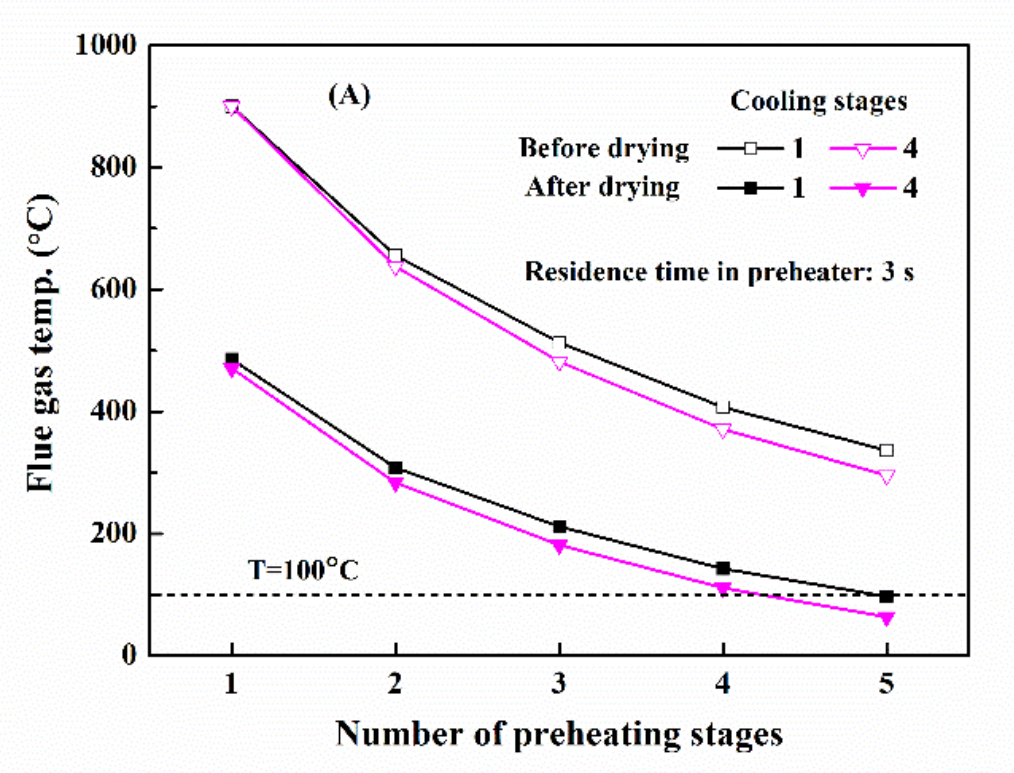

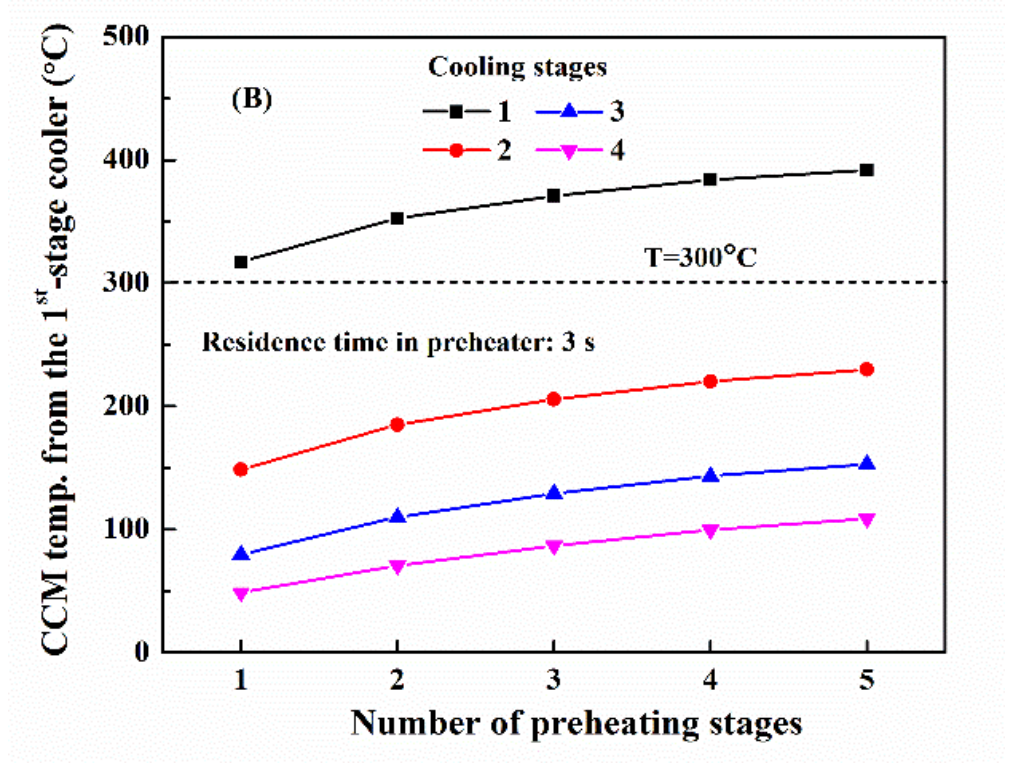

Figure 3.10 Influences of the cooling stage number and the preheating stage number on (A) flue gas temperatures before and after drying and (B) the CCM temperature from the 1st-stage cooler.

Table 3.3 Temperatures of solid in individual stage under different arrangement strategies.

Cooling stages	Preheating stages	Solid temperatures in individual heat-exchange stages (°C)								
		Preheating					Cooling			
		5	4	3	2	1	4	3	2	1
1	1	/	/	/	/	486	317	/	/	/
	2	/	/	/	308	605	353	/	/	/
	3	/	/	211	513	638	371	/	/	/
	4	/	143	407	570	646	384	/	/	/
	5	97	336	507	597	651	392	/	/	/
2	1	/	/	/	/	476	408	149	/	/
	2	/	/	/	293	599	462	185	/	/
	3	/	/	193	495	633	490	206	/	/
	4	/	124	387	558	643	509	220	/	/
	5	77	313	485	588	648	521	230	/	/
3	1	/	/	/	/	473	445	392	80	/
	2	/	/	/	287	597	512	260	110	/
	3	/	/	185	486	630	547	295	129	/
	4	/	116	377	553	641	570	319	143	/
	5	68	302	475	583	646	584	335	153	/
4	1	/	/	/	/	471	461	222	104	49
	2	/	/	/	284	595	537	299	155	71
	3	/	/	181	482	629	577	344	188	87
	4	/	111	371	550	640	603	375	213	100
	5	63	295	469	580	645	620	396	230	109

3.3.4 Effect of residence time in each preheater

The preceding pre-decomposition of magnesite supposes that the kinetic rate is substantially quick and the reaction is limited only by temperature. The effect of residence time varying in 1 to 5 s in combination with the reaction kinetics is considered herein for the system having two-stage cooling. Noting that the pre-decomposition occurs mainly in the first stage of preheating, the analysis is further simplified by considering only the 1st-stage preheater. **Figure 3.11**A clarifies that the longer the residence time is, the higher the conversion of magnesite pre-decomposition is. Nonetheless, extending the residence time (but above 1 s considering the actual possible values in the cyclone reactors) caused limited increase in pre-decomposition conversion. The conversion is below 10% for the residence time of 1s, while the maximal conversions of pre-decomposition are 12.5% and 14% for the residence times of 3 s and 5 s in the five-stage preheating system, respectively.

Figure 3.11B shows the corresponding temperatures of magnesite in the 1st-stage preheater in cases without and with pre-decomposition, decrease with the increase of residence time since the pre-decomposition is an adiabatic process. Obviously, the longer the residence time is, the greater the temperature reduction due to pre-decomposition in the first stage is. The maximal temperature reduction for the residence time of 5 s is around 160 °C.

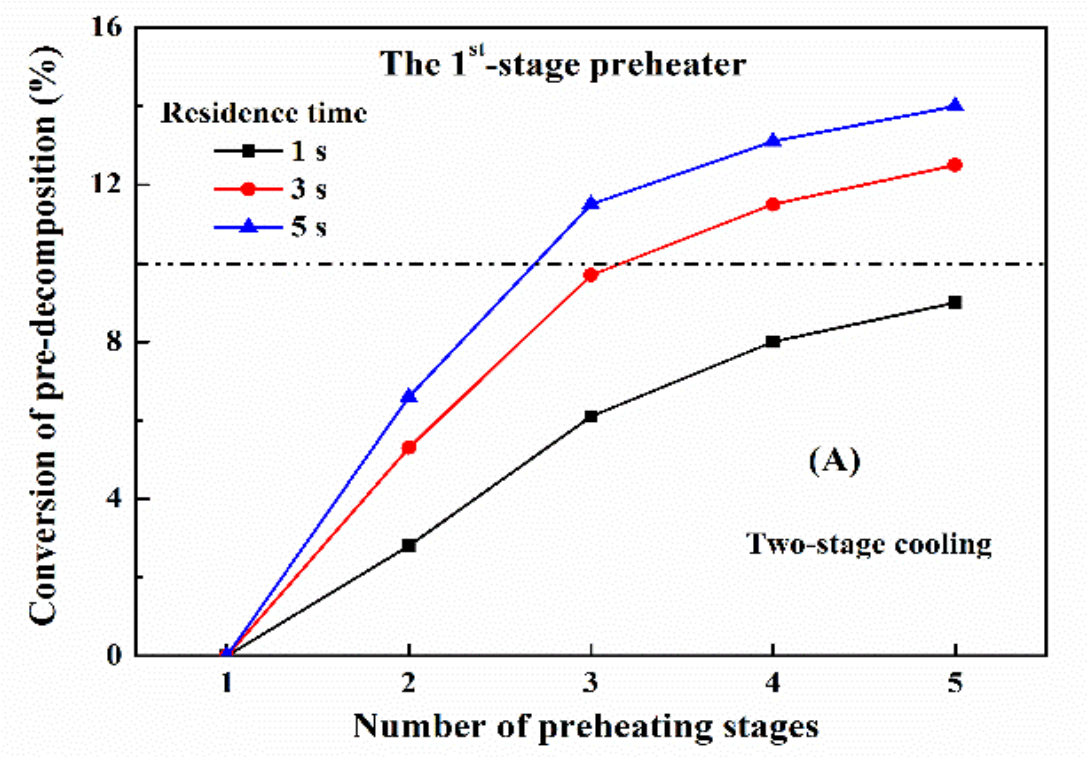

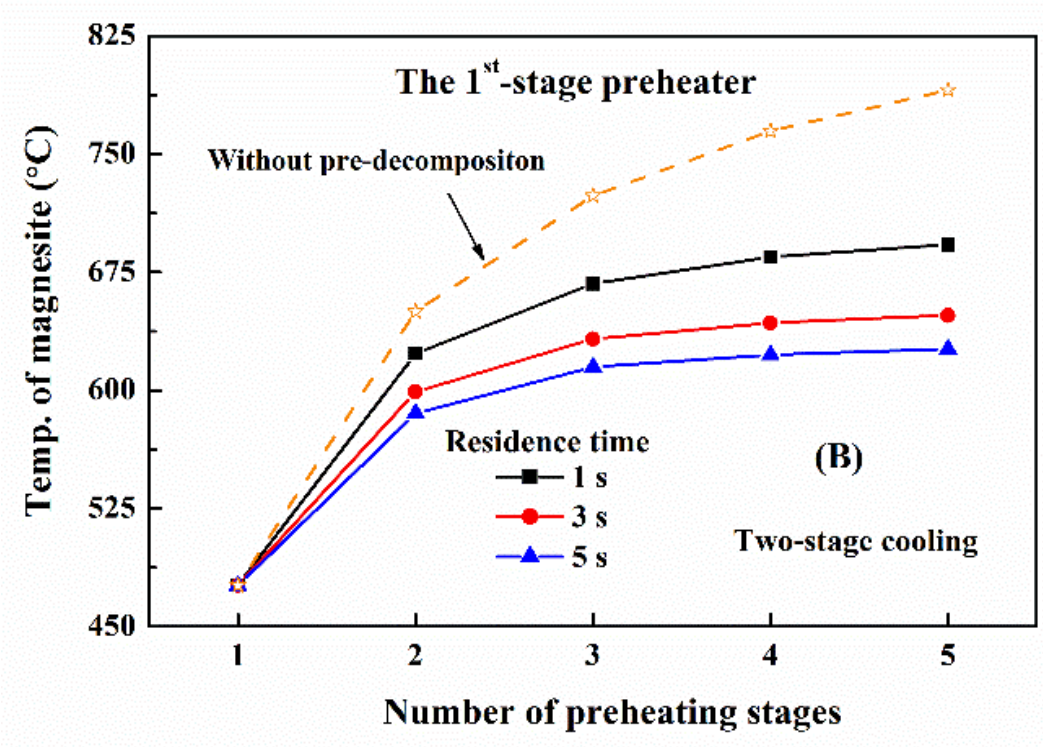

Figure 3.11 Variations with residence time of (A) conversion of magnesite pre-decomposition and (B) temperature of magnesite in the 1st-stage preheater.

Figure 3.12 shows the variation in temperature and energy efficiency of the TBFC with five stages of preheating that would lead to the most obvious pre-decomposition of magnesite. There are different influences of residence time on the temperatures of flue gas before and after drying and on the temperature of the final CCM. While longer residence time causes lower flue gas temperatures before and after drying, the temperature of CCM product becomes very slightly higher (see **Figure 3.12**A). The results correspond to the slightly higher conversion of magnesite pre-decomposition, which thus requires slightly less fuel gas for the calciner and consequently generates slightly lower volume of flue gas as well. For a specified treatment capacity, the temperatures of flue gas then must be slightly lower after its heat exchange with the fed magnesite. As a consequence, in **Figure 3.12**B the energy consumption decreases and the energy efficiency increases, although slightly, with raising the residence time from 1 s to 5 s.

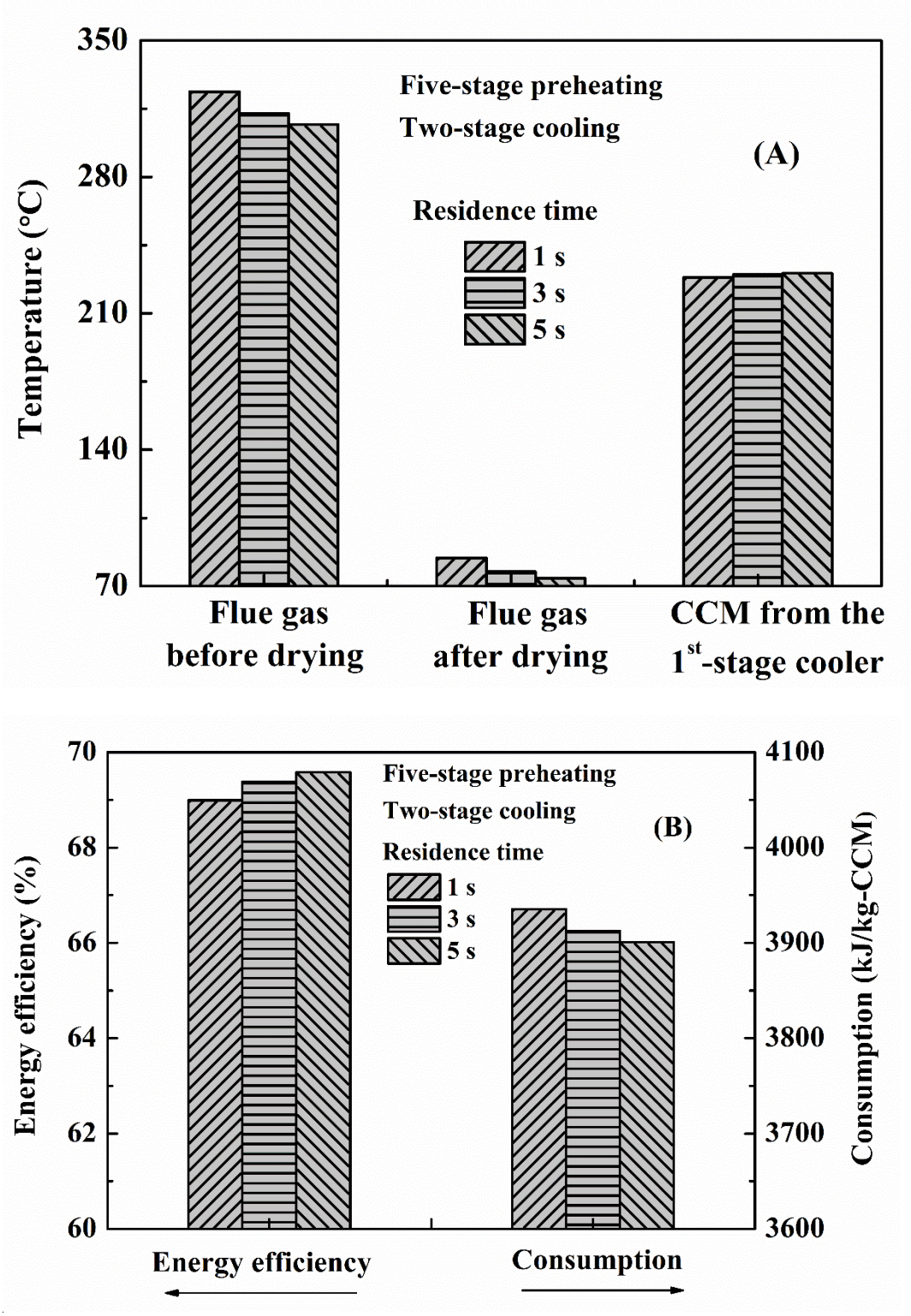

Figure 3.12 Variations with residence time of (A) characteristic temperatures and (B) energy consumption and efficiency corresponding to the conditions in Fig. 3.11.

3.3.5 Benchmark and application for light calcination

Comparison is made for the energy consumption and efficiency of the technologies represented by TBFC, MFC and RF. The TBFC process has two-stage cooling for CCM and four-stage preheating for fed magnesite. Simulations were performed according to the Aspen models shown in **Figure 3.6**. The estimated energy consumptions are about 4100, 7600, and 8400 kJ/kg-CCM, while the corresponding energy efficiencies are 66.8%, 37.2%, and 33.9% for the TBFC, MFC and RF processes, respectively. In order to further illustrate the superiority of the TBFC process over the MFC and RF, **Figure 3.13** shows further the allocations of consumed energy for the benchmarked technologies. Because there is not CCM cooling in RF, the energy loss via the sensible heat of CCM takes about 9.3%, which is much higher than that for TBFC (4.6%) and MFC (2.0%). For the MFC and RF processes, the energy losses via flue gas reaches about 60.8% and 56.8%, whereas this loss via flue gas can be as low as 28.6% for TBFC.

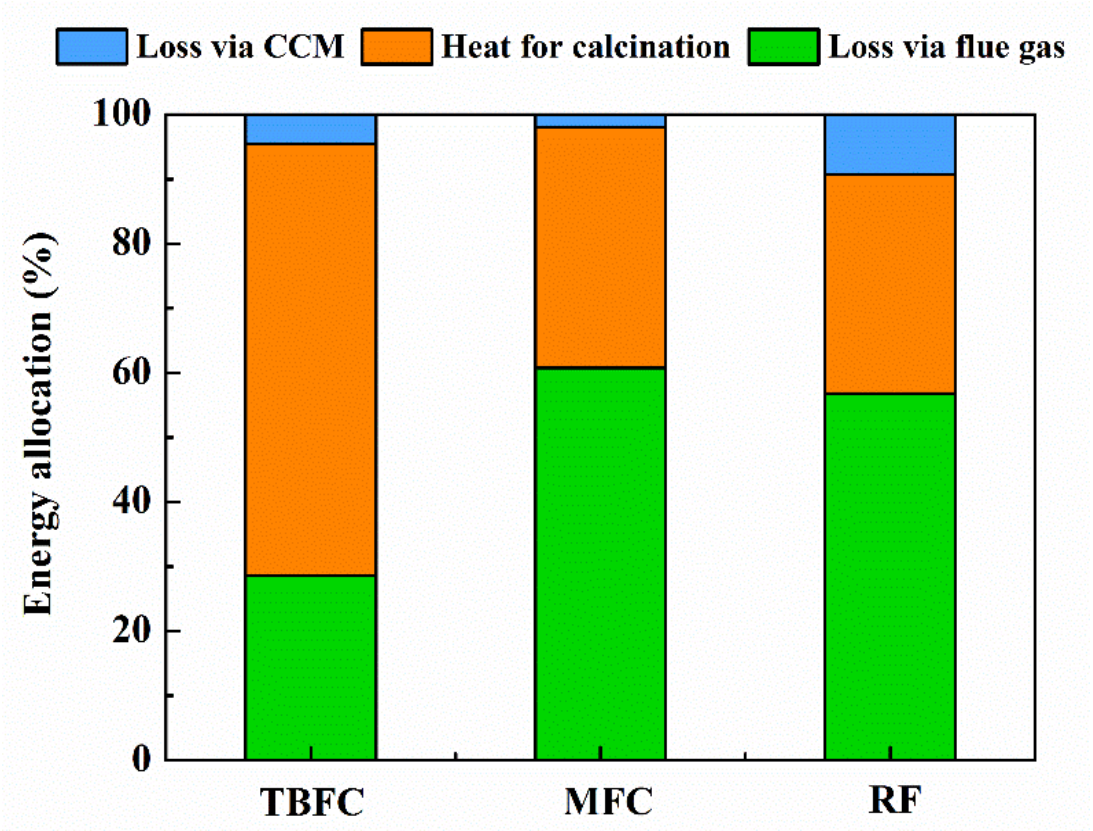

Figure 3.13 Allocation of consumed energy in processes of TBFC, MFC and RF.

Therefore, the heat loss via flue gas accounts for the major part of the consumed energy for MFC and RF, which is much higher than the loss via high-temperature CCM. For TBFC, the staged combustion of fuel gas ensured essentially the possibly lowest amount of flue gas, which contributes energy saving also via flue gas. Overall, the TBFC process saves energy by staged combustion of fuel gas, and further by the recovery and reutilization of the sensible heat carried with the calciner flue gas as well the CCM particles. The traditional RF and MFC technologies, however, are not integrated with such energy saving strategies thus causing its higher energy consumption and lower energy efficiency. As a consequence, the TBFC process occupies the obvious superiority as the stage-of-the-art technology for light calcination

of magnesite. Because of this, a demonstration plant of TBFC with a capability of 400,000 t/a magnesite is under construction in Liaoning province, China (shown in **Figure 3.14**), and it is going to be commissioned into commercial running in 2021.

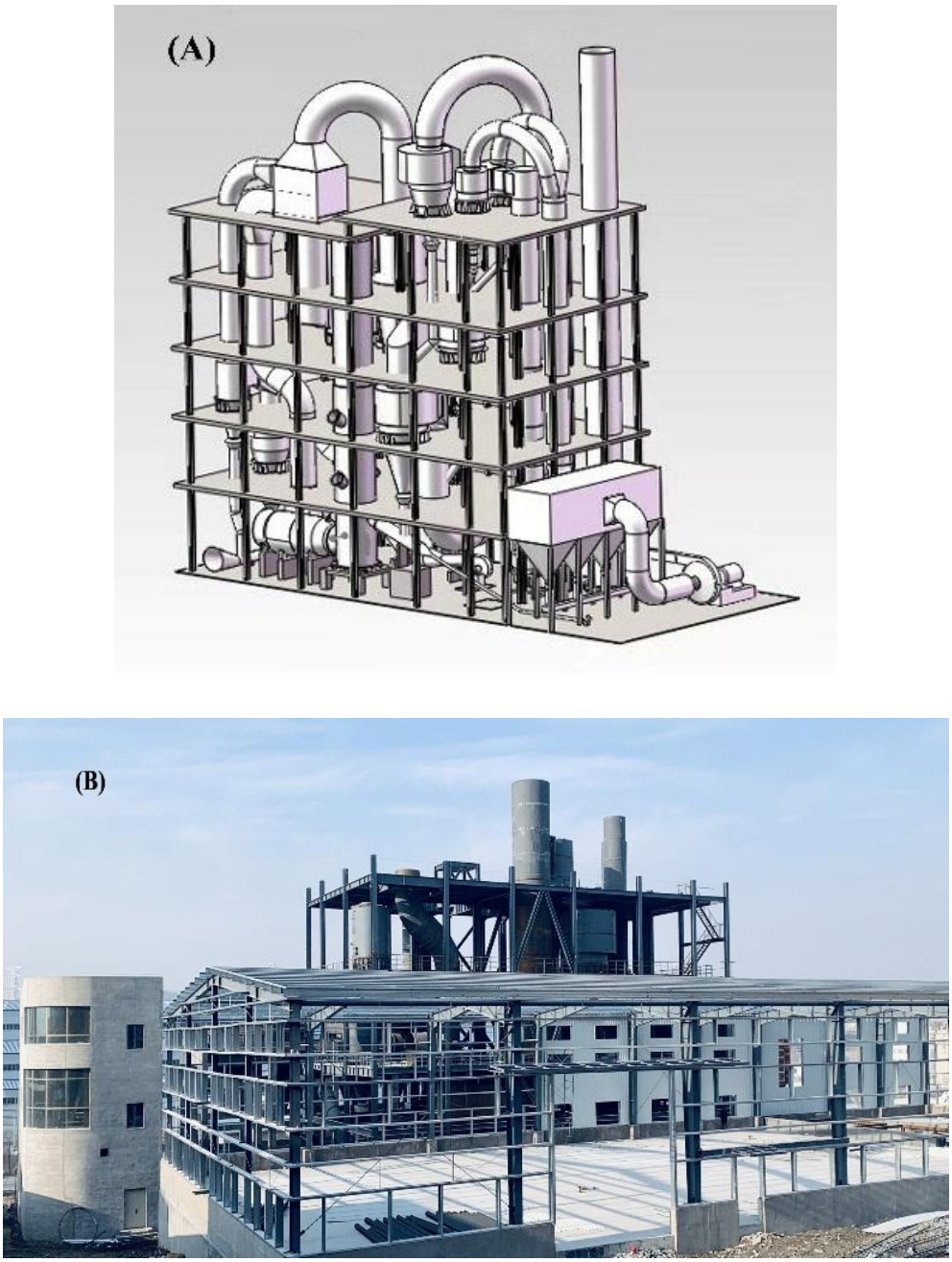

Figure 3.14 A demonstration plant under construction for TBFC: (A) three-D design and (B) a picture of plant site.

3.4 Conclusions

The so-called transport bed flash calcination (TBFC) process applied to magnesite has been systematically investigated via process simulation to optimize the energy-saving strategy for the technology. The process is featured with the staged combustion of fuel gas and the recovery, with further its reutilization inside the process of the sensible heat carried by the flue gas of calciner and also by the high-temperature caustic calcined magnesia (CCM) product. The lower energy consumption and higher energy efficiency are well identified for the investigated TBFC process in comparison with the traditional but typical reverberatory furnace (RF) and magnesite flash calciner (MFC).

Pre-decomposition of magnesite by the high-temperature calciner flue gas is considered on basis of the kinetics measured using a micro fluidized bed reaction analyzer (MFBRA) that allows the minimized effect of external diffusion on reaction. The result reveals that the pre-decomposition mainly occurs in the first stage of preheaters, and the maximal conversion under the cyclone preheating model conditions of this article is about 13%. The occurrence of pre-decomposition would slightly lower the energy consumption and increase the energy efficiency of the entire process while the residence time of magnesite above 1 s in the cyclone preheaters has limited effect on the available pre-decomposition rate.

Varying the number of preheating stages causes more pronounced rise in the energy efficiency than adjusting the same number of cooling stages does. In fact, the sensible heat carried with the calciner flue gas is much more, say by about 6 times, than with

the high-temperature CCM. The TBFC adopts staged feed of fuel gas along the calciner to allow the air equivalence ratio of about 1.2 for fuel gas combustion. This in turn reduces the volume of flue gas and contributes greatly the energy conservation. For TBFC, the preferred process arrangement is proved to be four-stage preheating for magnesite and two-stage cooling for CCM, and the corresponding energy consumption is about 4100 kJ/kg-CCM and energy efficiency is 66.8%. Comparing with the traditional light calcination furnaces such as the popularly used RF, the energy efficiency is almost doubly higher, say, from 34% to about 67%.

References

1. L. Wang, P. Tai, C. Jia, X. Li, P. Li, X. Xiong, Magnesium contamination in soil at a magnesite mining region of Liaoning province, China, Bull Environ. Contam. Toxicol. 2015, 95, 90-96.
2. L. Xiao, S. Dai, Introduction on the status of magnesite and its benefication methods in China (in Chinese), Non-ferrous Min. Metall. 2017, 33, 29-31.
3. Z. Zhao, X. Cui, D. Wang, Y. Chen, G. Bai, J. Li, X. Liu, Review of the metallogenie regularity of magnesite deposits in China, Acta Geol Sin-Engl. 2015, 89, 1747-1761.
4. Y.Quan, Production and application of magnesia refractories (in Chinese), Metallurgical Industry, Beijing, 2008.

5. Q. Chen, T. Wei, Status and prospect of China's magnesia raw materials (in Chinese), Refractories 2013, 47, 210-214.

6. N. José, H. Ahmed, B. Miguel, E. Luís, de B. Jorge, Magnesia (MgO) production and characterization, and its influence on the performance of cementitious materials: a review, Materials 2020, 13, 4752.

7. A.A. Pilarska, Ł. Klapiszewski, T. Jesionowski, Recent development in the synthesis, modification and application of $Mg(OH)_2$ and MgO: a review, Powder Technol. 2017, 319, 373–407.

8. G. Li, Z. Li, Y. Guo, F. Wu, N. Xu, Effect of calcination temperatures on microstructure and activity light burned magnesite powder (in Chinese), Refractories 2016, 50, 367-369.

9. W. Ren, B. Xue, C. Lu, Z. Zhang, Y. Zhang, L. Jiang, Evaluation of GHG emissions from the production of magnesia refractory raw materials in Dashiqiao, China, J. Clean. Prod. 2016, 135, 214-222.

10. L. Mo, M. Deng, M. Tang, A. Al-Tabbaa, MgO expansive cement and concrete in China: past, present and future, Cem. Concr. Res. 2014, 57, 1-12.

11. J. Zhu, N. Ye, J. Yang, Evaluation methods on corrected hydration activity in preparation of active MgO with calcined magnesite (in Chinese), Metal Mine 2013, 11, 88-91.

12. Q. Gao, G. Wei, X. Jiang, H. Zheng, F. Shen, Characteristics of calcined magnesite and its application in oxidized pellet production, J. Iron Steel Res. Int. 2014, 21, 408-412.

13. E. Tsiplakou, A. Pappas, C. Mitsiopoulou, M. Georgiadou, C.A. Georgiou, G. Zervas, Evaluation of different types of calcined magnesites as feed supplement in small ruminant, Small Ruminant Res. 2017, 149, 188-195.

14. N. Yang, P. Ning, K. Li, J. Wang, MgO-based adsorbent achieved from magnesite for CO_2 capture in simulate wet flue gas, J. Taiwan Inst. of Chem. E. 2018, 86, 73-80.

15. S.D. Stefanidis, S.A. Karakoulia, K.G. Kalogiannis, E.F Iliopoulou, A. Delimitis, H. Yiannoulakis, T. Zampetakis, A.A. Lappas, K.S. Triantafyllidis, Natural magnesium oxide (MgO) catalysts: a cost-effective sustainable alternative to acid zeolites for the in situ upgrading of biomass fast pyrolysis oil, Appl. Catal. B: Environ. 2016, 196, 155-173.

16. L. Mo, D.K. Panesar, Effects of accelerated carbonation on the microstructure of Portland cement pastes containing reactive MgO, Cement Concrete Res. 2012, 42, 769-777.

17. H. Ba, L. Bai, W. Zhao, Y. Ma, X. Yin, Review on preparation and processing of caustic calcined magnesite (in Chinese), Conserv. Util. Miner. Resour. 2017, 1, 84-89.

18. J. Li, Y. Zhang, S. Shao, S. Zhang, S. Ma, Application of cleaner production in a Chinese magnesia refractory material plant, J. Clean. Prod. 2016, 113, 1015-1023.
19. H. Li, M. Li, The choice and application of pollution control technique on flue dust from light sintering magnesium kiln (in Chinese), Environ. Prot. Sci. 1997, 2, 8-10.
20. Z. Li, Thoughts on magnesia refractory raw materials of Liaoning Province (in Chinese), Refractories 2011, 45, 382-385, 389.
21. D. Xu, Q. Jia, Study on the residence time distribution of powder in magnesite flash calciner (in Chinese), J. Xi'an U. Archit. Technol. 1987, 4, 95-100.
22. W. Jiang, W. Hao, X. Liu, Z. Han, J. Yue, G. Xu, Characteristic and kinetics of light calcination of magnesite in micro fluidized bed reaction analyzer (in Chinese), CIESC J. 2019, 70, 2928-2937.
23. C. Sun, B. Yan, C. Cai, Z. Han, G. Xu, Characteristics of reaction and product microstructure during light calcination of magnesite in transport bed (in Chinese), CIESC J. 2020, 71, 5735-5744.
24. X. Liu, G. Xu, S. Gao, Micro fluidized beds: wall effect and operability, Chem. Eng. J. 2008, 137, 302-307.
25. F. Wang, X. Zeng, S. Geng, J. Yue, S. Tang, Y. Cui, J. Yu, G. Xu, Distinctive hydrodynamics of a micro fluidized bed and its application to gas-solid reaction analysis, Energy Fuels 2018, 32, 4096-4106.

26. Y. Guo, Y. Zhao, S. Meng, D. Feng, T. Yan, P. Wang, S. Sun, Development of a multistage in situ reaction analyzer based on a micro fluidized bed and its suitability for rapid gas-solid reactions, Energy Fuels 2016, 30, 6021-6033.

27. X. Yang, Y. Liu, J. Yu, F. Jiang, Y. Han, G. Xu, W. Ge, Numerical simulation of mixing characteristics of trace sample and bed material in micro fluidized bed reaction analyzer (in Chinese), CIESC J. 2014, 65, 3323-3330.

28. J. Yu, X. Zeng, J. Zhang, M. Zhong, G. Zhang, Y. Wang, G. Xu, Isothermal differential characteristics of gas-solid reaction in micro-fluidized bed reactor, Fuel 2013, 103, 29-36.

29. X. Zeng, F. Wang, Y. Wang, A. Li, J. Yu, G. Xu, Characterization of char gasification in a micro fluidized bed reaction analyzer, Energy Fuels 2014, 28, 1838-1845.

30. Z. Han, J. Yue, S. Geng, D. Hu, X. Liu, S.B. Suleiman, Y. Cui, D. Bai, G. Xu, State-of-the-art hydrodynamics of gas-solid micro fluidized beds, Chem. Eng. Sci. 2021, 232, 116345.

31. Y. Ji, X. Zeng, J. Yu, J. Yue, A. Li, G. Xu, Steam gasification characteristics of coal char in micro-fluidized bed reaction analyzer (in Chinese), CIESC J. 2014, 65, 3447-3456.

32. X. Liu, W. Hao, K. Wang, Y. Wang, P. An, H. Zhang, J. Yue, D. Bai, G. Xu, Acquiring real kinetics of reactions in inhibitory atmosphere containing product gases using micro fluidized bed, AIChE J. 2021, e17325.

33. Z. Han, J. Yue, X. Zeng, J. Yu, F. Wang, S. Sun, H. Yao, G. Luo, X. Liu, Y. Sun, F. Ding, L. Fu, L. Shi, K. Wang, J. Yang, S. Wang, X. Chen, D. Bai, G. Xu, Characteristics of gas-solid micro fluidized beds for thermochemical reaction analysis, Carbon Resour. Convers. 2020, 3, 203-218.

CHAPTER 4

Influence of flue gas atmospheres and pressures on $CaCO_3$ decomposition through simulation

4.1 Introduction

The micro fluidized bed reaction analyzer (MFBRA) was first proposed by Xu [1] in 2005. As a novel thermal analyzer, MFBRA has become commercially available and can be a complementary and reliable way for the characterization of gas-solid reactions after extensive researches and developments [2-4] besides thermogravimetric analyzer (TGA). To investigate the mechanisms and kinetics of gas-solid reactions , a fluidized bed reactor in millimeter diameter is used as the isothermal differential reactor in an MFBRA [5]. Until now, MFBRA has been well applied in a variety of gas-solid reactions, such as pyrolysis [6-8], gasification [9,10], combustion [11,12] of solid fuels, calcination [4,13] and reduction [14-17] as well as catalytic reactions [18,19]. These applications have verified that MFBRA is reliable, effective, and adaptable to various gas-solids reactions. Due to the minimized effect of external diffusion on reaction, MFBRA would give high-accuracy kinetic data than TGA does.

In Chapter 3, the kinetic parameters obtained by measuring magnesite calcination in air using MFBRA is adopted to perform the process simulation. While for the industrial calcination process of magnesite, due to the heat supply by the combustion of fuel gas, the calcination of magnesite actually occurs under the atmosphere of flue gas. The flue gas is mainly composed of CO_2, H_2O, O_2, N_2 and the inhibition on the

reaction by the produced CO_2 gas could occur. Thus, the kinetic parameters obtained by measuring magnesite calcination in flue gas atmosphere using MFBRA is hoped. While, the difficulties arose as how to distinguish between product gas CO_2 and fluidized gas CO_2 because the reaction kinetics data are determined based on the measurement of time-series of product gas species in MFBRA. Liu *et al.* [20] introduced the isotope-tagging method to the gas-solid reaction using MFBRA, which has been employed in the research of heterogenous catalytic reactions [21,22]. Liu *et al.* proposed the deliberate selection of the raw reactants with isotopes labeling so that the isotopes contained in the product gas are different from those contained in the same component in fluidizing gas. Unfortunately, $Mg^{13}CO_3$ was not available while the similar carbonate $Ca^{13}CO_3$ was available.

The $CaCO_3$ decomposition in the presence of CO_2 could be found in some situations of practical applications. For example, the calcium looping process, which is an advanced and popular combustion technology, mainly includes the CaO carbonation reaction (i.e. CaO reacts with CO_2 to produce $CaCO_3$) and the $CaCO_3$ calcination (i.e. $CaCO_3$ decomposes into CaO and CO_2 in the presence of CO_2) reaction [23,24]. According to a few researches reported [25-31], the kinetics of calcination are influenced by the presence of CO_2 in atmosphere while it is not yet fully demonstrated. It should be noted that the strong inhibition of diffusion and lower rates of heat and mass transfer may cause TGA to provide inaccurate kinetics for reactions which occur in the atmosphere of product gas as reported by several researchers [13, 32-35]. For example, the

apparent activation energy was obtained as unreasonably high as more than 2000 kJ/mol under the 100% CO_2 atmosphere, with the reaction time in a few minutes [36], which does not match the reaction time reported for fluidized bed experiments of chemical looping.

Thus, Liu *et al*. [20] obtained the kinetics of $Ca^{13}CO_3$ decomposition in the presence of CO_2 by MFBRA to acquire the correct kinetics of reactions inhibited by the product gas containing atmosphere. Their results demonstrated that the apparent activation energy of reaction was increased due to the presence of CO_2 in the atmosphere. However, the rise in the apparent activation energy was obviously overestimated by TGA due to the excessive inhibition by the stagnant product gas inside sample crucible. **Figure 4.1** showed the comparison of activation energy with CO_2 concentration obtained from TGA and MFBRA measurements. It could be found that the apparent activation energy obtained from both MFBRA and TGA rose with the increase of CO_2 concentration, but the rise was significantly faster for TGA than for MFBRA. The ratio of the activation energy tested from TGA to that tested from MFBRA, which showed the difference more clearly, increased from about 1.9 in N_2 to 3.7 in the atmosphere with only 1% CO_2 and it increased up to about 8 when the CO_2 in the atmosphere is further increased. These results indicated that with the increase of CO_2 concentration in atmosphere, the inhibition of product gas diffusion from TGA sample to the surrounding atmosphere became more seriously. In the 100% CO_2 environment, the TGA provided the activation energy of 2047.2 kJ/mol, which was obviously too high

to be thought as reasonable. In comparison, the reaction activation energy obtained from MFBRA was 271.5 kJ/mol, which was more in line with expectations. It should be noted that the moderate rise in the activation energy for MFBRA with the increase of CO_2 concentration was mainly owing to the impact of thermal equilibrium, which was confirmed below.

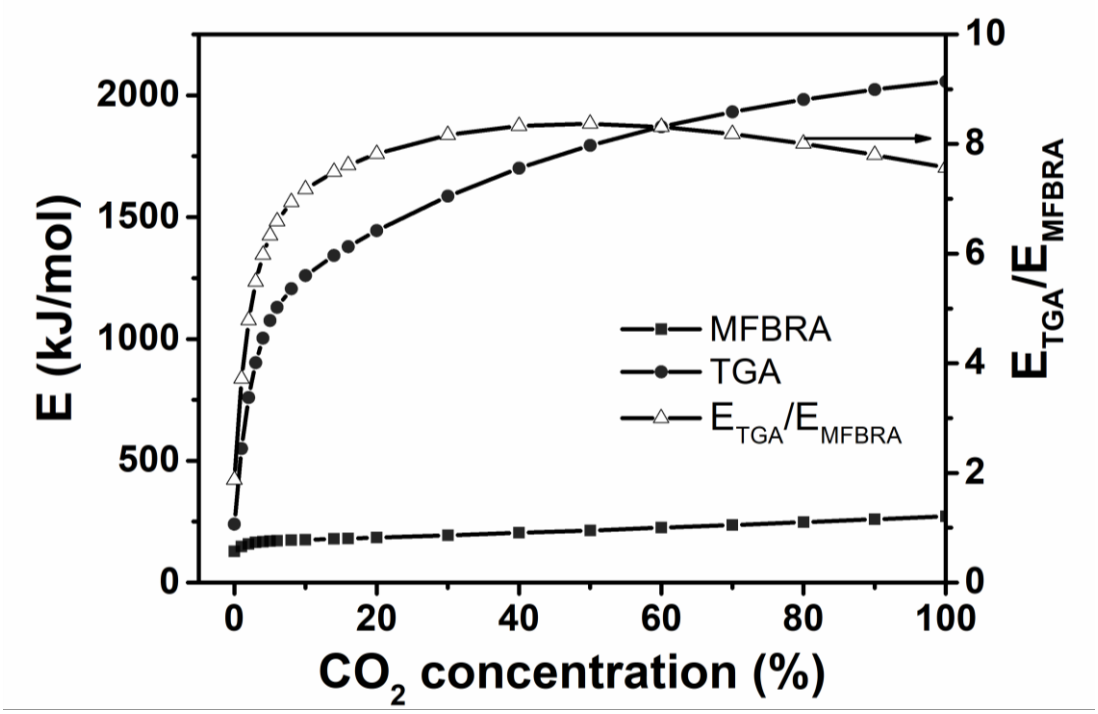

Figure 4.1 Relationship of activation energy with CO_2 concentration for $CaCO_3$ decomposition in MFBRA and in TGA. (Reprinted with permission from Ref 20).

Figure 4.2 showed the initial temperatures of $CaCO_3$ decomposition at different CO_2 concentrations obtained from TGA, MFBRA and simulation [20]. The process simulations for $CaCO_3$ decomposition at different CO_2 concentrations were conducted by Aspen Plus and the RGibbs model was adopted as the reactor to simulate the decomposition process. The CO_2 concentrations in a mixture of N_2 and CO_2 were

determined as 0 vol.%, 1 vol.%, 10 vol.%, 30 vol.%, 60 vol.% and 100 vol.%, respectively. It showed clearly that the initial temperature of $CaCO_3$ decomposition raised exponentially with the CO_2 concentration increasing. The initial decomposition temperature obtained by TGA was 580 °C in pure N_2, and it increased sharply to around 720 °C with only 1% CO_2 and further to about 935 °C in 100% CO_2. In comparison, for MFBRA, the initial decomposition temperatures obtained were lower than those obtained from TGA. The difference between MFBRA and TGA was 30 °C with 0% CO_2, and it rose up to about 100 °C with the CO_2 concentration over 10%. It is worth noting that the initial decomposition temperatures between MFBRA and thermal equilibrium simulation were quite close, which was consistent with the earlier analysis. It suggested that the gas diffusion in MFBRA was eliminated essentially and MFBRA was approaching to the real kinetics of reaction in the strongly suppressed atmospheres of product gas. Therefore, MFBRA was superior than TGA and was very capable of obtaining the real kinetics in such inhibitory atmospheres for the characterization of gas-solid reactions.

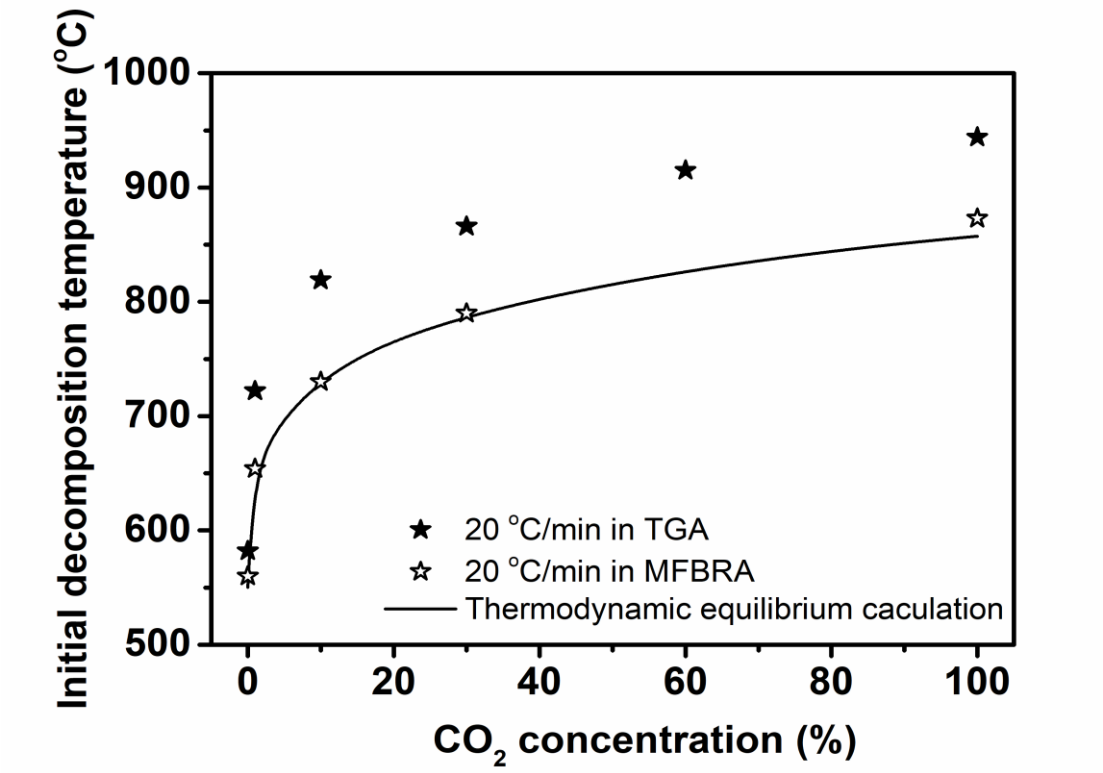

Figure 4.2 The initial temperature of $CaCO_3$ decomposition with different N_2/CO_2 mixtures at the heating rate of 20 °C/min in TGA, MFBRA and in the condition of thermodynamic equilibrium. (Reprinted with permission from Ref 20).

Following this, **Chapter 4** presents the detailed and comprehensive $CaCO_3$ decomposition under different flue gas atmospheres and different pressures through simulation to provide more fundamental and complete information for the reaction in the product gas which could strongly inhibited atmospheres and certain reference values for industrial applications.

4.2 Methods and models

For better understanding the influence of flue gas atmospheres and pressures on $CaCO_3$ decomposition, the simulations by Aspen Plus at a steady state condition were

conducted. Referred to the simulation results of the second work, herein, the two cases for different atmospheres of flue gas are considered. The flue gas from fuel gas combustion before magnesite calcination is considered as the case of flue gas 1 while the flue gas from fuel gas combustion also containing CO_2 produced by calcination is considered as the case of flue gas 2. The corresponding compositions of these two atmospheres are presented in **Table 4.1** and it is clear that the CO_2 concentration in flue gas 2 is much higher than that in the flue gas 1 while the other gases concentrations become lower consequently.

Figure 4.3 shows the Aspen Plus flow chart of decomposition of calcium carbonate. In the simulation, the types of $CaCO_3$ and CaO are selected as "solid" while the types of CO_2, H_2O, N_2, and O_2 are determined as "conventional". For the property, the IDEAL is employed as the base method. The RGibbs model is employed as the reactor to simulate decomposition process. For Aspen Plus simulations, the molar ratio of feeding flue gas and calcium carbonate is 9. The pressures of 0.1 atm, 0.5 atm, 1 atm, 5 atm, and 10 atm are determined for the influence of pressures on the decomposition of calcium carbonate.

Table 4.1 Composition of two different cases of flue gas.

Concentration (mol.%)	**Flue gas 1**	**Flue gas 2**
CO_2	8	32
O_2	4	3
N_2	72	53
H_2O	16	12

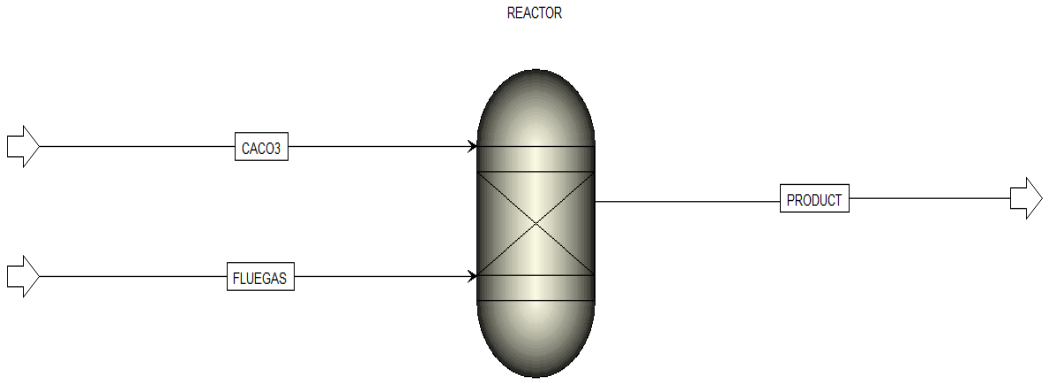

Figure 4.3 Aspen Plus flow chart of decomposition of calcium carbonate.

4.3 Results and discussion

4.3.1 Conversion and temperature in two different cases of flue gas

Figure 4.4 shows the variation of conversion with temperature for $CaCO_3$ decomposition in different atmospheres of flue gas at atmospheric pressure. When the temperature of reaction is increased, the conversion of $CaCO_3$ decomposition increases in both the atmospheres of flue gas 1 and 2. Compared with the result of flue gas 1, the conversion of $CaCO_3$ decomposition increases more significantly and sharply. As shown in **Figure 4.5**, for the $CaCO_3$ decomposition in the flue gas 2, both the initial decomposition temperature and complete decomposition temperature are higher than those in the flue gas 1. And the increase of initial decomposition temperature is more obviously than the complete decomposition temperature. In the atmosphere of flue gas 1, $CaCO_3$ starts to decompose around 709 °C and complete the decomposition at 745 °C, while the corresponding initial decomposition temperature and complete

decomposition temperature in the atmosphere of flue gas 2 are about 775 °C and 786 °C, respectively. As stated earlier, the main difference for these two cases of flue gas is the gas composition especially the CO_2 concentration. The CO_2 concentration of flue gas 2 reaches to 32% while the corresponding value of flue gas 1 is 8%. These results indicates that CO_2 seriously inhibits the decomposition of $CaCO_3$. And the inhibition seems to be more obvious on the initial decomposition temperature compared with the complete decomposition temperature. The higher CO_2 concentration of flue gas may lead to a smaller and higher whole temperature range for the decomposition of $CaCO_3$.

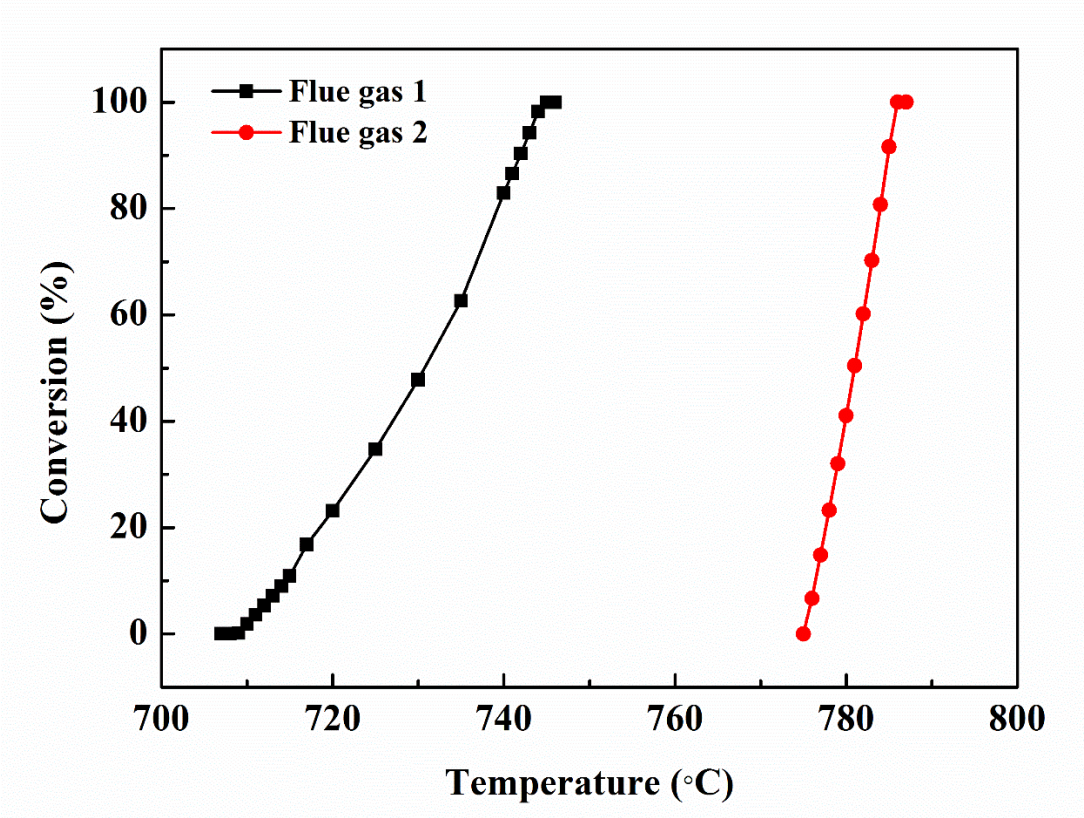

Figure 4.4 Variation of conversion with temperature for $CaCO_3$ decomposition in different atmospheres of flue gas at atmosphere pressure.

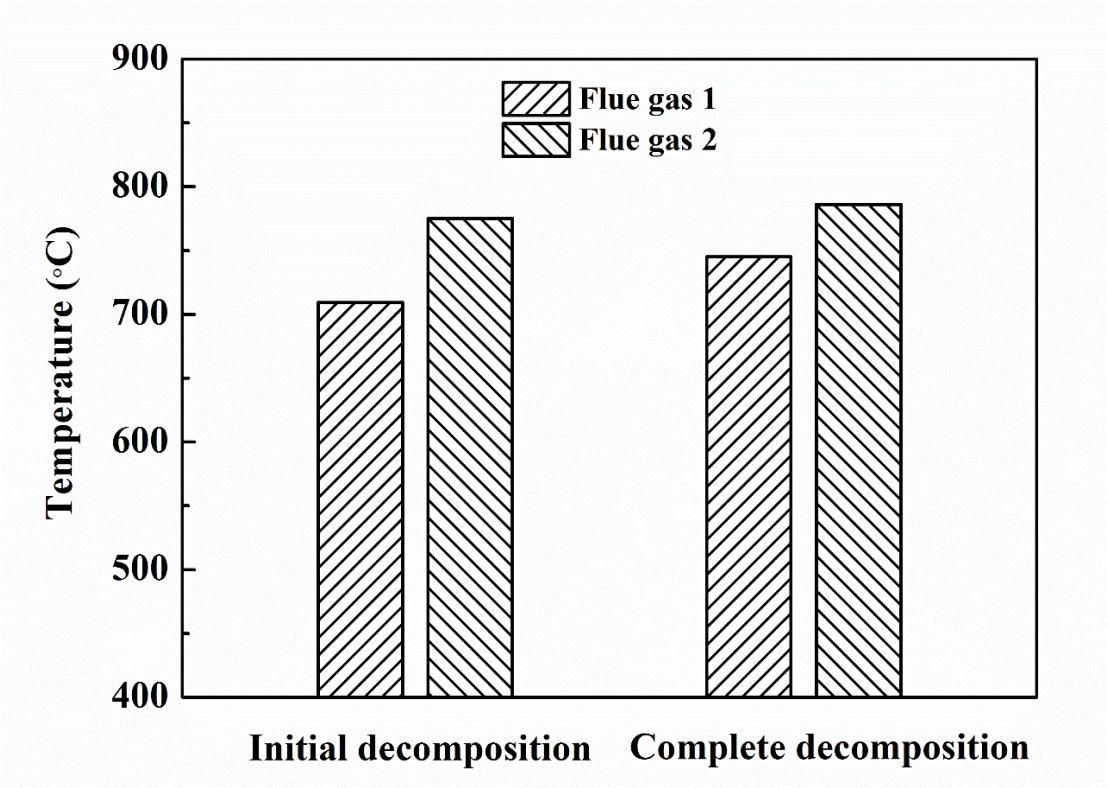

Figure 4.5 Variations with different flue gas atmospheres of initial decomposition temperature and complete decomposition temperature of $CaCO_3$ at atmosphere pressure.

4.3.2 Conversion and temperature in different pressures

Figure 4.6 shows the variation of conversion with the temperature for $CaCO_3$ decomposition under different pressures in the atmosphere of flue gas 1. Consistent with the earlier results, the conversion of $CaCO_3$ decomposition increases with the increase in the temperature of reaction at the pressures ranging from 0.1 to 10 atm. The increase trend is similar while the conversion of $CaCO_3$ decomposition under 0.1 atm seems to be a little shaper than that under 10 atm. The decrease of pressure is favorable for the decomposition of $CaCO_3$. In other words, for a same conversion, a lower temperature of decomposition of $CaCO_3$ can be realized under a lower pressure of

reaction. The variation of conversion with the temperature for $CaCO_3$ decomposition under different pressures in the atmosphere of flue gas 2 is presented in **Figure 4.7**. As expected, the results are similar to those of flue gas 1 but with a shaper trend.

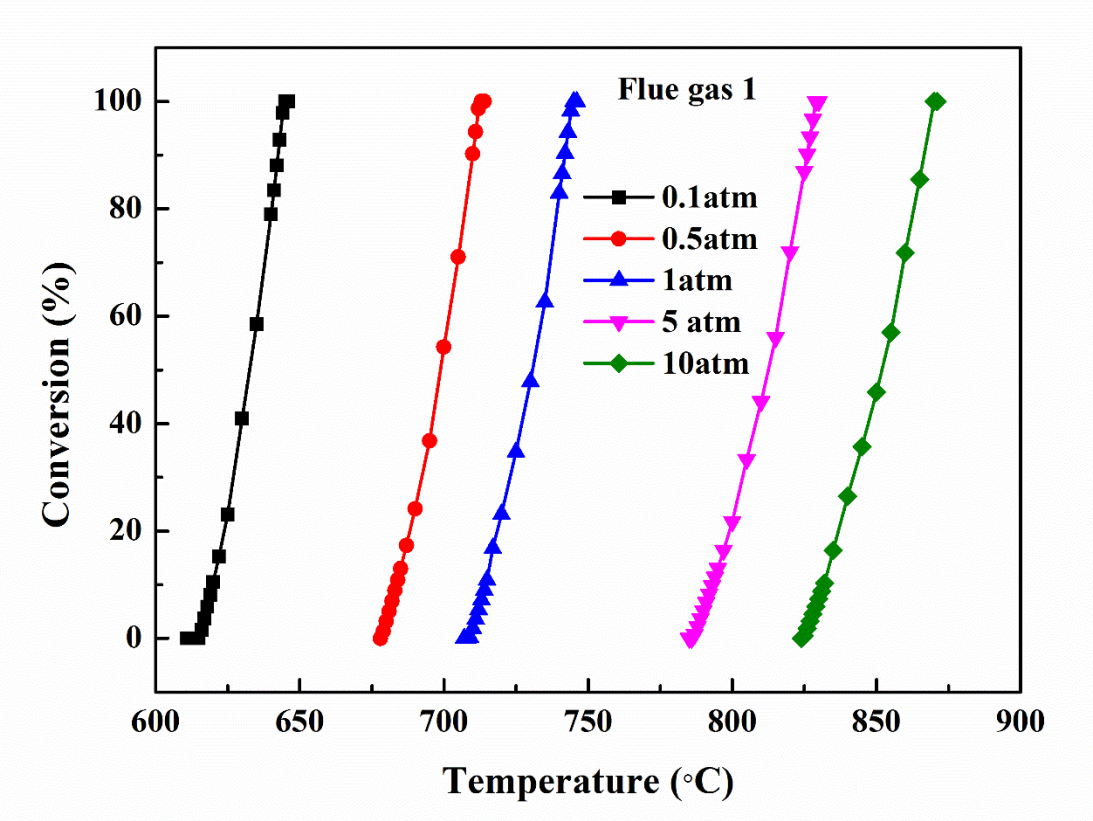

Figure 4.6 Variation of conversion with temperature for $CaCO_3$ decomposition under different pressures in the atmosphere of flue gas 1.

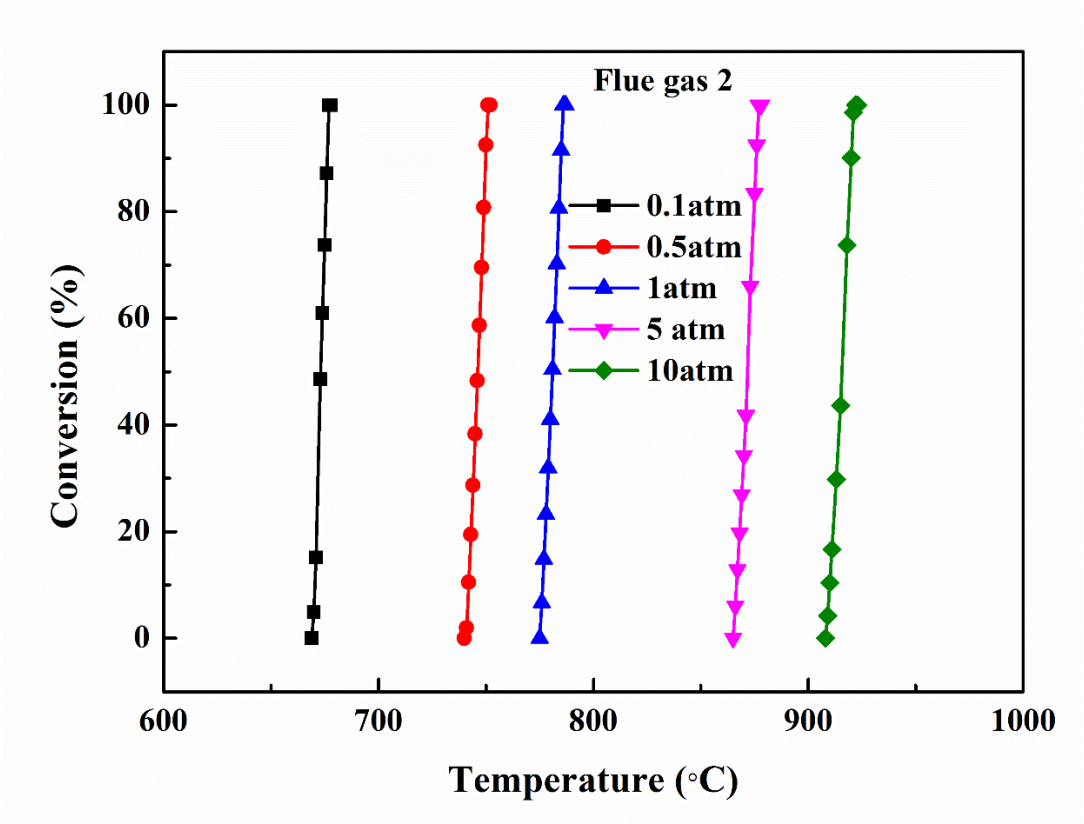

Figure 4.7 Variation of conversion with temperature for $CaCO_3$ decomposition under different pressures in the atmosphere of flue gas 2.

The variations with pressure of initial decomposition temperature of $CaCO_3$ in different flue gas atmospheres are shown in **Figure 4.8**. The initial temperature of $CaCO_3$ decomposition increases with the increase of reaction pressure for both the flue gas 1 and 2. In the case of flue gas 1, with the pressure reduction from 1 atm to 0.1 atm, the corresponding initial decomposition temperatures can be reduced from 709 °C to 615 °C while it can be increased to 825 °C under 10 atm. In the case of flue gas 2, the initial decomposition temperatures under 0.1 atm, 1 atm and 10 atm are 669 °C, 775 °C and 908 °C, respectively. The pressure seems to influence initial decomposition temperature a little obviously for a higher CO_2 concentration atmosphere (i.e., flue gas

2) than that for a relative low CO_2 concentration atmosphere (i.e., flue gas 1). **Figure 4.9** shows the variations with pressure of complete decomposition temperature of $CaCO_3$ in different flue gas atmospheres. The complete decomposition temperature of calcium carbonate also increases with the increase of pressure in the reactor. With the pressure ranging from 1 atm to 0.1 atm, the corresponding complete decomposition temperatures decrease from 745 °C to 645 °C while it increases to 870 °C under 10 atm in the case of flue gas 1. In the case of flue gas 2, the initial decomposition temperatures can increase from 677 °C to 922 °C with the pressure increase from 0.1 atm to 10 atm. These results suggests that the increase in pressure inhibits the decomposition of $CaCO_3$ including both initial decomposition and complete decomposition temperatures.

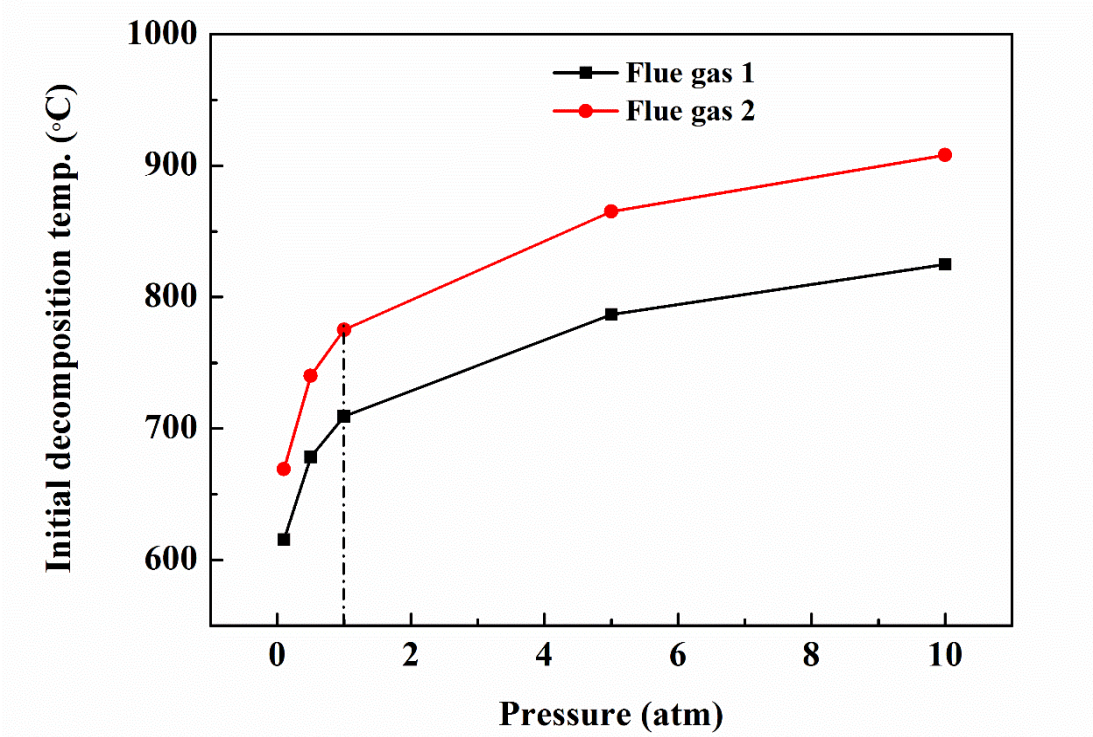

Figure 4.8 Variations with pressure of initial decomposition temperature of $CaCO_3$ in different flue gas atmospheres.

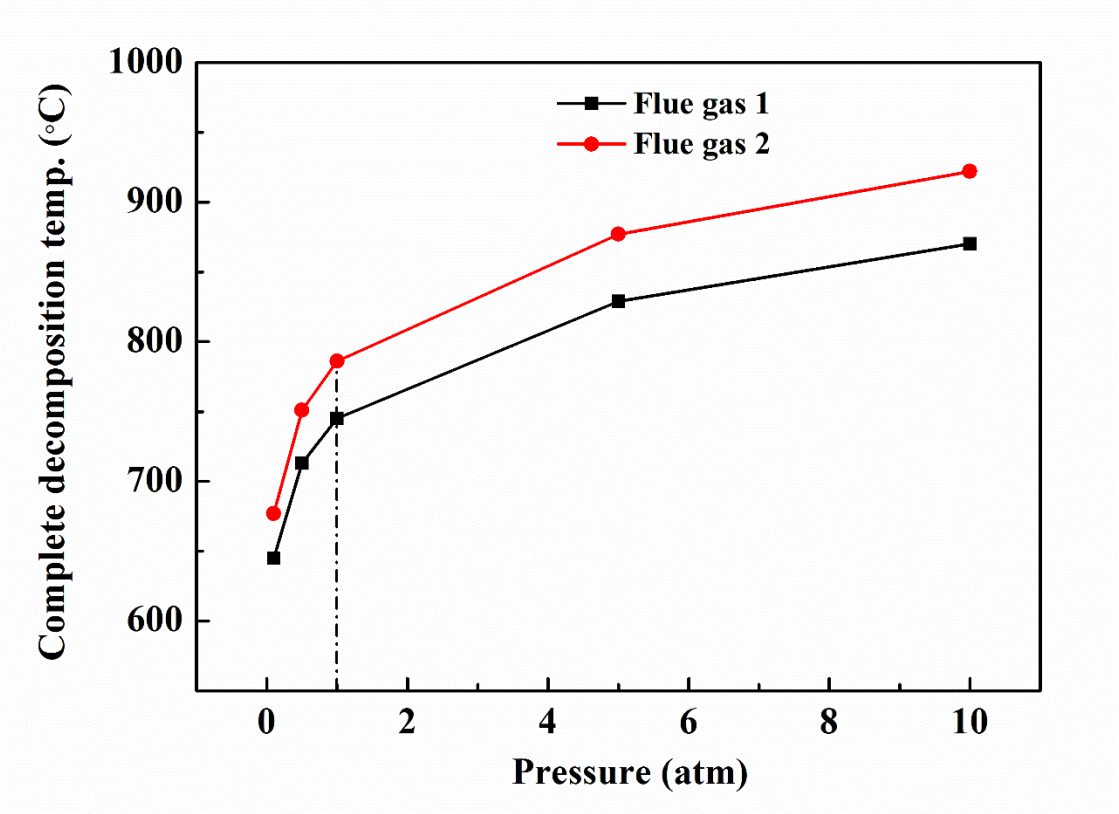

Figure 4.9 Variations with pressure of complete decomposition temperature of $CaCO_3$ in different flue gas atmospheres.

4.4 Conclusions

This work systematically investigates the detailed and comprehensive $CaCO_3$ decomposition under different flue gas atmospheres and different pressures through simulation to provide more fundamental and complete information for the reaction kinetics in the product gas strongly inhibited atmospheres and certain reference value for industrial applications. Compared with the result of flue gas 1, the conversion of $CaCO_3$ decomposition in the case of flue gas 2 increase more significantly and sharply. For the $CaCO_3$ decomposition in the flue gas 2, both the initial decomposition temperature and complete decomposition temperature are higher than those in the flue

gas 1. These results indicates that CO_2 seriously inhibits the decomposition of $CaCO_3$. And the inhibition seems to be more obvious on the initial decomposition temperature compared with the complete decomposition temperature. The higher CO_2 concentration of flue gas may lead to a smaller and higher whole temperature range for the decomposition of $CaCO_3$. Both the initial temperature and complete temperature of $CaCO_3$ decomposition increase with the increase of reaction pressure for both the flue gas 1 and 2. The decrease of pressure is favorable for the decomposition of $CaCO_3$.

References

1. G. Xu, Micro fluidized bed reaction kinetics analyzer, the instrument development project of Chinese Academy of Sciences, China, Project number Y2005014. 2005.
2. X. Liu, G. Xu, S. Gao, Micro fluidized beds: Wall effect and operability, Chem Eng J. 2008, 137, 302-307.
3. J. Yu, J. Zhu, J. Yue, L. Sun, X. Liu, G. Xu, Development and application of micro kinetic analyzer for fluidized bed gas-solid reactions, CIESC Journal. 2009, 60, 2669-2674.
4. J. Yu, J. Yue, Z. Liu, L. Dong, G. Xu, J. Zhu, Z. Duan, L. Sun, Kinetics and mechanism of solid reactions in a micro fluidized bed reactor, AIChE J. 2010, 56, 2905-2912.

5. S. Geng, Z. Han, J. Yue, Y. Li, X. Zeng, D. Lai, J. Yu, G. Xu, Conditioning micro fluidized bed for maximal approach of gas plug flow, Chem Eng J. 2018, 351, 110-118.
6. Y. Liu, Y. Wang, F. Guo, X. Li, T. Li, C. Guo, J. Chang, Characterization of the gas releasing behaviors of catalytic pyrolysis of rice husk using potassium over a micro-fluidized bed reactor, Energy Convers Manage. 2017, 136, 395-403.
7. W. Gao, M.R. Farahani, M.K. Jamil, M.K. Siddiqui, HMA. Siddiqui, M. Imran, R. Rezaee-Manesh, Kinetic modeling of pyrolysis of three Iranian waste oils in a micro-fluidized bed, Petrol Sci Technol. 2017, 35, 183-189.
8. J. Yu, C. Yao, X. Zeng, S. Geng, L. Dong, Y. Wang, S. Gao, G. Xu, Biomass pyrolysis in a micro-fluidized bed reactor: Characterization and kinetics, Chem Eng J. 2011, 168, 839-847.
9. F. Wang, X. Zeng, R. Shao, Y. Wang, J. Yu, G. Xu, Isothermal gasification of in situ/ex situ coal char with CO_2 in a micro fluidized bed reaction analyzer, Energy Fuels. 2015, 29, 4795-4802.
10. X. Zeng, F. Wang, Y. Wang, A. Li, J. Yu, G. Xu, Characterization of char gasification in a micro fluidized bed reaction analyzer, Energy Fuels. 2014, 28, 1838-1845.
11. Y. Fang, G. Luo, C. Chen, J. Li, H. Zhao, R. Duan, L. Chen, K. Li, H. Yao, Combustion kinetics of in-situ char and cold char in micro-fluidized bed, J Combust Sci Technol. 2016, 22, 148-154.

12. Y. Fang, R. Zou, G. Luo, J. Chen, Z. Li, Z. Mao, X. Zhu, F. Peng, S. Guo, X. Li, H. Yao, Kinetic study on coal char combustion in a micro fluidized bed, Energy Fuels 2017, 31, 3243-3252.
13. W. Jiang, W. Hao, X. Liu, Z. Han, J. Yue, G. Xu, Characteristic and kinetics of light calcination of magnesite in micro fluidized bed reaction analyzer (in Chinese), CIESC J. 2019, 70, 2928-2937.
14. H. Chen, Z. Zheng, Z. Chen, W. Yu, J. Yue, Multistep reduction kinetics of fine iron ore with carbon monoxide in a micro fluidized bed reaction analyzer, Metall Mater Trans B. 2017, 48, 841-852.
15. Y. Song, Y. Wang, W. Yang, C. Yao, G. Xu, Reduction of NO over biomass tar in micro-fluidized bed, Fuel Process Technol. 2014, 118, 270-277.
16. H. Chen, Z. Zheng, Z. Chen, XT. Bi, Reduction of hematite (Fe_2O_3) to metallic iron (Fe) by CO in a micro fluidized bed reaction analyzer: A multistep kinetics study, Powder Technol. 2017, 316, 410-420.
17. J. Li, X. Liu, L. Zhou, Q. Zhu, H. Li, A two-stage reduction process for the production of high-purity ultrafine Ni particles in a micro-fluidized bed reactor, Particuology 2015, 19, 27-34.
18. S. Geng, Z. Han, Y. Hu, Y. Cui, J. Yue, J. Yu, G. Xu, Methane decomposition kinetics over Fe_2O_3 catalyst in micro fluidized bed reaction analyzer, Ind Eng Chem Res. 2018, 57, 8413-8423.

19. F. Guo, Y. Dong, Z. Lv, P. Fan, S. Yang, L. Dong, Kinetic behavior of biomass under oxidative atmosphere using a micro-fluidized bed reactor, Energy Convers Manage. 2016, 108, 210-218.
20. X. Liu, W. Hao, K. Wang, Y. Wang, P. An, H. Zhang, J. Yue, D. Bai, G. Xu, Acquiring real kinetics of reactions in inhibitory atmosphere containing product gases using micro fluidized bed, AIChE J. 2021, e17325.
21. J. Happel, Transient tracing, Chem Eng Sci. 1978, 33, 1567.
22. J. Happel, I. Suzuki, P. Kokayeff, V. Fthenakis, Multiple isotope tracing of methanation over nickel catalyst, J Catal. 1980, 65, 59-77.
23. T. Shimizu, T. Hirama, H. Hosoda, K. Kitano, M. Inagaki, K. Tejima, A twin fluid-bed reactor for removal of CO_2 from combustion processes, Chem Eng Res Des. 1999, 77, 62-68.
24. D.P.Harrison, Sorption-enhanced hydrogen production: a review, Ind Eng Chem Res. 2008, 47, 6486-6501.
25. I. Avila, P.M. Crnkovic, F.E. Milioli, K.H. Luo, Thermal decomposition kinetics of Brazilian limestones: effect of CO_2 partial pressure, Environ Technol. 2012, 33, 1175-1182.
26. I. Martinez, G. Grasa, R. Murillo, B. Arias, J.C. Abanades, Kinetics of calcination of partially carbonated particles in a Ca-Looping system for CO_2 capture, Energy Fuels 2012, 26, 1432-1440.

27. B. Gonzalez, G.S. Grasa, M. Alonso, J.C. Abanades, Modeling of the deactivation of CaO in a carbonate loop at high temperatures of calcination, Ind Eng Chem Res. 2008, 47, 9256-9262.

28. T. Darroudi, A.W. Searcy, Effect of CO_2 pressure on the rate of decomposition calcite, J Phys Chem. 1981, 85, 3971-3974.

29. J.C. Maya, F. Chejne, C.A. Gómez, S.K. Bhatia, Effect of the CaO sintering on the calcination rate of $CaCO_3$ under atmospheres containing CO_2, AIChE J. 2018, 64, 3638-3648.

30. J. Khinast, G.F. Krammer, C. Brunner, G. Staudinger, Decomposition of limestone: The influence of CO_2 and particle size on the reaction rate, Chem Eng Sci. 1996, 51, 623-634.

31. F. Garcia-Labiano, A. Abad, L.F. de Diego, P. Gayan, J. Adanez, Calcination of calcium-based sorbents at pressure in a broad range of CO_2 concentrations, Chem Eng Sci. 2002, 57, 2381-2393.

32. J. Yu, X. Zeng, J. Zhang, M. Zhong, G. Zhang, Y. Wang, G. Xu, Isothermal differential characteristics of gas-solid reaction in micro-fluidized bed reactor, Fuel 2013, 103, 29-36.

33. A. Jess, A-K. Andresen, Influence of mass transfer on thermogravimetric analysis of combustion and gasification reactivity of coke, Fuel 2010, 89, 1541-1548.

34. A. Mueller, H.D. Haustein, P. Stoesser, T. Kreitzberg, R. Kneer, T. Kolb, Gasification kinetics of biomass- and fossil-based fuels: comparison study using fluidized bed and thermogravimetric analysis, Energy Fuels 2015, 29, 6717-6723.

35. B. Nowak, O. Karlstrom, P. Backman, A. Brink, M. Zevenhoven, S. Voglsam, F. Winter, M. Hupa, Mass transfer limitation in thermogravimetry of biomass gasification, J Therm Anal Calorim. 2013, 111, 183-192.

36. Y. Zheng, K. Song, B. Chi, C. Zheng, Decomposition kinetics of $CaCO_3$ in CO_2 atmosphere, J Huazhong Univ of Sci Technol (Nature Science). 2007, 35, 87-89.

CHAPTER 5

Conclusions and prospects

5.1 Conclusions

In this study, we mainly focus on the high energy efficiency for light calcination of magnesite for caustic-calcined magnesia (CCM) production through a two-stage fluidized bed gasification system with a transport bed flash calcination process. Firstly, a two-stage fluidized bed gasification (TSFBG) system for fuel gas production was systematically simulated by Aspen Plus to identify the effect of pre-drying for coal with its initial water content varying from 10-65 wt% on gasification performance, particularly energy efficiency. Then, a transport bed flash calcination (TBFC) process applied to magnesite considering pre-decomposition of magnesite during preheating on basis of the kinetics was systematically investigated through process simulation to optimize the energy-saving strategy. Finally, the detailed and comprehensive $CaCO_3$ (similar carbonate as $MgCO_3$) decomposition under different flue gas atmospheres and different pressures through simulation were conducted to provide more fundamental and complete information for the reaction in the product gas strongly inhibited atmospheres and certain reference value for industrial applications. The following results were obtained:

- For the TSFBG system, the higher the water content, the greater the reduced energy efficiency through the pre-drying of coal. When the initial water content is below

26 wt%, $\Delta\eta_{LHV}$ increases by about 1.4% with every 5 wt% increase in water content. The $\Delta\eta_{LHV}$ further increases from about 4.4% to 6.9% when the initial water content of coal is increased from 26 to 65 wt%. An analysis of energy allocations demonstrates that the heat loss due to the pre-drying of coal is mainly responsible for the reduction in energy efficiency. The η_{LHV} of the TSFBG system without the pre-drying of coal using the air/steam as gasification agent reaches its maximum of about 91% at an initial water content of 26 wt%. The η_{LHV} at a high initial water content of 50 wt% is comparable with that at a low initial water content of 10 wt%. For TSFBG using the air/steam without the pre-drying, the preferred initial water content of coal is below 50 wt%. Replacing air with oxygen increases energy efficiency by about 1% to 2% for the TSFBG systems with and without the pre-drying of coal when the initial water content of coal is between 10-65 wt%. Variation in the sensible heat of the product gas is responsible for this difference in energy efficiency. The TSFBG without the pre-drying using the oxygen/steam as the gasification agent shows advantages over using air/steam, especially at a high water content.

- The TBFC process is featured with the staged combustion of fuel gas and the recovery, with further its reutilization inside the process of the sensible heat carried by the flue gas of calciner and also by the high-temperature caustic calcined magnesia (CCM) product. The lower energy consumption and higher energy efficiency are well identified for the investigated TBFC process in comparison with

the traditional but typical reverberatory furnace (RF) and magnesite flash calciner (MFC). Pre-decomposition of magnesite by the high-temperature calciner flue gas is considered on basis of the kinetics measured using a micro fluidized bed reaction analyzer (MFBRA) that allows the minimized effect of external diffusion on reaction. The result reveals that the pre-decomposition mainly occurs in the first stage of preheaters, and the maximal conversion under the cyclone preheating model conditions of this study is about 13%. The occurrence of pre-decomposition would slightly lower the energy consumption and increase the energy efficiency of the entire process while the residence time of magnesite above 1 s in the cyclone preheaters has limited effect on the available pre-decomposition rate.

- For TBFC process, varying the number of preheating stages causes more pronounced rise in the energy efficiency than adjusting the same number of cooling stages does. In fact, the sensible heat carried with the calciner flue gas is much more, say by about 6 times, than with the high-temperature CCM. The TBFC adopts staged feed of fuel gas along the calciner to allow the air equivalence ratio of about 1.2 for fuel gas combustion. This in turn reduces the volume of flue gas and contributes greatly the energy conservation. For TBFC, the preferred process arrangement is proved to be four-stage preheating for magnesite and two-stage cooling for CCM, and the corresponding energy consumption is about 4100 kJ/kg-CCM and energy efficiency is 66.8%. Comparing with the traditional light

calcination furnaces such as the popularly used RF, the energy efficiency is almost doubly higher, say, from 34% to about 67%.

- The CO_2 seriously inhibits the decomposition of $CaCO_3$ and the inhibition seems to be more obvious on the initial decomposition temperature compared with the complete decomposition temperature. The higher CO_2 concentration of flue gas may lead to a smaller and higher whole temperature range for the decomposition of $CaCO_3$. Both the initial temperature and complete temperature of $CaCO_3$ decomposition increase with the increase of reaction pressure for different CO_2 concentration of flue gas. The decrease of pressure is favorable for the decomposition of $CaCO_3$.

5.2 Prospects

In this study, the clean and efficient light calcination of magnesite for CCM production through the two-stage fluidized bed gasification system with the transport bed flash calcination process was realized. While, for the industrial application in the future, the following works should be done:

- The kinetic data of magnesite calcination in the atmosphere of flue gas using MFBRA should be measured for achieving an accurate process analysis. And pre-decomposition of magnesite during the preheating could be further improved.
- For the TBFC process with the staged combustion of fuel gas, the branch pipe positions for staged fuel gas are essential for designing reactor structures and

corresponding optimization is needed in order to achieve uniform temperature distribution along the calciner.

- Results in this work indicated that the sensible heat carried with the calciner flue gas is much more than with the high-temperature CCM. Thus, it is recommended to explore fuel gas combustion with oxygen for a higher energy efficiency since it can effectively reduce the sensible heat carried with flue gas.

List of publications, presentations and awards

Publications

1) **Ping An**, Zhennan Han, Kangjun Wang, Jiguang Cheng, Zhongkai Zhao, Yohanes Andre Situmorang, Jenny Rizkiana, Abuliti Abudula, Guoqing Guan, Energy-Saving Strategy for a Transport Bed Flash Calcination Process Applied to Magnesite, Carbon Resources Conversion, 2021, 4: 122-131.

2) **Ping An**, Zhennan Han, Kangjun Wang, Jiguang Cheng, Jianhong Zhou, Jenny Rizkiana, Abuliti Abudula, Guoqing Guan, Dingrong Bai, Guangwen Xu, Process Analysis of a Two-Stage Fluidized Bed Gasification System With and Without Pre-Drying of High-Water Content Coal, The Canadian Journal of Chemical Engineering, 2021, 99: 1498-1509.

3) Zhongkai Zhao, Yohanes Andre Situmorang, **Ping An**, Jingxuan Yang, Xiaogang Hao, Jenny Rizkiana, Abuliti Abudula, Guoqing Guan, A Biomass-Based Small-Scale Power Generation System with Energy/Exergy Recuperation, Energy Conversion and Management, 1 January 2021, 227:113623.

4) Zhongkai Zhao, Yohanes A. Situmorang, **Ping An**, Nichaboon Chaihad, Jing Wang, Xiaogang Hao, Guangwen Xu, Abuliti Abudula, Guoqing Guan, Hydrogen Production from Catalytic Steam Reforming of Bio-Oils: A Critical Review, Chemical Engineering & Technology, 2020, 43(4): 625-640.

5) Yohanes Andre Situmorang, Zhongkai Zhao, **Ping An**, Tao Yu, Jenny Rizkiana, Abuliti Abudula, Guoqing Guan, A Novel System of Biomass-Based Hydrogen Production by Combining Steam Bio-Oil Reforming and Chemical Looping Process, Applied Energy, 2020, 268: 115122.

6) Yohanes Andre Situmorang, Zhongkai Zhao, **Ping An**, Jenny Rizkiana, Tirto Prakoso, Abuliti Abudula and Guoqing Guan, A Small-scale Power Generation System Based on Biomass Direct Chemical Looping Process with Organic Rankine Cycle, Chemical Engineering and Processing - Process Intensification, 2021, 163: 108361.

Conference presentations

1) **Ping An**, Zhennan Han, Abuliti Abudula, Guoqing Guan, Dingrong Bai, Guangwen Xu, Effects of Water Contents in fuels on Gasification Characteristics of a Low-Tar Two-Stage Fluidized Bed Gasification System, The 7th Young Scholars' Symposium on Coal Chemical Industry, Xi'an, China, November 5-7, 2020.

2) **Ping An**, Zhennan Han, Jiguang Cheng, Akihiro Yoshida, Abuliti Abudula, Guoqing Guan, Guangwen Xu, Effect of Drying on the Lignite Gasification in a Two-Stage Fuidization System, 2019 CIESC Annual Meeting, Qingdao, China, October 17-20, 2019.

3) **Ping An**, Zhennan Han, Jiguang Cheng, Abuliti Abudula, Guoqing Guan,

Guangwen Xu, Effects of Drying on Two-Stage Fluidized-Bed Coal Gasification Process by Simulation, The First International Symposium of Young Scholars on Carbon Resources Conversion (YSCRC-2019), Shenyang, China, October 11-14, 2019.

4) Situmorang Yohanes Andre, 趙 忠凱, **安 萍**, Jenny Rizkiana, 于 涛, 阿布里提, 官 国清, CO_2-Recycling Biomass Gasification System for Hydrogen Production with Water Gas Shift and Membrane-based CO_2 Capture, 化学工学会第51回秋季大会、岩手大学、2020年9月24-26日(On line).

5) 趙 忠凱，ヨハネス・アンドレ・シツモラング，**安 萍**，吉田 暁弘，阿布 里提，官 国清，メタンの乾式改質とメタンの部分酸化を組み合わせることによる高効率CO_2変換のためのエクセルギー再生システム，第29回日本エネルギー学会大会，富山国際会議場ネット会議、2020年8月5日～7日.

6) Zhongkai Zhao，Yohanes Andre Situmorang，**Ping An**，Akihiro Yoshida，Abuliti Abudula，Guoqing Guan, An Exergy-recuperative Biomass-utilized Power Generation System, 7th Asian Conference on Biomass Science in Koriyama, Japan, December 10, 2019.

Awards

1) **安 萍**, 弘前大学表彰, 2021 年 3 月 5 日.

2) **Ping An**, "Best Oral Presentation" at "The First International Symposium of Yong Scholars on Carbon Resources Conversion (YSCRC-2019)" in Shengyang, China, October 11-14, 2019.

Curriculum vitae

Education:

- 2018.10-present, Hirosaki University, Safety System Engineering, Doctoral Course
- 2014.09-2017.06, Tianjin University, Chemical Engineering, Master Degree
- 2010.09-2014.07, East China University of Science and Technology, Chemical Engineering and Technology, Bachelor Degree

Work experience:

2017.07-present, Shenyang University of Chemical Technology, Research Assistant